Behaviour of saturated sand under different triaxial loading and liquefaction

by

Samuel Tadesse

Thesis submitted to the Faculty of Civil and Environmental Engineering, Norwegian University of Science and Technology, in partial fulfilment of the requirements for the degree of Doctor of Engineering.

Department of Geotechnical Engineering
Norwegian University of Science and Technology

October, 2000

The committee for the appraisal of this thesis
was comprised of the following members:

Associate professor Lars Bo Ibsen, Ph.D., Geotechnical Engineering Laboratory, Department of Civil Engineering, Aalborg University, Aalborg, Denmark.

Dr. Arne Aasmund Skotheim, Dr. Ing., Geovest AS, Molde, Norway.

Professor emeritus Nilmar Janbu, Dr. Sc., Department of Geotechnical Engineering, Norwegian University of Science and Technology, Trondheim, Norway.

Professor Steinar Nordal, Dr. Ing., (Administrator), Department of Geotechnical Engineering, Norwegian University of Science and Technology, Trondheim, Norway.

Abstract

An experimental investigation of the monotonic and cyclic loading behaviour of a saturated uniform medium sand under triaxial conditions is presented. The tests performed in connection with this consisted of undrained monotonic compression and extension, drained monotonic compression and undrained cyclic triaxial loading.

In order to study the influence of the initial relative density and confining pressure on the behaviour of sand, samples were prepared at different initial density and then tested under various levels of confining pressures. The test results indicated that the behaviour of the sand under triaxial tests are both density-dependent and pressure- dependent.

In undrained monotonic triaxial testing, all of the stress paths for the sand tested passed through a state of phase transformation. This state is defined by a point in a q-p' plane at which the mean effective stress increment, $\Delta p'$, is zero. The test results have shown that for loose sands the steady state and phase transformation are almost the same and describe ultimate failure. On the other hand, dense sands exhibited relatively low strains and high stiffness up to this point. It was also observed however, that in these soils large strains occurred after the phase transformation point.

A series of monotonic tests carried out under drained and undrained conditions of loading, have clearly indicated that the steady state line obtained at large strain level is the same for the two tests. This indicates that

the large strain level needed to develop the steady state is able to transform the initial soil structure to a new soil structure which is the same for all samples tested under these two conditions of loading.

A series of tests on isotropically consolidated samples were performed using undrained cyclic loading condition. The results showed that, for a given void ratio, the effective stress state at which the sample starts to develop significant amount of strains is found the same as the phase transformation line obtained from undrained monotonic loading. Furthermore, two different kinds of cyclic failure were observed from the test results, depending on whether the sand was initially loose or dense. For loose sand, flow liquefaction occurred where the effective stress path crossed the phase transformation line and axial strains rapidly accelerated to failure. In the case of dense sand cyclic mobility was evident, where the effective stress path crossed the phase transformation line and then cycled through or close to zero mean effective stress conditions while the cyclic axial strain increased at steady rate to large values. The liquefaction strength was defined in terms of the number of cycles to cause a double amplitude axial strain of 5% for both types of failure. A relationship was established between the cyclic strengths and the effective stress ratios at the phase transformation states obtained from undrained monotonic tests. The suggested relationship enables the cyclic strengths of the sand to be estimated from the results of undrained monotonic tests.

Acknowledgements

I wish to express my sincere and deepest gratitude to my advisor Professor Steinar Nordal, for his inestimable assistance, guidance and advice during all the steps of the present work. The many helpful discussions with him contributed towards my better understanding of Geotechnical Engineering. His kindness and support will always be remembered.

I would like to thank the entire staff of the Department of Geotechnical Engineering and SINTEF Geotechnical Engineering for helpful discussions and encouragements throughout the present work. In particular thanks should be given to Jomar Finseth for his endless patience to solve all the technical problems of the triaxial apparatus and Kjell Rokskåg for solving the electrical and data acquisition problems. I would also like to thank Dr. Steve Perkins for his valuable comments and suggestions.

Special thanks are due to Professor Kåre Senneset for his support and kindness and my friend Kudzi Mawire for his nice discussions and encouragements.

The author wishes to express his gratitude to the Faculty of Civil and Environmental Engineering at the Norwegian University of Science and Technology for financial support which made this investigation possible.

Lastly, the author would like to thank his beloved wife Eden Seyoum and his children Nebiyu, Nahome and Gelila for their encouragements and supports.

Notations

Latin letters

a	attraction
A	area
A_o	initial area
B	Skempton's pore pressure parameter
C_u	uniformity coefficient
d	grain size
d_{50}	diameter of the soil particles for which 50% of the particle are finer
d_{60}	diameter of the soil particles for which 60% of the particles are finer
D	diameter of sample
D_r	relative density
e	void ratio
e_c	void ratio after consolidation
e_{crit}	critical void ratio
e_i	initial void ratio
e_{max}	maximum void ratio
e_{min}	minimum void ratio
E_m	young's modulus of membrane

g_o	non dimensional shear modulus number
G	shear modulus
G_s	specific gravity of sand
G_u	unloading shear stiffness
k_o	non dimensional bulk modulus number
K	bulk modulus
L	length of sample
L_o	initial length of sample
M	slope of failure line in p'-q stress space
n	stress dependency exponent
n	porosity
n_{max}	maximum porosity
n_{min}	minimum porosity
N	normal force
N	number of cycles
P_a	1atm=100kPa
p'	mean effective stress
q	deviatoric stress
q_{cyc}	cyclic deviatoric stress
S	normalized membrane penetration
t_m	thickness of membrane
u	pore water pressure

V	volume of sample
V_o	initial volume of sample
V_m	volume change caused by membrane penetration

Greek letters

γ	shear strain
ε	strain
ε_a	axial strain
ε_p	volumetric strain
ε_p^e	elastic volumetric strain
ε_p^p	plastic volumetric strain
ε_q	shear strain
ε_q^e	elastic shear strain
ε_q^p	plastic shear strain
ε_r	radial strain
η	effective stress ratio in p'-q stress space
η_{pt}	effective stress ratio at phase transformation state
η_{pte}	effective stress ratio at phase transformation state on the extension side
σ	axial stress

σ_1	major principal stress
$\frac{\sigma_1}{\sigma_3}$	principal stress ratio
σ_2	intermediate principal stress
σ_3	minor principal stress
σ_3	cell pressure
σ_{3crit}	critical confining pressure
τ	shear stress
τ_{cyc}	cyclic shear stress
τ_{max}	maximum shear stress
τ_{oct}	octahedral shear stress
ϕ	friction angle

Abbreviations

CCV	consolidated constant volume
CCV87%	consolidated constant volume test on a sample of 87% relative density
CD	consolidated drained
CD30%	consolidated drained test on a sample of 30% relative density
CD57%	consolidated drained test on a sample of

	57% relative density
CD87%	consolidated drained test on a sample of 87% relative density
CU	consolidated undrained
CU30%	consolidated undrained test on a sample of 30% relative density
CU57%	consolidated undrained test on a sample of 57% relative density
CU87%	consolidated undrained test on a sample of 87% relative density
CUC	consolidated undrained cyclic
CUC30%	consolidated undrained cyclic test on a sample of 30% relative density
CUC57%	consolidated undrained cyclic test on a sample of 57% relative density
CUC87%	consolidated undrained cyclic test on a sample of 87% relative density
NTNU	Norwegian University of Science and Technology
PTL	phase transformation line
SSL	steady state line
URD30%	unloading-reloading consolidated drained

	test on a sample of 30% relative density
URD87%	unloading-reloading consolidated drained test on a sample of 87% relative density
URD87%	unloading-reloading consolidated und-rained test on a sample of 87% relative density

Table of contents

Chapter 1
Introduction, scope and organization

1.1 Introduction.

Liquefaction is one of the major causes of ground or geotechnical failures and it has been observed in almost all of the large earthquakes that have occurred. The name liquefaction has been used to describe all those phenomena that are related with the undrained response of cohesionless material where an important build up in pore water pressure and a significant amount of deformation occur. However, the mechanisms causing them are different. These phenomena may be categorised into two main groups; namely flow liquefaction and cyclic mobility.

During cyclic loading induced by earthquake shaking, the grains of soil tend to move to form a denser arrangement. If the water in the pore spaces is unable to drain away to accommodate the compaction, the pore water pressure increases. This decreases the effective intergranular stress and

the soil becomes weaker and more deformable. In very loose cohesionless soils, the rise in pore water pressure can be extremely large due to collapse of the soil structure and there can be a very significant loss of strength and deformation. This phenomenon is called flow liquefaction. If the sand is dense, pore water pressures still develop during seismic shaking and may become large enough to reduce its effective intergranular stress to zero. But since the sand is dense it does not undergo flow deformation. However, the pore water pressure does reduce the stiffness of the sand and the strength at small strains. Therefore deformations tend to increase with the duration of seismic loading and become large enough in some cases to constitute failure. This phenomenon is called cyclic mobility.

The behaviour of saturated sands during drained or undrained triaxial tests is determined by the initial nature and distribution of the contacts between grains, by the void ratio of the sand assembly and by the mean effective stress level. The relative importance of these different factors on the soils stress-strain characteristics varies as the magnitude of the shear strain increases. The initial intergranular contact conditions and stress level strongly influence the stress-strain characteristics at small strains and also the inherent anisotropy. Void ratio and stress level govern volume change characteristics at intermediate to large strains (Georgiannou, V.N. Burland, J.B.and Hight, D.W. 1990).

In the past four decades, Geotechnical researchers have focused increased attention on the behaviour of saturated sands under different loading conditions as a result of a number of developments have been made, including the establishment a relation between the cyclic stress ra-

tio and the N value of the SPT test (Seed 1979), and the evaluation of seismic liquefaction potential from residual strength of consolidated-undrained static triaxial tests (Poulos et al. 1985). Because many of the researchers approached the topic from different perspectives and described their results in a variety of forms, the existing literatures on the behaviour of saturated sands under different loading conditions contains some contradiction. Therefore, further work is still needed to give a straight forward and fundamental explanation about the behaviour of this soil.

1.2 Scope of the study.

The investigation described in this thesis entailed an experimental study of the monotonic and cyclic behaviour of uniform medium saturated sand. All the tests have been performed using the triaxial apparatus. The main objectives of the research were as follows:

a) The experimental study of the undrained and drained behaviour of saturated sand under monotonic and cyclic loading conditions.

b) To study the mechanisms of strain development as a consequence of flow liquefaction and cyclic mobility during cyclic loading.

c) On the basis of the experimental results, to develop a relationship between undrained monotonic and cyclic test results, which enables prediction of the cyclic shear strength from the monotonic test results.

1.3 Organization of the thesis.

The thesis has been organized as follows:

In Chapter 2, a critical review of literature relevant to this study, is presented. The equipment used for monotonic and cyclic loading tests is described in Chapter 3. The Chapter also includes a description of the material used in this study, the testing procedure and the method of sample formation.

Chapter 4 deals with the experimental study of the behaviour of the material under drained and undrained monotonic loading. The effects of initial relative density and confining pressure on the drained and undrained response are discussed.

In Chapter 5 the response of the material to cyclic loading conditions is examined. The effects of initial density on the development of axial strains is studied. The results from Chapters 4 and 5 are used to establish a relationship between monotonic and cyclic loading conditions.

Finally, the principal conclusions of the study and recommendations for the future work are given in Chapter 6.

Chapter 2
Literature Review

2.1 Introduction.

The liquefaction of saturated cohesionless soils during earthquakes is one of the major causes of damage to all types of Civil engineering structures. This phenomenon was best illustrated in the Niigata and the Alaska earthquakes of 1964, where severe damage was experienced by buildings, embankments, and natural slopes.

The high incidence of liquefaction during earthquakes, together with its potential for damage, has made the phenomenon a prime subject of concern in earthquake engineering.The seismic design of nuclear power plants and other critical facilities routinely includes evaluation of the liquefaction potential of saturated cohesionless soil layers. The design of new and the inspection of old earth dams in seismic areas is carried out considering the possibility of liquefaction of the dam and /or its foundation when

saturated cohesionless soils are involved. Due to its complexity, the mechanism of the liquefaction phenomenon is not yet completely understood and a large amount liquefaction research is still being done.

At present, the term liquefaction is often used in a broad sense for several phenomena where either loss in strength or stiffness reduction takes place in a saturated cohesionless soil mass leading to large deformation of the ground. However, in order to understand the actual soil behaviour it is of great importance to distinguish between these two different phenomena: flow liquefaction and cyclic mobility.

Cyclic mobility is a phenomenon where there is a significant reduction in the stiffness of the soil mass associated with a rising in the pore water pressure caused by cyclic loading. It is important to point out that during the occurrence of this phenomenon, the soil mass does not show significant loss in strength, however, large deformations can be developed due to the degradation of stiffness. Perhaps, the most common outcome of the large build-up in the pore water pressure is the appearance of sand blows in the ground surface usually called sand boils.

During seismic loading, the level of deformation undergone by the soil mass, due to cyclic mobility, can be unacceptable for some structures, and consequently this phenomenon can generate an important amount of damage to structures. Most probably in all large earthquakes this phenomenon has been the cause of great losses of property and life (Verdugo,1992).

On the other hand, flow liquefaction has been observed in loose saturated cohesionless soil masses and its main features are the large amount

soil involved in the failure, the short time of a few minutes that it takes to bring it failure and the very flat slope that is finally reached by the flowing soil mass. This kind of failure can be triggered not only by earthquakes, but also by any other disturbance that is fast enough to induce a high pore pressure in the soil mass.

Because flow liquefaction involves a loss in strength, in general, it is much more catastrophic than cyclic mobility and the failure compromises a more significant amount of soil mass. For example, the 1920 Kansu, China, earthquake induced several flow failures as much as 1 mile in length and breadth, killing an estimated 200,000 people (U.S. Geological Survey Professional Paper,1981).

Therefore, it is clear that efforts must be made in order to understand in more detail the soil behaviour and specially the undrained response of saturated cohesionless soils which can be unstable and deform largely during fast loading condition, e.g., in earthquakes.

2.2 Volume change in cohesionless soils.

Unlike with other engineering materials, like steel and concrete, soils can undergo a large amount of volume change depending on the initial state of stresses and density when they are subjected to shear stresses. This tendency for volume change has been shown to have a tremendous effect on the strength of the soil mass. The volume change that takes place during loading is mainly due to the contraction or expansion of the voids in the soil mass and it was first pointed out by Reynolds (1885) in the last century. Reynolds discovered that shear deformation of sand is

accompanied by volume changes, and in particular that dense granular materials increase in volume when sheared. This property of granular materials Reynolds termed “dilatancy.” He demonstrated this property for lead shot and for sand by means of the following experiment. A closed rubber bag filled with dense, saturated material was found to be completely rigid. When the bag was connected to an open graduated vessel containing water, and then deformed, water was pulled into the material.

However, it was only in the 1930s that professor Casagrande realized the actual importance of the volumetric strain in the soil response developing the concept of critical density or critical void ratio from the observation of the volumetric strains in dense and loose sands.

2.3 The critical void ratio concept.

In 1936 Casagrande reported his concept of critical void ratio. This concept was based on the results of direct shear box tests conducted as part of Casagrande’s investigation of sands for Fort Peck and Franklin Falls Dams. Typical results of Casagrande‘s direct shear box tests are shown in Fig.2.1 for both loose and dense specimens of sands. Both tests were conducted with the same normal effective stress, which was held constant during shear, and careful measurements were made of the volume changes during shear. Shear of a dense sand at constant normal effective stress causes an initial compaction followed by an increase in void ratio; at large displacement a constant void ratio is reached. Conversely, shear of a loose sand shows a continuing decrease in void ratio until a constant void ratio is reached. The void ratio at large displacement for both loose and

dense specimens was the same. This ultimate common void ratio was termed the critical void ratio by Casagrande. In this state, the soil continues to deform under constant strength and constant volume, hence the soil behaves as a frictional fluid.

Initially, Casagrande thought that the critical void ratio or critical density was a unique constant value for a given soil, but later he realized that the critical void ratio is a function of normal effective stresses, the greater the normal stress the smaller the critical void ratio. Therefore, in the e - $\log \sigma'_n$ plane the critical void ratio can be represented by a single curve as the E - line illustrate in Fig.2.1 (Casagrande 1975). This diagram indicates that any initial state above the E - line should decreases its void ratio when it is sheared, and on the other hand, any initial state represented by a point below the E - line should eventually increase its void ratio when it is subjected to shear stress.

Taylor (1948) added that for undrained conditions, dense sands generally develop greater strength when volume changes are prevented during shear, and loose sands show a decrease in strength. The critical void ratio is one at which shearing under undrained loading conditions does not lead to a change in shear strength.

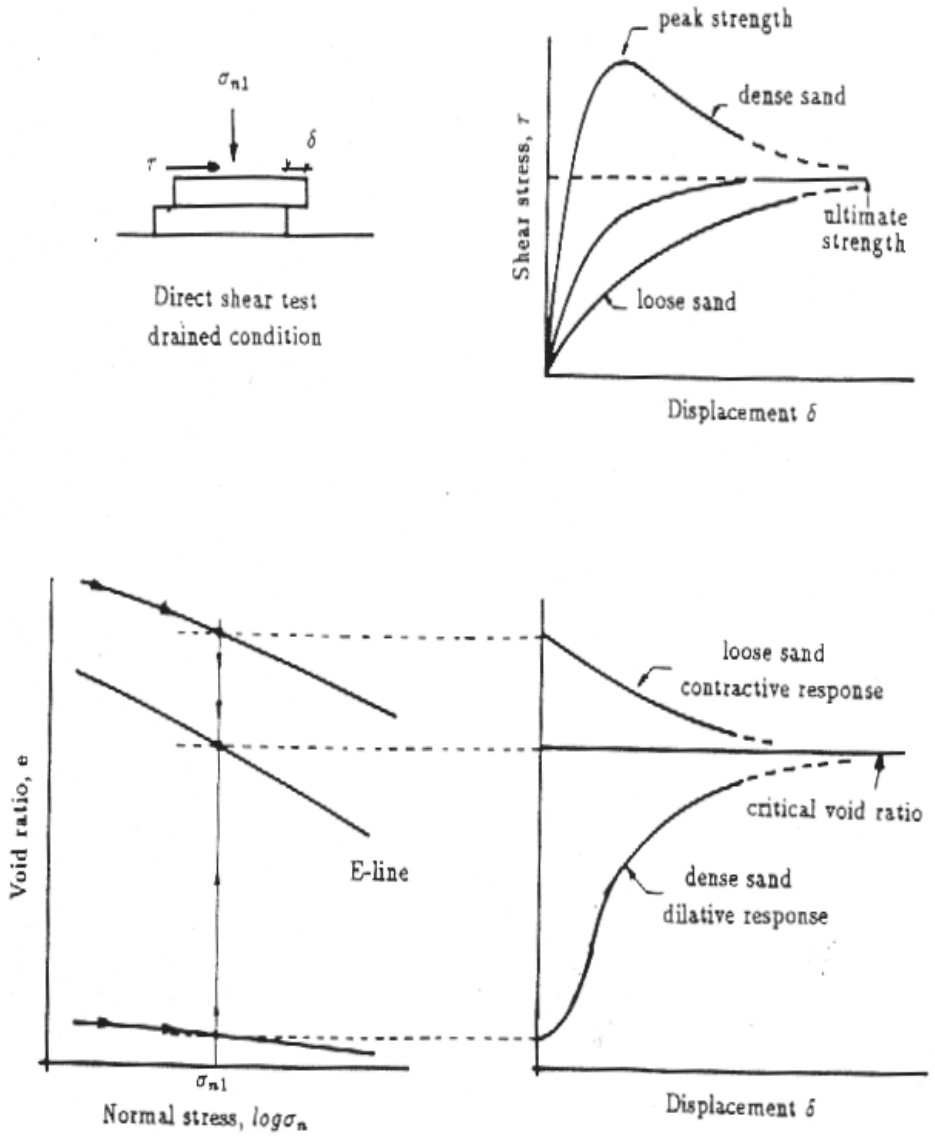

Figure 2.1 Casagrande's critical void ratio from direct shear box tests (Casagrande 1975).

Castro (1969) conducted a series of monotonic undrained, monotonic drained and cyclic undrained tests using the conventional triaxial apparatus. Fig. 2.2 shows the set of these experimental results obtained by him for Banding sand. As can be observed, the experiments support the idea of the existence of two critical void ratio lines. One line, the e_f line is obtained from undrained tests while the e_s line, which plots above the e_f line, is obtained from drained tests and therefore should be similar to the E-line originally defined by Casagrande. From this figure it is seen that, for a given void ratio the e_f line yields a residual undrained strength much smaller than that given by the e_s line. This was explained by Casagrande and Castro using the concept of the “flow structure” as defined by A.Casagrande; i.e during a liquefaction failure the structure of a fully saturated sand changes rather abruptly into a “minimum resistance structure”, or “flow structure”, which differs in the arrangement of the grains from the “normal structure” of a sand that governs the stress-strain behaviour during drained tests.

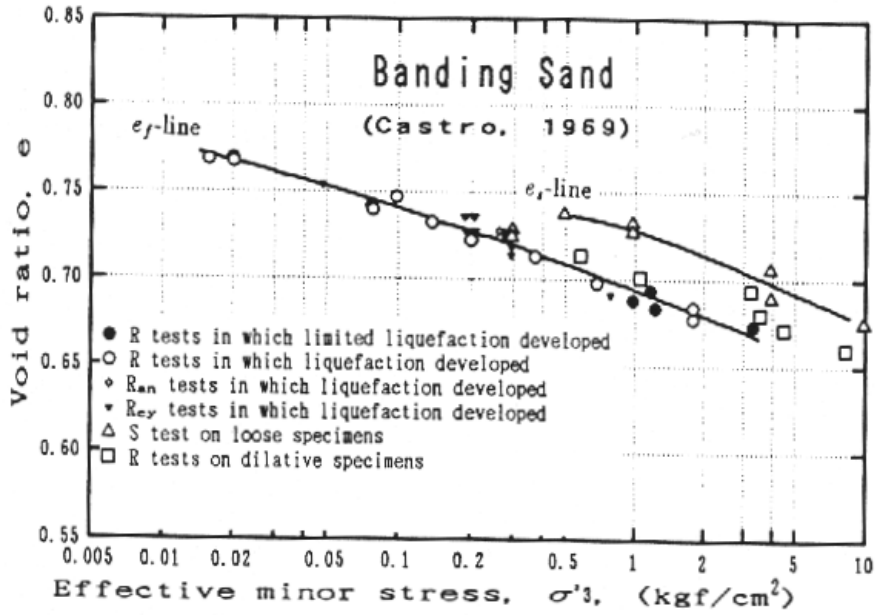

Figure 2.2 Summary of triaxial tests on Banding sand (Castro 1969).

2.4 Steady state.

Steady state is an outgrowth of Casagrande‘s (1936) concept of critical void ratio for characterizing the flow-slide behaviour of sands. Present understanding of steady state is drawn in large part from the work of Castro (1969). Further investigations of undrained response and liquefaction of sands Castro(1975), Casagrande(1976), Poulos (1971, 1981), Castro and Poulos (1977), Castro et.al (1982) and Vaid and Chern (1984) were based on monotonic triaxial compression tests. Observations from these have led to the wide acceptance of steady state as a unique property for a given sand.

At the heart of the steady state is the concept of the steady state deformation, which has been defined by Poulos (1981) as “the steady state deformation for any mass of particles is that state in which the mass is continuously deforming at constant volume, constant normal effective stress, constant shear stress, and constant velocity. The steady state deformation is achieved only after all particle orientation has reached a statistically steady state condition and after all particle breakage, if any, is complete, so that the shear stress needed to continue deformation and the velocity of deformation remain constant.”

For example, according to Poulos (1981), the steady state deformation occurs during undrained tests on fully saturated loose sands after liquefaction has been achieved. During the steady state deformation, the original structure of the specimen has been completely destroyed and reworked into a new “flow structure,” as it was originally proposed by Casagrande and indicated in the previous section.

With the aforementioned definition, the critical void ratio line becomes the steady state line and represents the locus of states in which a soil can flow at constant volume, constant effective normal stress, and constant shear stress (Castro and Poulos, 1977). Therefore, the actual representation of the steady state line should be accomplished in a three dimensional plot by means of three independent quantities which can be selected as follows (Verdugo, 1992).

1.A parameter that express the relative amount of voids in the soil mass, as for example void ratio, porosity or relative density.

2.An effective normal stress parameter, for instance, the first stress

invariant.

$$I_1 = p' = (\sigma'_1 + \sigma'_2 + \sigma'_3)/3 \tag{2.1}$$

3.A parameter that represents the level of shear stress attained by the soil mass, for example, the maximum shear stress,

$$\tau_{max} = (\sigma_1 - \sigma_3)/2 \tag{2.2}$$

the deviator stress,

$$q = \sigma_1 - \sigma_3 \tag{2.3}$$

or the octahedral shear stress,

$$\tau_{oct} = \frac{1}{3}\left((\sigma_1 - \sigma_3)^2 + (\sigma_1 - \sigma_2)^2 + (\sigma_2 - \sigma_3)^2\right)^{1/2} \tag{2.4}$$

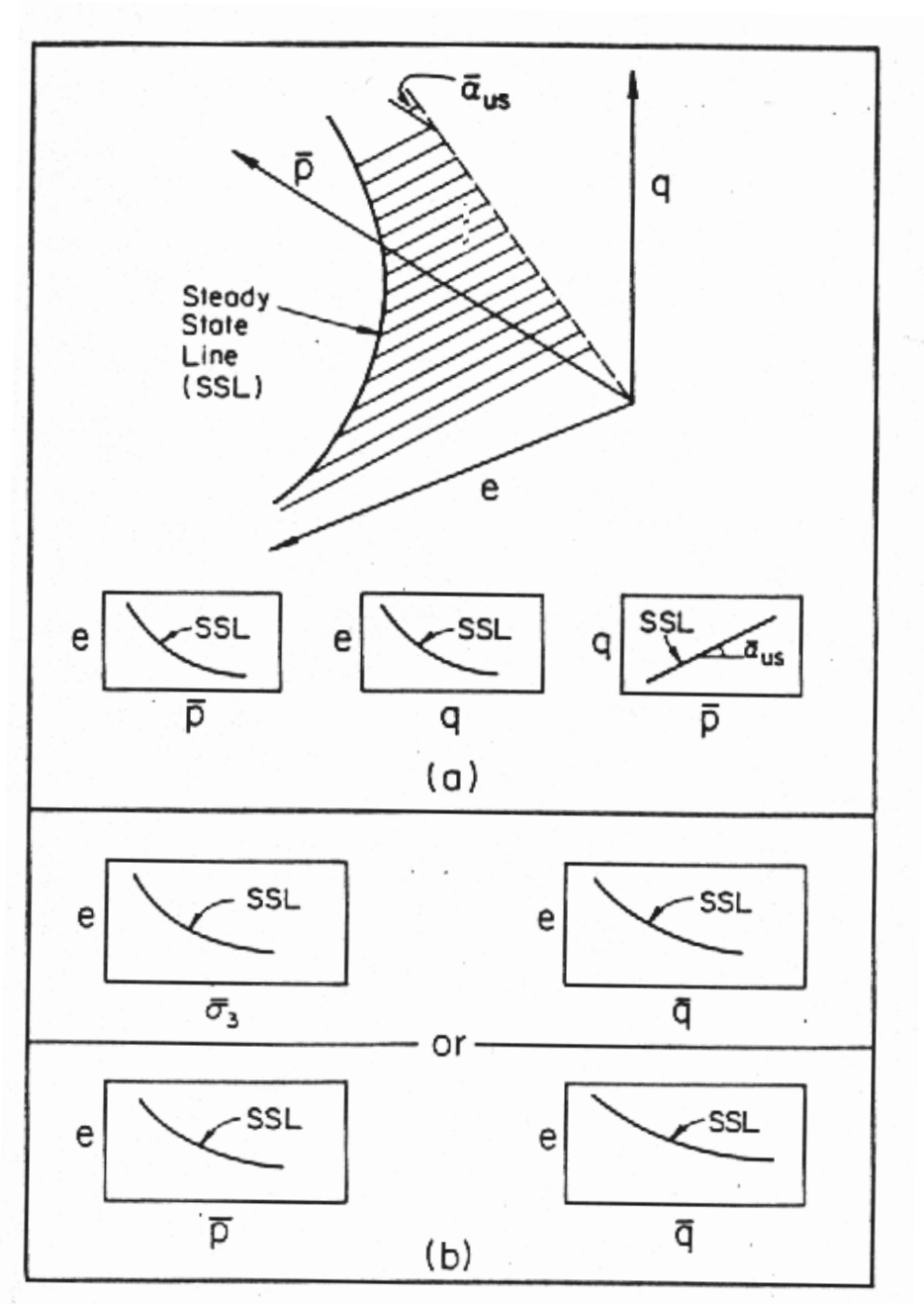

Figure 2.3 Representation of the steady state line (Vasquez et al. 1988).

The most common representation of the steady state seems to be in terms of void ratio, e, effective mean stress, p', and deviator stress, q. However, given the difficulties of a three-dimensional plot, it is preferable to use three two dimensional plots, where each plot corresponds to the projection of the steady state line on the planes of the e-p'-q space. Figure 2.3 sketches the actual steady state line in a three dimensional diagram and the three projections in the corresponding planes.

2.5 Behaviour of saturated sand under monotonic undrained shear.

Several studies have been conducted to provide a better understanding of the undrained behaviour of saturated sand under monotonic loading. Some of the pioneering work in this field has been performed by Seed and Lee (1967), Castro (1969), Ishihara et al. (1975), Casagrande (1976), Castro and Poulos (1977), Poulos (1981), and Castro et al. (1982). In addition, several recent studies Been and Jefferies (1985); Alarcon-Guzman (1988); Vaid and Chern (1985); Sladen et al. (1985); Mohammed and Dobry (1986); Vaid et al. (1989); Ishihara (1993) have made significant contributions to the understanding of the undrained behaviour of saturated sands. The focus of these studies was to relate the undrained strength of sand to its initial state in order to allow for the prediction of the potential for a saturated sand to liquefy. In other words, most of the investigations focused on the influence of the consolidation pressure and the associated void ratio of the sand on the undrained behaviour of the saturated sand under monotonic loading.

The undrained behaviour of isotropically consolidated saturated sand under monotonic loading is accompanied by a change in the excess pore-water pressure, which, in turn leads to different forms of undrained behaviour. This behaviour was found to be characterized by three regions in a state diagram, shown schematically in Figure 2.4 (a) by considering the behaviour of sand samples A, B and C consolidated with the same effective pressure but having different void ratios after consolidation.

First, there is a region in the state diagram within which a sand exhibits marked strain softening behaviour, i.e., after the peak point of the stress - strain curve, which occurs at a small strain (about 1-2%), there is a marked reduction in strength until the shear stress stabilizes at an ultimate or residual strength, regardless of the shear strain amplitude. This is referred to as “flow deformation” and the residual strength is called “steady-state strength.” The corresponding plot in the q-p‘space (sample A, curve a in Figure 2.4(c)) shows a pronounced peak, after which it moves continuously downwards until reaching the failure envelope at the steady-state point (point a in Figure 2.4 (b), (c) and (d)). The pore-water pressure shown in Figure 2.4(c) always increases until steady state flow, when it remains constant. Castro has found that steady-state strength was solely a function of the initial void ratio of the sand. Thus, Castro suggested that the locus of the steady-state strength in a void ratio logarithm of effective minor stress diagram defines a unique line that is referred to as the F-line.This line is widely referred to as the steady-state line.

Secondly, there is a transition region in the state diagram in which samples would only exhibit limited liquefaction as shown by sample B in Figure 2.4(a). The induced pore-water pressure-strain response (curve b in Fig-

ure 2.4 (c)) of samples exhibiting limited flow typically consists of a rapid increase in excess pore-water pressure up to small strain of about 1-2%; this pore-water pressure remains essentially constant to strains of about 10-15%. After further deformation, the sample has a tendency to dilate and pore-water pressure decreases slightly. A typical stress-strain curve is thus characterized by a deviator stress that peaks at small strains, remaining essentially constant, then increasing slightly when the sample dilates at strains in excess of 10-15%.

Finally, there is a region in the state diagram within which a sand exhibits solely strain hardening behaviour, as shown by sample C in Fig.2.4 (curve c). Typically after an initial increase in pore-water pressure, dilation results in a decrease in pore-water pressure and the effective stress path follows the steady-state envelope (Castro 1969; Alarcon-Guzman et al. 1988).

Castro (1969) defined a transition region by the P line and the L line, which are parallel to the F line (Figure 2.4 (a)). Samples above the L line would liquefy (i.e., strain-softening behaviour), whereas those below the P line would experience strain-hardening. Samples consolidated within the P and L lines would develop limited liquefaction. According to Alarcon-Guzman et at. (1988), the L line is the same as the critical void ratio (CVR) line obtained from drained tests.

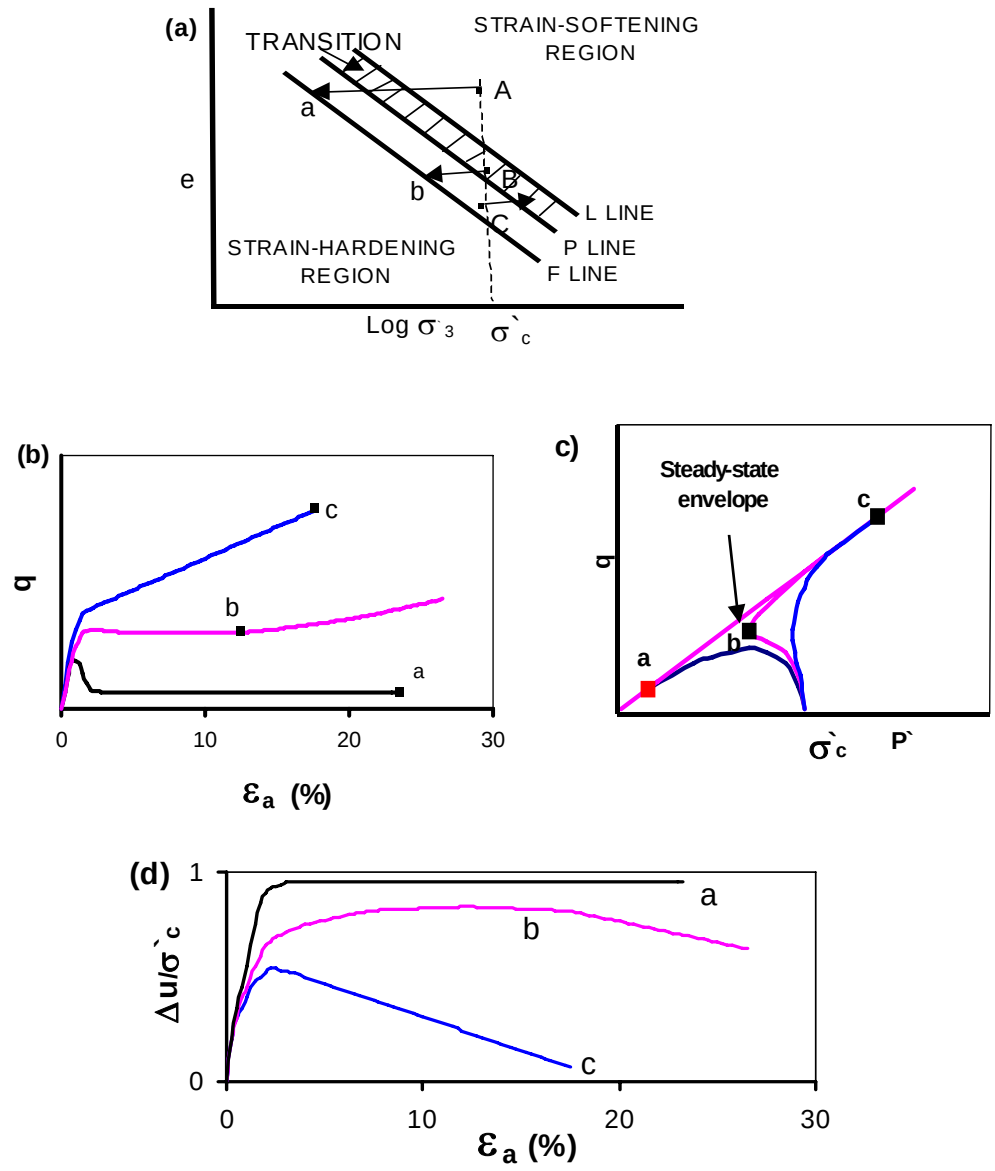

Figure 2.4 Schematic behaviour of sands (Castro 1969): (a) State diagram; (b) Stress versus strain; (c) Deviatoric stress versus effective mean stress; (d) Normalized pore water pressure versus strain.

2.6 Behaviour of saturated sand under monotonic drained shear.

In a drained test, the sample is first consolidated under an effective cell pressure of σ'_3. After consolidation is complete, the sample is gradually sheared by increasing deviatoric stress. Shear is conducted under open drainage and the test is performed sufficiently slowly to prevent any rise in the pore water pressure. During shear, the cell pressure under which the sample was consolidated, remains constant.

Figure 2.5 shows the set-up of a drained triaxial test including a volume change measurement device by reading the water level within a vertical glass tube. This method requires that the sand is and remains saturated during the test. As was mentioned in the previous section, the initial void ratio has an influence on the stress -strain and volume change responses. In triaxial compression, the level of effective confining pressure also has a considerable influence on the behaviour of the soil. The effect of the level of effective confining pressure and initial void ratio on shear strength has been studied by Lee and Seed (1967c), Vesic and Clough (1968), Lo and Roy (1973), Lee (1977), Holtz and Kovacs (1981), Miura et al. (1984) and Tatsuoka et al. (1986) among others. From all these research very consistent conclusions have been obtained. When void ratio and level of effective confining pressure interact as it is shown on figures 2.6 (drained loose sand) and 2.7 (drained dense sand): a loose sand sheared at a very low confining pressure behaves nearly like a dense sand at medium effective confining pressure. On the opposite, a dense sand loaded at very high effective confining pressure looks like a loose sand at medium pressure.

Figure 2.8 shows volumetric strain at failure (points at failure are shown as small arrows in Fig. 2.7) versus void ratio at the end of consolidation, from the data in Figures 2.6 and 2.7 for various confining pressures (other data have been added as well). It can be seen from this figure that for a given confining pressure the volumetric strain decreases (becomes more negative) as the void ratio increases. According to Lee (1965), the critical void ratio is the void ratio at failure when the volumetric strain is zero. Thus for various values of confining pressure in Fig. 2.8, critical void ratio is the void ratio when $(\Delta V)/V_o$ =0.

The relationship between critical void ratio and confining pressure (it is called critical confining pressure because this is the effective confining pressure at which zero volumetric strain occurs at failure for a given void ratio, Lee (1965)) determined from the data in Figure 2.8 is presented in Figure 2.9. The data in this figure indicated that for all practical purposes the critical confining pressure and critical void ratio for this sand are uniquely related to each other. For loose sand, the critical void ratio varies considerably with small changes in confining pressure, while for dense sand small changes in void ratio causes large changes in the critical confining pressure. Furthermore, at combinations of pressure and void ratio falling below the critical void ratio line, samples tend to dilate, whereas at combinations of pressure and void ratio above the line, samples tend to compress during static load application (Lee and Seed, 1966 and1967).

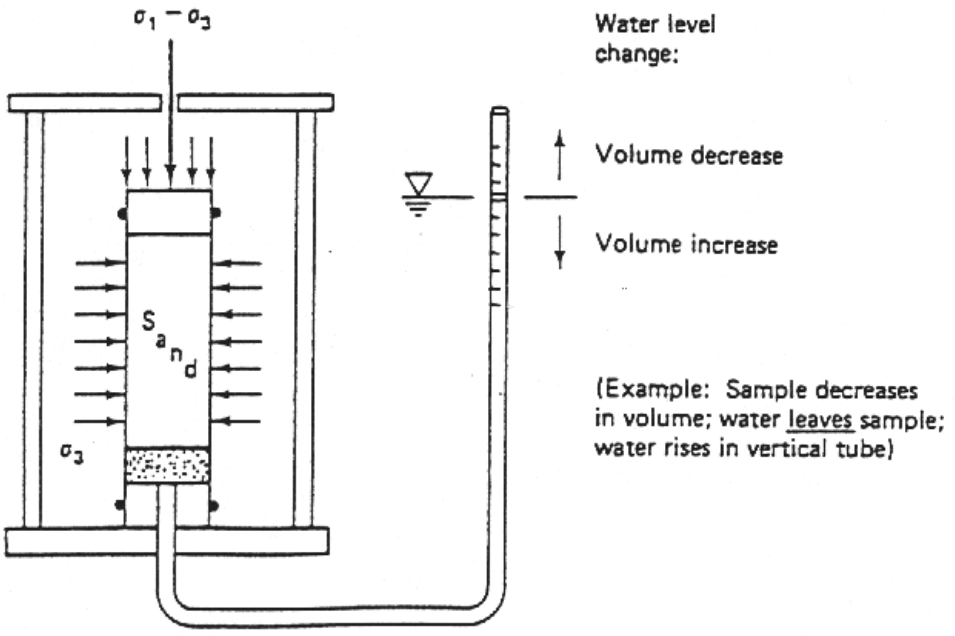

Figure 2.5 Scheme of drained triaxial test on a sample of saturated sand, with measurments of volume change.

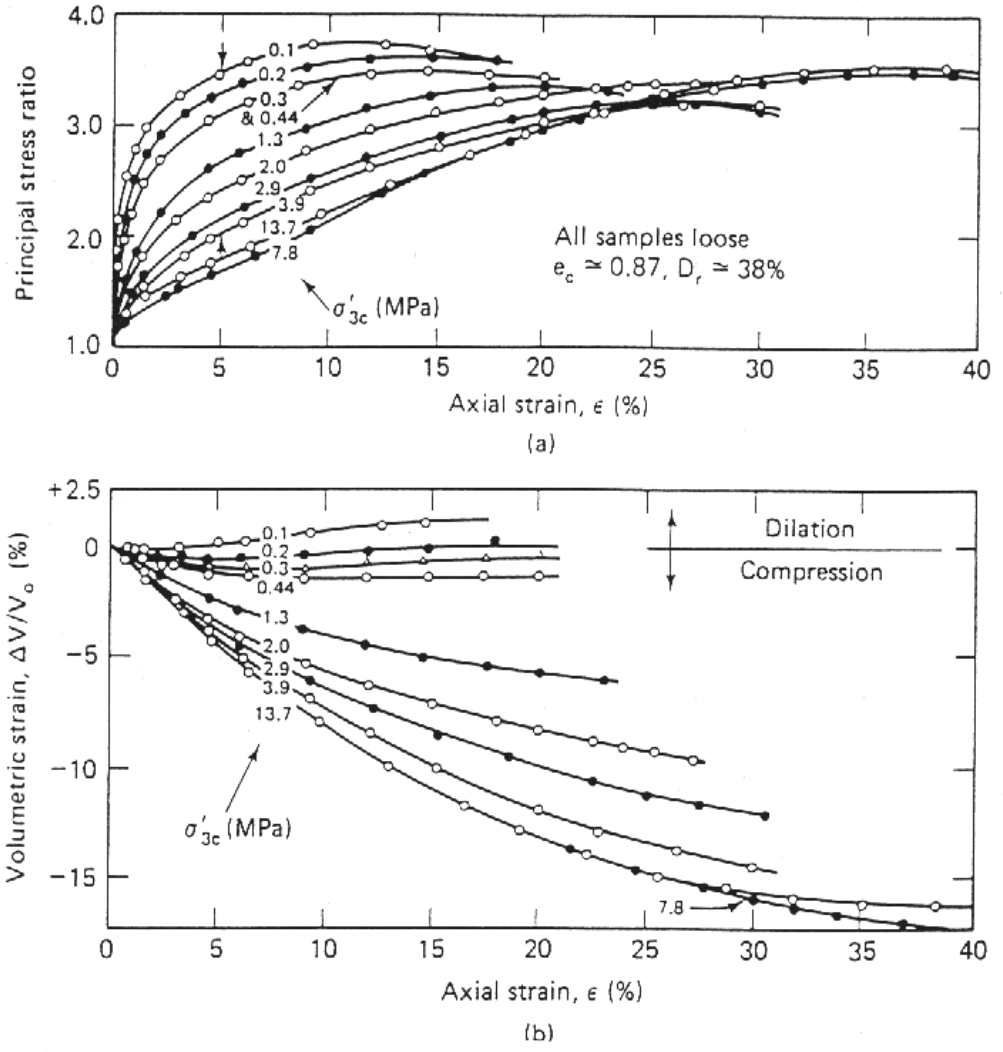

Figure 2.6 Typical drained triaxial test results on loose Sacramento River sand: (a) Principal stress ratio versus axial strain; (b) Volumetric strain versus axial strain (Lee 1965).

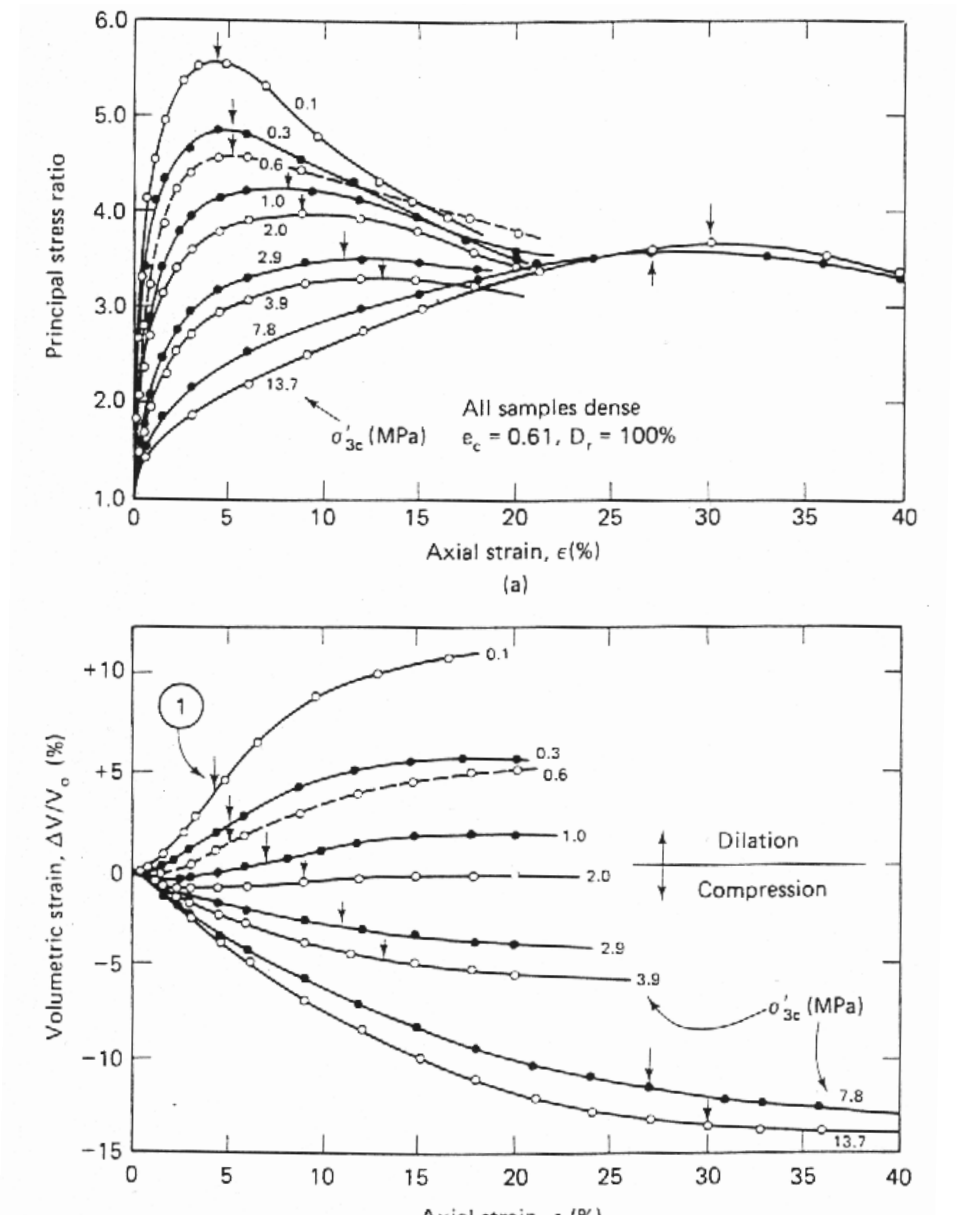

Figure 2.7 Typical drained triaxial test results on dense Sacramento River sand: (a) Principal stress ratio versus axial strain; (b) Volumetric strain versus axial strain (Lee 1965).

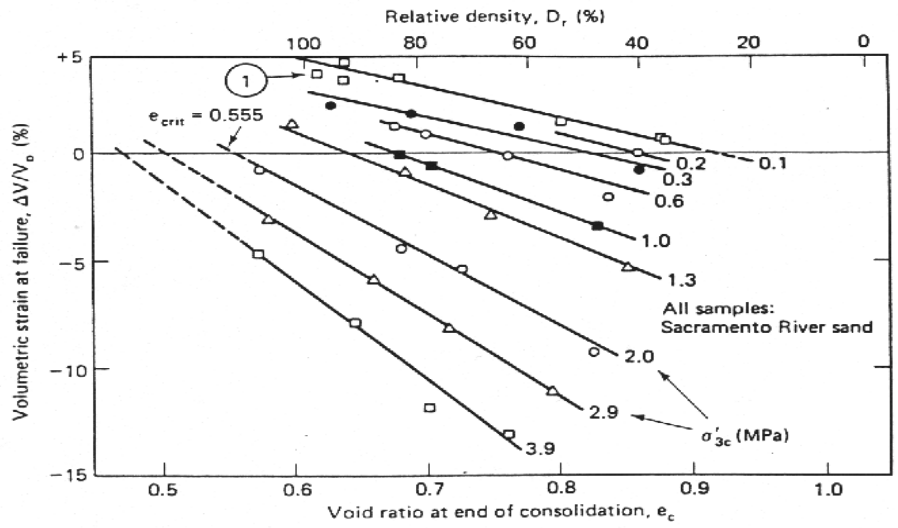

Figure 2.8 Volumetric strain at failure versus void ratio at end of consolidation for drained triaxial tests at various confining pressures (Lee 1965).

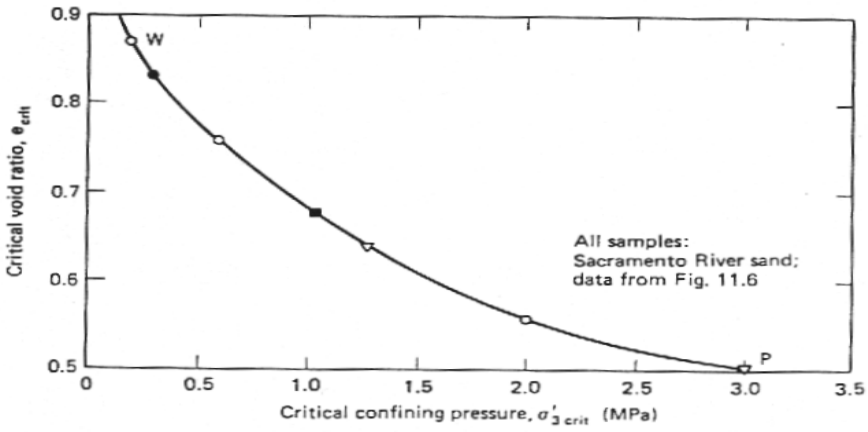

Figure 2.9 Critical void ratio versus pressure conditions from drained triaxial tests (Lee 1965).

2.7 Liquefaction.

Liquefaction is a physical process that may take place during earthquakes or other rapid loading and may lead to ground failure. As a consequence of liquefaction, clay-free soil deposits, primarily sands, temporarily lose strength and behave as viscous fluids rather than as solids. Seismic waves, primarily shear waves passing through a saturated granular soil layer, distort the granular structure and cause some loosely packed particles to collapse. Disruptions of the particulate structure generated by these collapses cause transfer of load from grain-to-grain contacts in the soil layer to the pore water. This transfer of load increases pressure in the pore water, either causing drainage to occur or, if drainage is restricted, a sudden buildup of pore-water pressure. When the pore-water pressure rises to about the pressure caused by the weight of the overlying soil, the effective stress becomes zero, the sand layer behaves like a fluid rather than like a solid for a short period. In this condition, large deformations can occur easily (Youd, 1984b).

Liquefaction of a sand in this way may develop at any zone of a deposit where undrained structural collapse during shaking occur. Such a zone may be at the surface or at some depth below the ground surface, depending only on the state of the sand and the induced motions.

However, liquefaction of the upper layers of a deposit may also occur, not as a direct result of the ground motions to which they are subjected, but because of the development of liquefaction in an underlying zone of the deposit. Once liquefaction develops at some depth in a mass of sand, the excess water pressures in the liquefied zone will dissipate by flow of

water in the upward direction. If the hydraulic gradient becomes sufficiently large, the upward flow of water will induce a “quick” or liquefied condition in the surface layers of the deposit (Seed and Lee, 1966).

Table 1. gives a list of previous major earthquakes accompanied by liquefaction. While the early investigations of this phenomenon were apparently motivated by the dramatic occurrence of liquefaction during the earthquakes in Alaska and Niigata in 1964, the imputes for prompting the study of liquefaction has been supplied incessantly by a series of large earthquakes that have occurred since then throughout seismically active regions of the world.

For the last three decades after 1964, great advances have been made in the recognition of the liquefaction phenomenon and the development of the technology for mitigation of the risk associated with this phenomenon. However, many aspects still need to be investigated.

The liquefaction phenomenon by itself may not be particularly damaging or hazardous. Only when it is accompanied by some form of ground displacement or ground failure is it destructive to all types of engineering structures which are founded or buried in saturated sand. Adverse effects of liquefaction can take many forms. These include: lateral spreads; ground oscillation; loss of bearing capacity; settlement; and increased lateral pressure on retaining structures.(Figure 2.10)

Table 2.1 A list of known recent earthquakes accompanied by liquefaction (Talaganove 1986).

Earthquake	Year	Magnitude
Alaska, USA	1964	8.4
Niigata, JAPAN	1964	7.5
Caracas, VENEZUEL	1967	-
Tokachi-Oki, JAPAN	1968	7.9
Peru	1970	7.8
Madan, NEW GUINEA	1970	7.0
San Fernando, USA	1971	6.5
Haicheng, CHAINA	1974	-
Guatemala	1976	7.6
Friuli, ITALY	1976	6.5
Tangshan, CHAINA	1976	7.7-7.9
SanJuan, ARGETINA	1977	7.2-7.4
Vrancea, ROMANIA	1977	7.2
Miyagi-Ken-Oki, JAPAN	1978	7.4
Montenegro, YUGOSLAVIA	1979	7.2
Imperial Valley, USA	1979	-
Mammoth Lakes, USA	1980	6.0
Nihonkai-Chubu, JAPAN	1983	7.7

Cracked highway, Alaska, USA,1964

Retaining wall damage and lateral spreading Kobe,Japan,1995

Sand boils, LomaPrieta, USA, 1989

A building sank in and tipped 22^0, Nigata, Japan, 1964

Lateral displacement of a quay wall, Kobe, Japan,1995

Collapsed bridge, Niigata, Japan, 1964

Figure 2.10 Damages caused by liquefaction during some earthquakes.

2.8 Behaviour of saturated sand under cyclic loading.

During an earthquake an element of soil in the ground is subjected to a complex system of deformations resulting from the erratic sequence of ground motions induced by the earthquake. However, for many deposits, a major part of the soil deformations may be attributed to the upward propagation of shear waves from underlying layers so that an element of soil, such as that shown in Figure 2.11(a), may be considered to be subjected to a series of cyclic shear strains or stresses that reverse directions many times during the earthquake, as shown in Figures 2.11(b) and (c). If the ground surface is approximately horizontal, then before the earthquake there is no shear stress on the horizontal plane. During the earthquake the normal stress on this plane remains constant while cyclic shear stresses are induced for the duration of ground shaking.

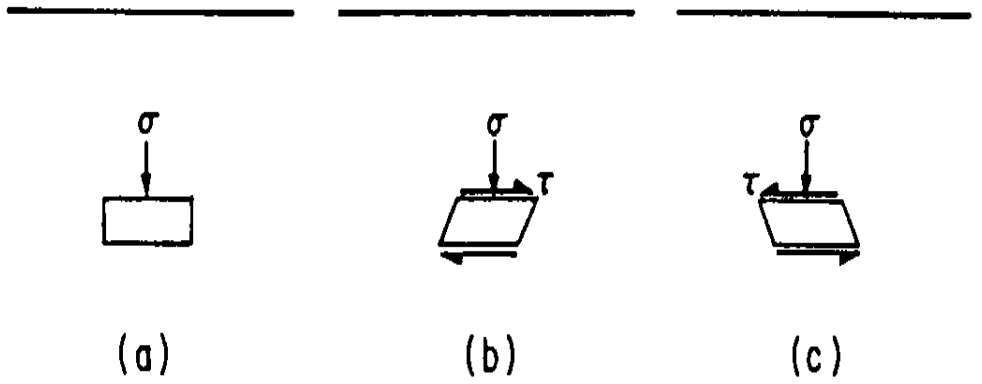

Figure 2.11 Idealized stress conditions for an element of soil below ground surface during an earthquake (Seed and Lee 1966).

Such deformation conditions may be reproduced approximately in the laboratory by cyclic loading triaxial compression tests as shown in Figure 2.12. These loadings, like those occurring during an earthquake, have to be considered as undrained with respect to the permeability of large soils masses, even in sandy soils, because the duration of an earthquake is on the order of minutes.

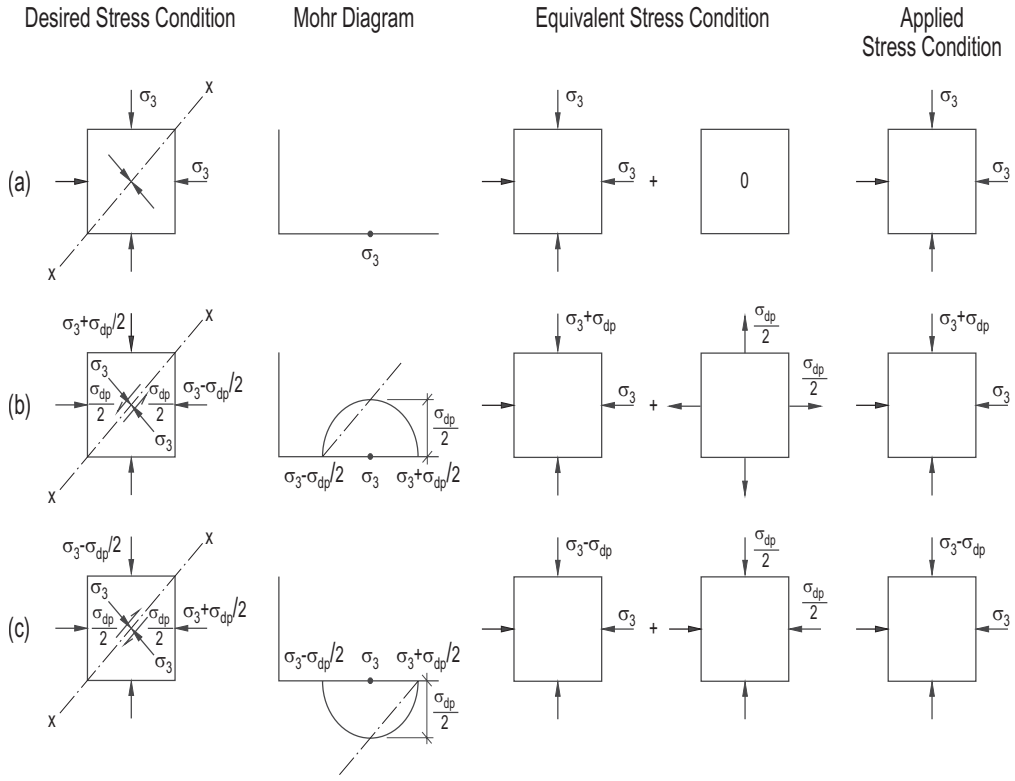

Figure 2.12 Stress conditions for triaxial test on saturated sand under simulated earthquake loading conditions (Seed and Lee 1966).

Cyclic triaxial tests followed by monotonic triaxial tests on loose and dense samples of Sacramento river sand were carried out by Seed (1966). The results of a typical cyclic loading test on a sample of loose sand (D_r=38%) are shown in Figure 2.13. During the first eight cycles of stress application the sample showed no noticeable deformation although the pore-water pressure built up gradually. However, during the ninth stress cycle, the pore-water pressure suddenly increased to a value equal to the externally applied confining pressure and the sample developed large strains which, in the tenth cycle, exceeded 20%; in fact, the soil had liquefied, the effective confining pressure was reduced to zero, and over a wide range of strains the soil could be observed to be in a fluid condition. When cyclic loading was stopped, the pore water pressure in the sample was equal to the applied confining pressure. After cyclic loading, the sample was subjected to static loading applied at a constant rate of strain, as shown in Figure 2.13(b). It is readily apparent that the sample did not exhibit any resistance, deforming continuously without change in pore water pressure during a level of strain of as large as 20%. However, thereafter the specimen develops a dilative behaviour decreasing the pore water pressure which leads to the development of shear resistance again.

Typical results of a cyclic loading test on a sample of dense sand (D_r = 78%) are shown in figure 2.14. During the first 9 cycles, the deformation is very small although the pore-water pressure has increased by about 50% of the applied confining pressure. At close to 12 stress cycles, the pore water pressure starts to reach the applied confining pressure at the instant of zero deviator stress, in other words, at the time when there is no shear stress acting on the sample. Associated with this condition it is observed that the strain amplitude increases markedly, but in contrast to

loose samples, the level of strain gradually increases with the stress cycles. In fact, even though, from stress cycle number 13, the condition zero effective stress is reached at each instant of zero shear stress, the axial strain of the sample does not exceed 10% after 20 stress cycles. Hence the response of dense sands does not show the sudden development of large strain observed in the case of loose samples.

The subsequent application of monotonic loading indicates that the sample starts to dilate, and therefore, starts to regain its strength at a much smaller strain of the order of 5%. Liquefied layers of denser sand will therefore regain their strength at much smaller deformations than loose sand.

From a set of experimental results carried out on cyclic triaxial tests similar to those described above, Seed and Lee introduced the following criteria to define liquefaction (Seed and Lee 1966; Lee and Seed 1967a).

- Failure:- Some level of strain which would be associated with a failure from a practical point of view.

- Complete liquefaction:- When the sample deforms without shear resistance over a wide range of strain

- Partial liquefaction:- when a sample exhibits no resistance to deformation over a range of strain smaller than that defined as failure.

- Initial Liquefaction:- When a soil first exhibits any degree of partial liquefaction during cyclic loading. This occurs when the pore water pressure reaches the initial effective confining pressure for the first

time.

This terminology was later the cause of some confusion that probably still exists among geotechnical engineers regarding the distinction between liquefaction with loss of strength and liquefaction as a phenomenon that induces significant deformation. Flow failure necessarily involves a loss of strength and accordingly, a soil mass can flow even kilo meters before stopping. However, the cyclic response analysed by Seed and Lee is mainly related to a gradual increment of strains associated with the build up in the pore water pressure caused by cyclic loading. In the next section the difference between these phenomena will be discussed in more detail.

Figure 2.15 shows for three different densities, the applied cyclic loading versus the number of cycles, in logarithm scale, required to cause failure according to the criteria defined above (Lee and Seed 1967a). It can be seen from this figure that:

- The stress amplitude required to induce some level of strain in a given number of cycles increases with the density of the sand.

- Initial liquefaction can be induced almost regardless of the density of the sample.

- In the case of loose samples, the condition of initial liquefaction and the condition of a level of axial strain of 20% are achieved almost simultaneously, but in the case of dense samples, the number cycles needed to reach these conditions are significantly different; between 200 and 500 times different.

Figure 2.16 from Lee and Seed (1967) shows for three different densities, the initial effective confining pressure against the cyclic stress amplitude required to induce both a certain amount and initial liquefaction in 100 cycles. From these results Seed and Lee concluded that the higher the confining pressure, the greater the cyclic stress amplitude required to induce failure. Furthermore, the main conclusion that can be drawn from the cyclic tests discussed above is that loose as well as dense sand can develop large pore water pressure when they are subjected to cyclic loading, which induces a progressive increase in the level of deformation.

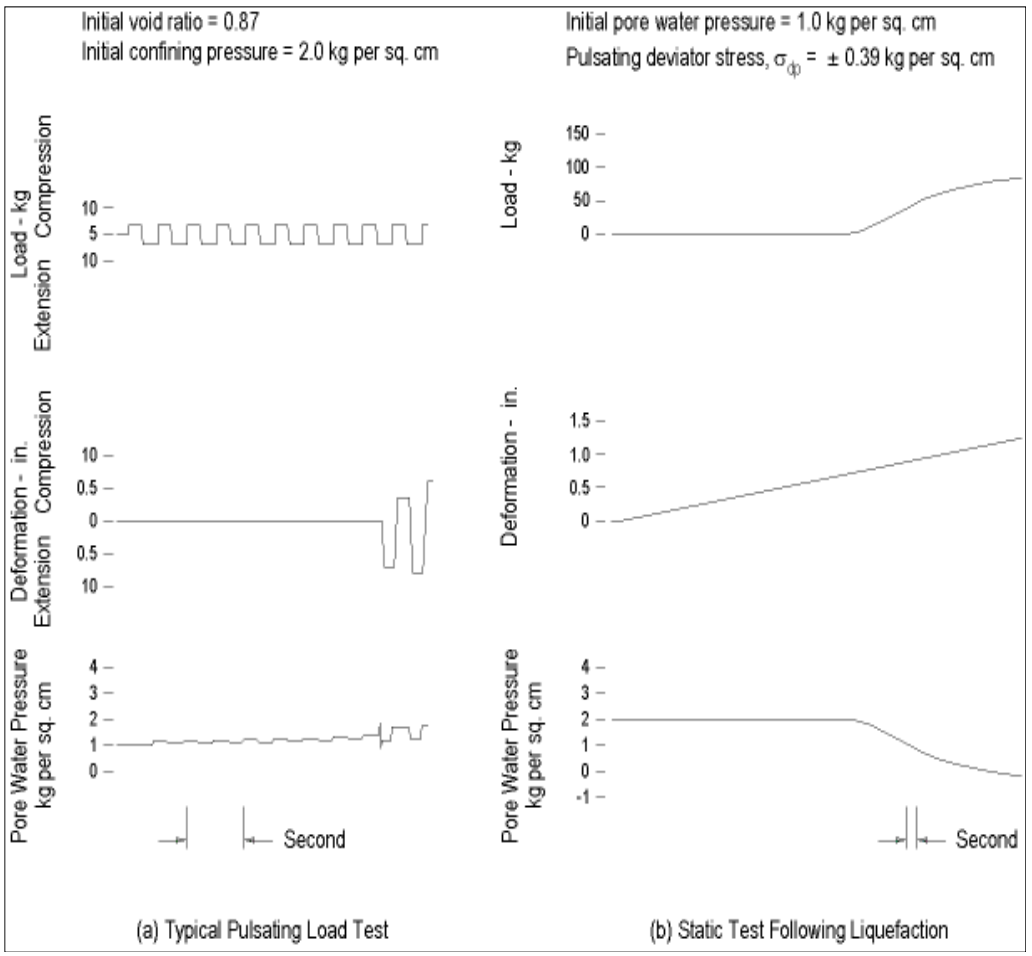

Figure 2.13 Cyclic triaxial test on loose sands (Seed and Lee, 1966).

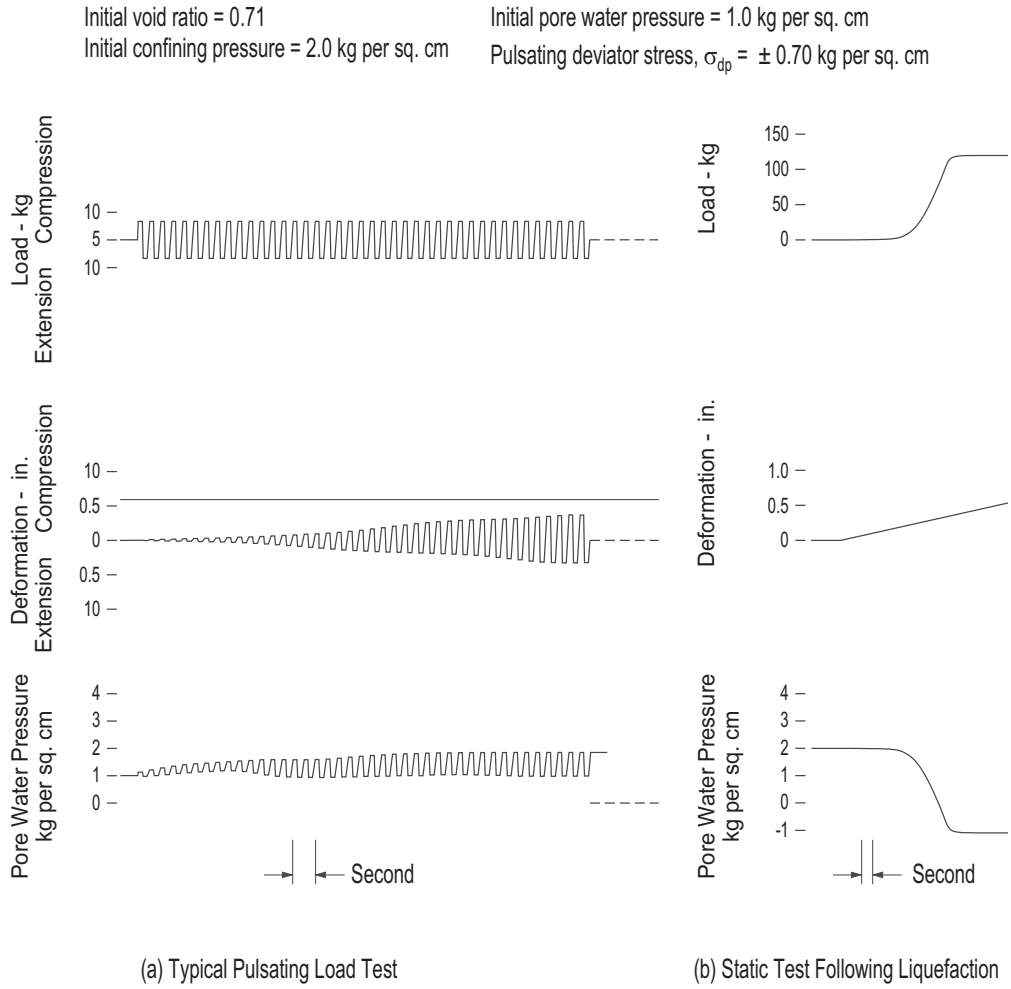

Figure 2.14 Cyclic triaxial test on dense sands (Seed and Lee, 1966).

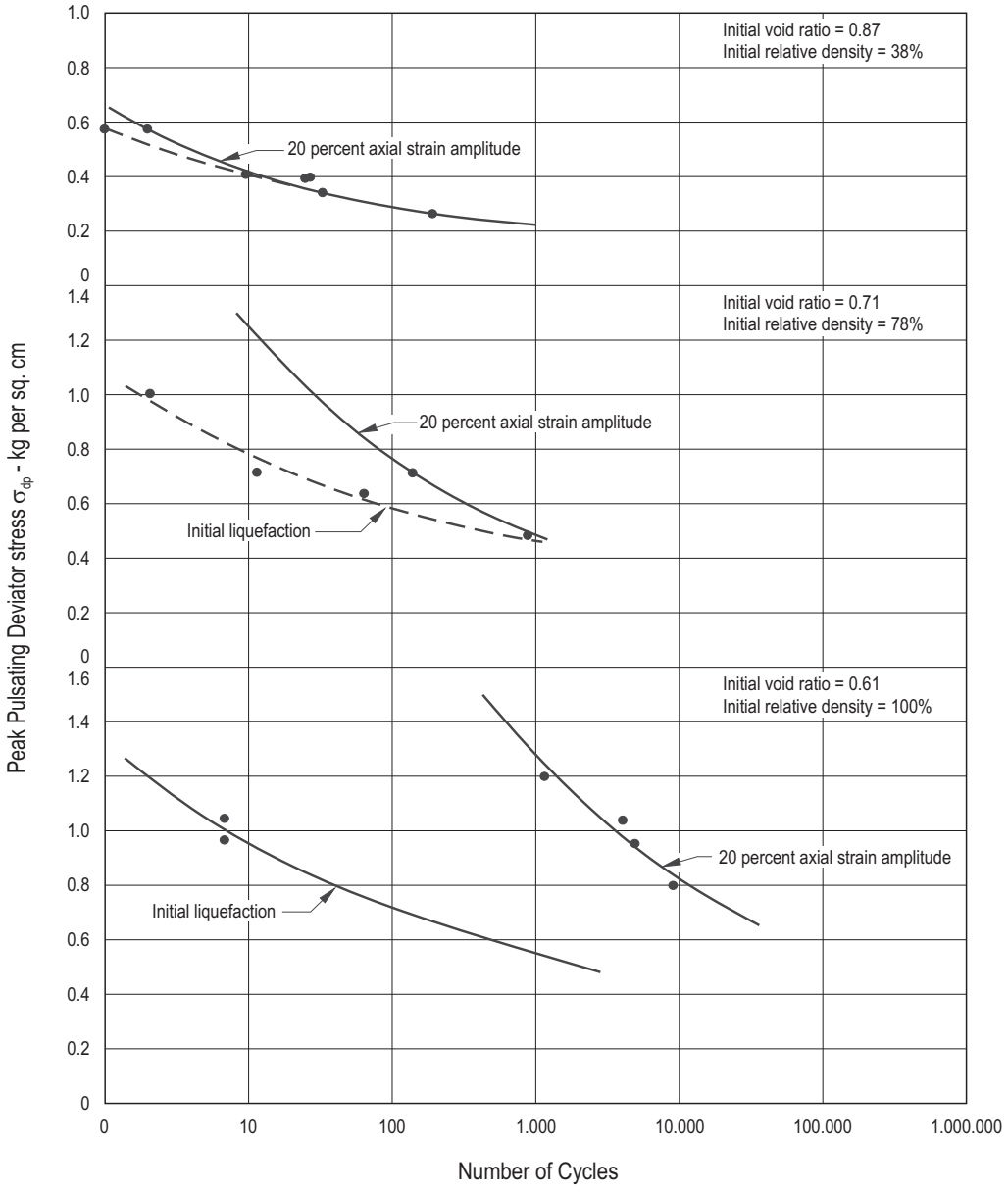

Figure 2.15 Effect of density and failure criterion on cyclic stress causing failure (Lee and Seed,1967).

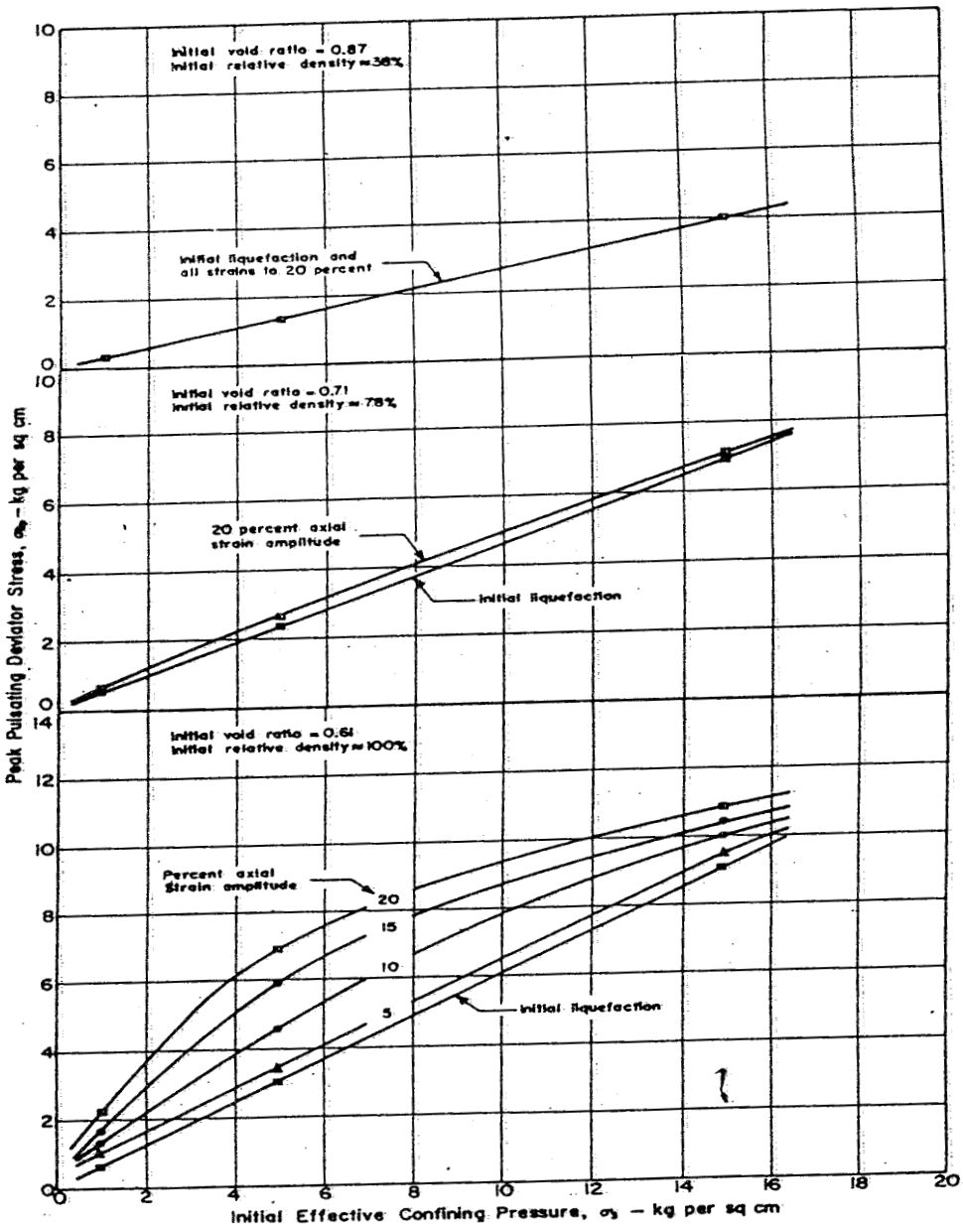

Figure 2.16 Cyclic stresses required to cause failure in 100 cycles (Lee and Seed,1967).

2.9 Phase transformation state from undrained loading.

As it was discussed in the previous section, Figure 2.17 shows sets of possible effective stress paths for undrained monotonic shear tests. The lowest effective stress path is for loose sands and demonstrates purely contractive behaviour and it migrates to the far left of the diagram, where steady-state conditions are achieved (Castro,1975; Castro and Poulos, 1977; Vaid and Chern, 1985; Poulos et al., 1985; Vaid et al., 1989). Dense sands, however, pass through a phase transformation state after an initial contractive period and dilate to a steady-state point. The term “phase transformation“ was first used by Ishihara et al. (1975) to describe a state at which the stress path turns its direction in q-p‘ plane. Normally this is referred to as the point associated with a maximum pore water pressure. But according to Nordal and a paper by Ibsen and Lade (1997) the knee described above does not clearly define the location of the phase transformation state, the most consistent definition is one that is independent of the total stress path. The phase transformation state is therefore best defined as the point at which the effective stress path has a vertical tangent. This definition is consistently used in this study to locate the phase transformation state in a q-p‘plane.

In undrained test, the total change in volumetric strain, $\Delta\varepsilon_p$, is normally assume to be approximately zero. At the phase transformation state defined by mean effective stress increment, $\Delta p'$, is zero, the elastic volumetric strain, $\Delta\varepsilon_p^e$, is also zero. Consequently, the plastic volumetric strain increment, $\Delta\varepsilon_p^p$, is also zero. Since change in plastic shear strain, $\Delta\varepsilon_q^p$, is greater than zero, one may realize that at the phase transformation state

there is no coupling between the responses in shear and volume, or in other word there is no dilation. The straight line that joins the states in the q-p‘ planes is called phase transformation line. Luong (1980) defined a similar concept of a “characteristic state” under drained conditions where the behaviour changed from contractive to dilative. But later it was redefined by Ibsen and Lade (1997) as the stress state where the total change in volumetric strain, $\Delta\varepsilon_p$, becomes zero for the first time in a test with p‘= const. From the results of undrained and drained triaxial compression tests, Chu (1995) suggested that for contractive sands, the steady, critical, characteristic and phase transformation states are the same and describes ultimate flow behaviour. On the other hand, Chu showed that for dilative sands, the principal effective stress ratio $(\sigma'_1)/(\sigma'_3)$ at the phase transformation and characteristic states was the same but quite different from that at the critical state.

It is recognized that for dilative (or partially contractive) sands a significant amount of strain due to cyclic or monotonic loading starts to develop only after the effective stress state of the sample crosses the phase transformation state (Vaid and Chern 1985b).

The location of the phase transformation line in the p‘-q stress space depends on the relative density and type of sand (Alarcon-Guzman, Leonards, and Chameau, 1988). For initially contractive specimens, the angle of phase transformation, ϕ_{pt}, is slightly smaller than the large strain angle of shear resistance, ϕ. In this case, initial liquefaction is likely to develop during the first few unloading stages after the stress path crosses the phase transformation line. As the relative density of the sand increases, the phase transformation line moves away from the failure line, since

dilation would prevail at much lower stress ratios (Ishihara 1985). Accordingly, in dense sands, many cycles of loading and unloading may be required to reach a condition of zero effective stress after crossing the phase transformation line for the first time. Once initial liquefaction develops, a certain amount of shear strain is required to remobilize a given shear resistance. The resistance obtained is then a function of the relative density of the sand (Seed and Lee 1966;Selig and Chang 1981; Youd 1977).

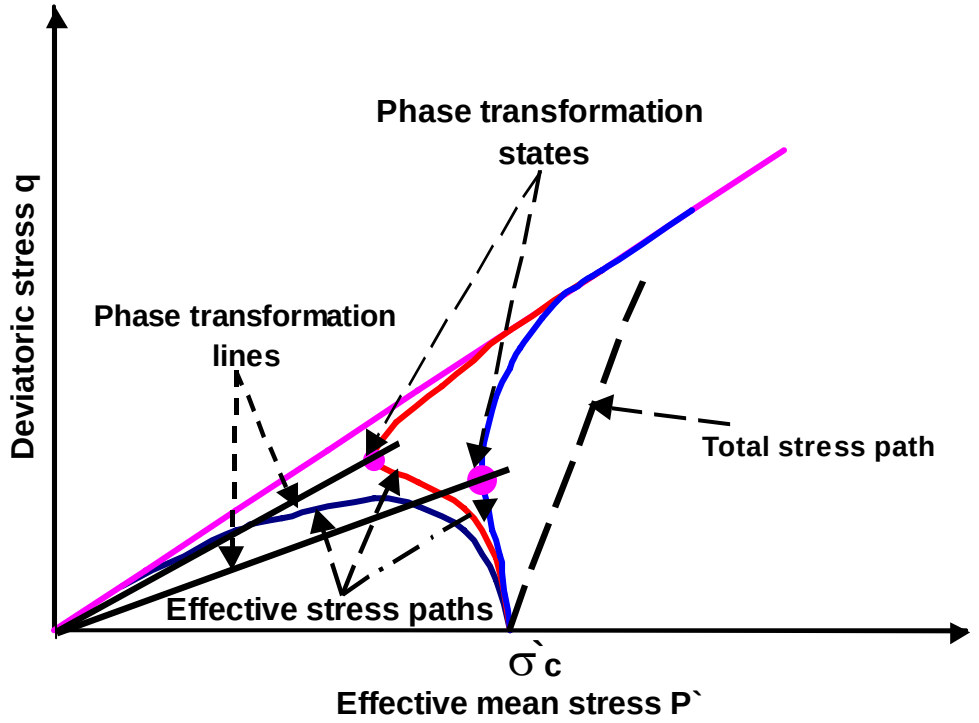

Figure 2.17 Idealized stress paths for undrained monotonic shear tests.

2.10 Flow liquefaction and cyclic mobility.

The term liquefaction has actually been used to describe a number of related phenomena. Because the phenomena can have similar effects, it can be difficult to distinguish between them. These phenomena can be divided into two main categories: flow liquefaction and cyclic mobility.

A simple means for understanding the difference between flow liquefaction and cyclic mobility as observed in the laboratory is through the use of the state diagram, shown in Figure 2.18, as was presented by Castro and Poulos (1977). The axes are void ratio and effective minor principal stress, σ'_3 **,.**The steady state line shown represents the locus of states in which a soil can flow at constant void ratio, constant effective minor principal stress and constant shear stress. The void ratio at the steady state is the same as defined by Casagrande.

Flow liquefaction is the result of undrained failure of a fully saturated highly contractive (loose) sand, starting at C and ending with steady-state flow at constant volume and constant σ'_3 as shown in Fig. 2.18. During undrained flow, the soil remains at point A in the state diagram. Saturated sand whose initial point is above point Q has zero strength and is also neither dilative nor contractive. The strength of this soil after liquefaction will be zero.

Flow liquefaction failures are characterized by the sudden nature of their origin, the speed with which they develop, and the large distance over which the liquefied material often move.

When a fully saturated dilative sand starting at point D is loaded monotonically (statically) under undrained condition it moves slightly to the left of point D but then it will move horizontally toward the steady-state line as load is increased. If a new test is started at point D by applying cyclic loading and following the behaviour by plotting the average void ratio and effective stress each time the applied cyclic load passes through zero. In this case, according to Castro and Poulos, the state point moves horizontally to the left, because the average void ratio is held constant and the pore water pressure rises due to cyclic loading. The magnitude of pore water pressure buildup in the cyclic test will depend on the magnitude of the cyclic load, the number of cycles, the type of test, and the soil type, to name a few variables. In particular, it has been observed in the laboratory that in triaxial tests for which the hydrostatic stress condition is passed during cycling, and if a large enough number of cycles of sufficient size are applied, the state point for the average conditions in the specimen eventually reaches zero effective stress at point B each time the hydrostatic stress state is reached. During this time, strains develop and the specimen softens. If these strains are large enough, one can say that the specimen has developed cyclic mobility. Subsequent application of undrained monotonic loading, after the specimen has developed cyclic mobility, moves the state point to the right toward the steady-state line, and the resistance of the specimen increases.

Deformations due to cyclic mobility develop incrementally and are much smaller than those developed by flow liquefaction. They can only take place during the application of cyclic loading, whereas flow liquefaction can be triggered by a load which is either static or dynamic.

The summary of the differences between flow liquefaction and cyclic mobility are indicated in table 2.2

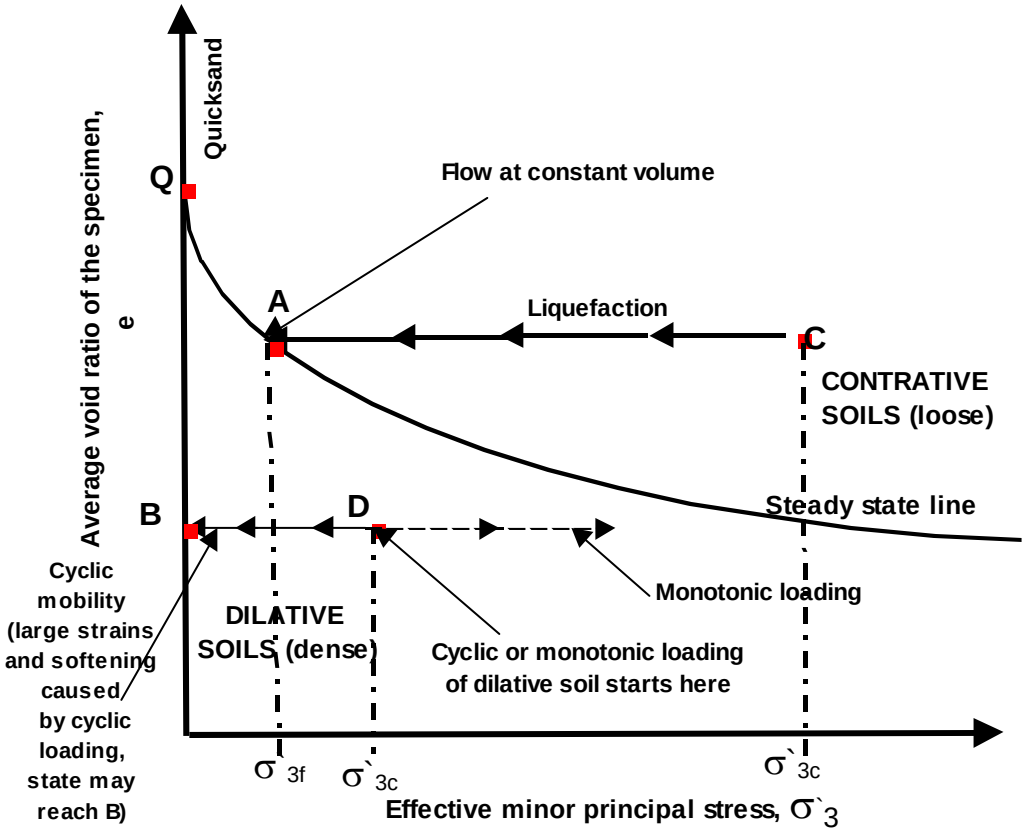

Figure 2.18 Undrained tests on fully saturated sands depicted on state diagram (Castro and Poulos, 1977).

Table 2.2 Differences between flow liquefaction and cyclic mobility (Verdugo 1992).

FLOW LIQUEFACTION	CYCLIC MOBILITY
It involves a loss in shear strength.	It does not entail any loss in shear strength.
Only such states above a particular boundary in the e-p'plane are susceptible to undergo flow liquefaction.	Loose as well as dense cohesionless soils under low or high overburden pressure can develop cyclic mobility.
It may be triggered only when driving forces are greater than the undrained steady state strength.	If there is no chance for a flow liquefaction, the bigger the driving forces, the bigger the cyclic strength.
It can be triggered by either cyclic or static loading, as long as the load is fast enough to put the soil under undrained condition.	It can be developed only during the application of undrained cyclic loading.
During flow liquefaction, the effective stresses drop to constant values which are equal to solely in the case of extremely loose sandy soil.	For reversed amplitude of cyclic stress, cyclic mobility is associated with momentarily zero effective stresses.

FLOW LIQUEFACTION	CYCLIC MOBILITY
During flow liquefaction, the soil mass deforms continuously under its residual shear strength.	During cyclic mobility, the soil mass undergoes cyclic deformation without mobilize necessarily its ultimate shear resistance.
Flow liquefaction involve remarkably large deformation of several kilo meters, mainly depending on the difference (shear stress-steady state strength) and the geometry of the problem itself.	Cyclic mobility usually compromise a moderate level of deformation, but sufficiently large to cause damage.
The higher the effective overburden pressure, the higher the possibility of the soil mass to be in such that induce flow failure.	The higher the effective overburden pressure, the more difficult it is to build up pore pressure, and therefore to develop cyclic mobility.
The residual strength is known if the void ratio is known.	Only the deformation that takes place in a sample are known.

2.11 Factors affecting liquefaction potential.

Factors which have some effect on the liquefaction potential of sands were studied by different investigators, among them Lee and Fitton (1969) Castro and Poulos (1977) Seed and Idriss (1971) and Hird and Hassona (1990) were the few. The main findings include 1, soil type; 2, relative density or void ratio; 3, initial confining pressure; 4, intensity of ground shaking; and 5, duration of ground shaking.

Soil type:- Uniformly graded soils are more susceptible to liquefaction than well graded soils because the reduced tendency for volumetric strains of well graded soils decreases the amount of excess pore water pressures that can develop during undrained conditions. Fine sands are more prone to liquefaction than coarse grained ones, this is because of that a more permeable soils will allow the build up in pore water pressures to dissipate and so liquefaction will not occur as easily.

Relative density:- Since the classical work of Casagrande (1936), it has been generally recognized that the susceptibility of a given soil to liquefaction is greatly dependent on its void ratio or relative density. It is the one which greatly affects the densification and hence the development of pore water pressure during vibration. The results of a series cyclic triaxial tests performed on samples of saturated sand at different void ratios and a confining pressure of 1 Kg per sq. cm is shown in Fig. 2.19. From this result it is apparent that the cyclic stress required to cause initial liquefaction in a given number of cycles increases with the initial density.

Initial confining pressure:- When a large initial confining pressure is applied to a soil, the intensity of vibration or the number of particular stress cycles must be large for the stress to be transferred to the pore water pressure. Therefore, high initial confining pressure reduces the possibility of liquefaction. The effect of confining pressure on the liquefaction potential is clearly shown in Fig. 2.20. The curves shown in this figure were obtained from cyclic triaxial tests conducted at the same initial void ratio and three different confining pressures. While the curves are similar in shape, their position is governed by the initial effective confining pressure. As the confining pressure increases, the curves shift upward on the diagram.

The intensity of ground shaking:- For a soil in a given condition and under a given confining pressure, the possibility of liquefaction to take place depends on the magnitude of the stresses or strains induced in it by the earthquake. These in turn are related to the intensity of ground shaking.

Duration of ground shaking:- The duration of ground shaking is a significant factor in determining liquefaction because it determines in a general way the number of significant stress or strain cycles to which a soil is subjected. All laboratory studies of soil liquefaction under cyclic loading conditions show that for any given stress or strain level, the onset of liquefaction depends on the application of a requisite number of stress or strain cycles.

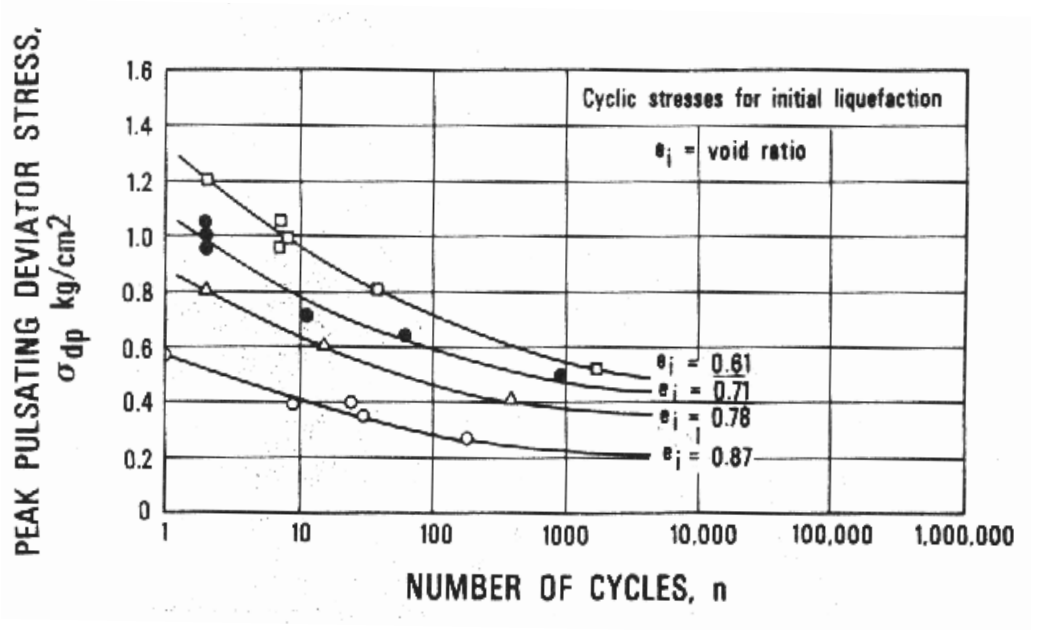

Figure 2.19 Effect of density on the cyclic stress causing initial liquefaction, σ'_3 = 1 kg per sq. cm (Seed and Lee,1965).

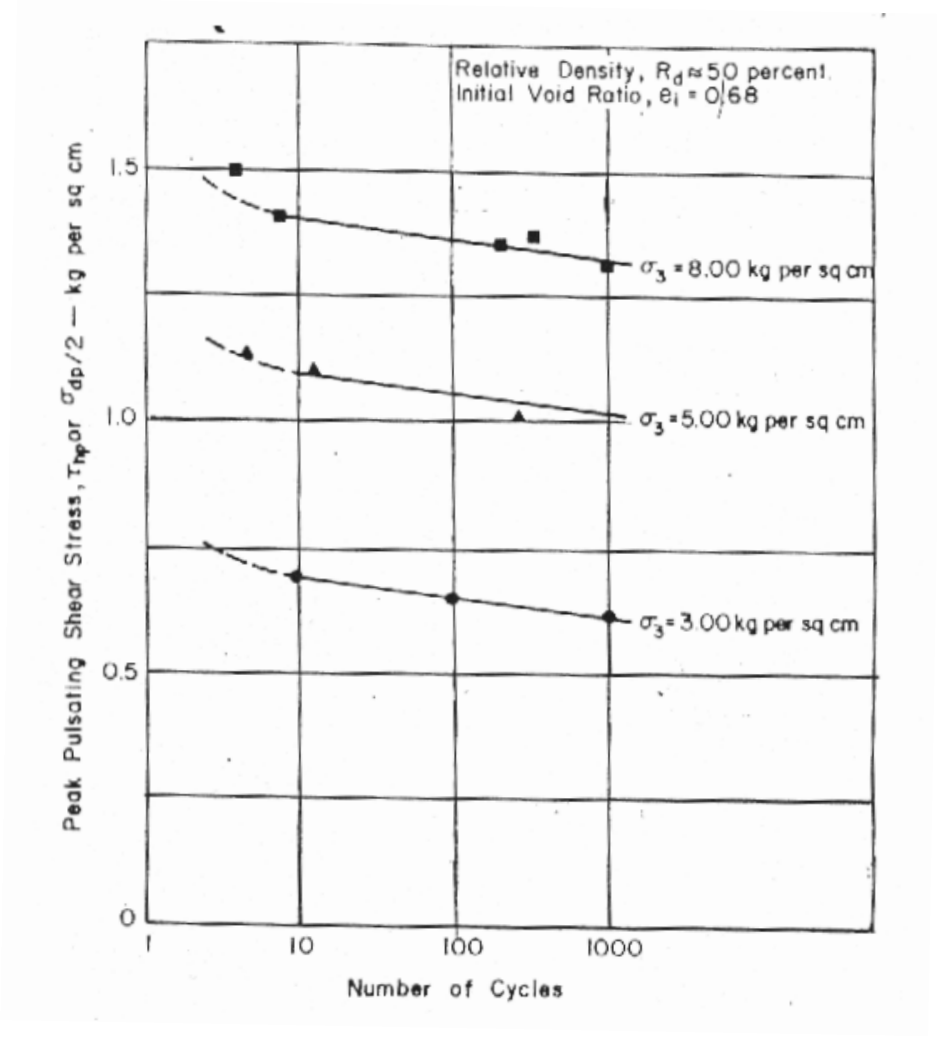

Figure 2.20 Effect of confining pressure on the cyclic stress causing initial liquefaction (Peacock and Seed 1968).

Chapter 3
Laboratory testing equipment, material and procedure

3.1 Introduction.

The experimental work of this investigation has been done using the conventional triaxial test. This test is the most widely used procedure for investigating several important properties of soil behaviour such as: stiffness, strength, dilatancy, stress-strain relationships and anisotropy among others. The triaxial test has been used for research as well as for determination of parameters for the design of real projects.

In this type of test, a cylindrical sample is sealed in a water-tight rubber

membrane and enclosed in a cell in which it can be subjected to fluid (usually water) pressure. The sample sits in the cell between a rigid base and a rigid cap. This configuration immediately creates specific boundary conditions. In the field the boundary conditions can not be exactly known nor can they be completely simulated by any laboratory test. In this sense, laboratory measurements have always to be seen as an approximation of what may actually occur in the field. According to Baldi et al (1986), the world-wide use of the triaxial test in geotechnical engineering is because of the following advantages:

- Relative simplicity of drainage control and measurement of pore pressure.

- Ability to measure axial and volumetric strains.

- Use of solid cylindrical specimens, which can be conveniently obtained from a tube sampler or easily trimmed from block samples.

- Versatility of the equipment, which may be used for a variety of determinations besides triaxial strength and stiffness such as for instance, consolidation and permeability parameters, wave velocity, dynamic parameters and so forth.

On the other hand, the conventional triaxial test has some limitations, perhaps the most important are being the influence of end restraint and sample height.

For the conventional triaxial test to be useful in obtaining the stress-strain behaviour of a soil, it is desirable that a homogenous state of

stress and strain should exist in the sample. Only if this state of homogeneity can be assumed can the stresses and the strains in the sample be calculated from the external loads and displacements in a simple manner. With regard to the state of strain in triaxial samples, experimental work by Kirkpatrick and Belshaw (1968) and Kirkpatrick and Younger (1970,1971) showed that for sands, several nonuniform conditions existed in samples tested with rough (non lubricated) platens. In addition to the above, Ibsen (1994) has also found that samples with a height to diameter ratio of 2 developed nonuniformities in strain resulting in measurements of incorrect stress-strain relations of the material. During undrained conditions the nonuniform development in volumetric strain results in inner draining and internal variation in porosity. A high degree of homogeneity of strain may be found in tests performed on samples tested with the sample height equal to the diameter and with smooth end platens. The technique used in the present research to avoid the significant non homogeneity, is explained in the next section.

3.2 Test equipment.

A static/dynamic load triaxial cell unit was used in the current study. The equipment was built at the Department of Geotechnical Engineering NTNU (Fig. 3.1). The equipment‘s measuring systems consisted of:

- Axial load:- The axial load applied to the samples was measured by a load transducer installed in the top frame and connected directly to the axial piston. The transducer has a maximum capacity of 25KN.

- Pore water pressure:- In the case of an undrained test, pore water pressure was measured by a pressure transducer connected to the top and bottom of the sample. The maximum capacity of the pore water transducer was 700KPa.

- Axial deformation:- The axial deformation of the sample was measured by a linear variable differential variable transducer (LVDT), which was connected directly to the axial piston. The gauge has an accuracy of 0.01mm and a maximum elongation of 30mm.

- Volume change:- The volume change of the samples, during consolidation and drained tests was measured by a calibrated electronic burette connected to the top and to the bottom of the samples. A burette graduated to 0.1cm^3 was used for all tests.

To ensure homogeneous stress and strain conditions, all the tests were performed on cylindrical samples with a height and diameter equal to 54mm, and bounded by lubricated as well as enlarged end plates (Fig.

3.2). Both end plates (enlarged diameter of 62.9mm) were made from polished glass with a center hole for drainage. A 7mm diameter and 3mm-thick porous stones were placed in the hole during the test. A silicon grease-rubber interface was placed between the plates and the samples.

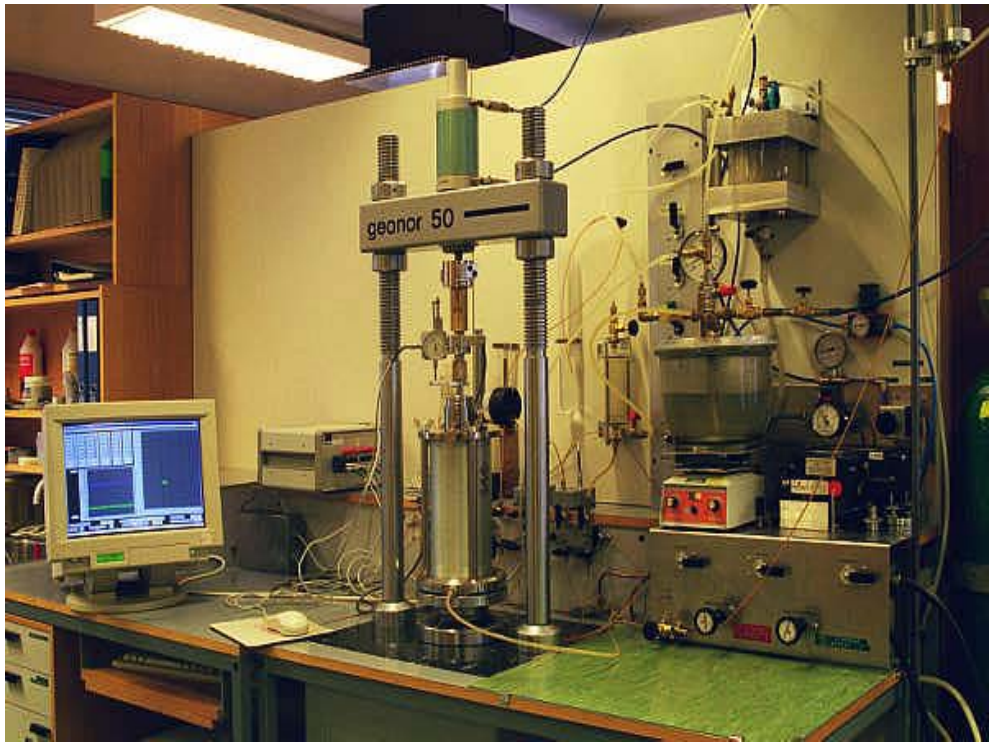

Figure 3.1 Triaxial test equipment.

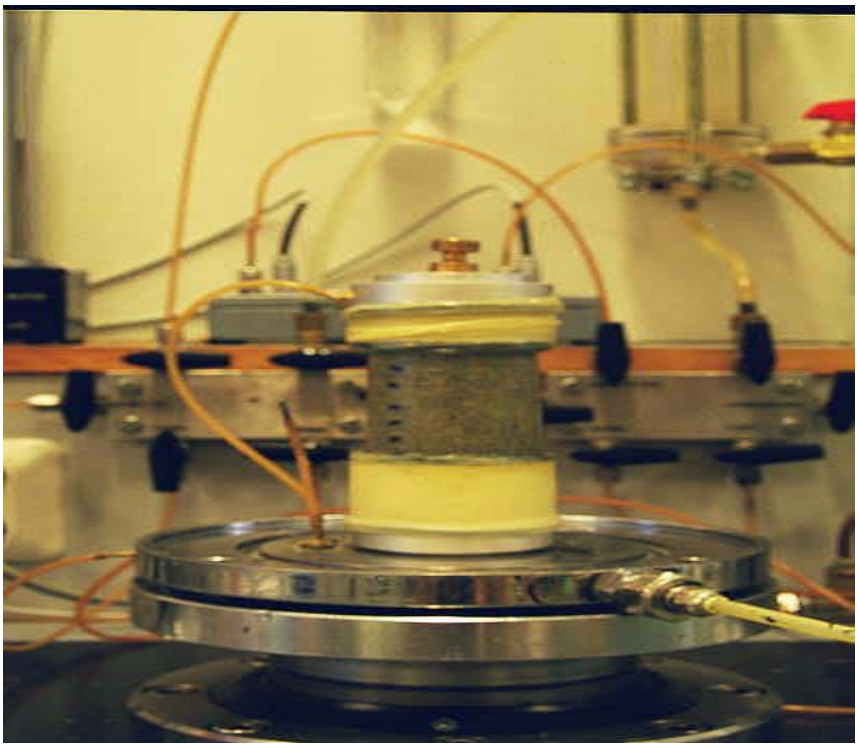

Figure 3.2 Typical sample with height equal to the diameter and smooth heads before testing

3.3 Membrane penetration.

Experimental investigations on the stress-strain behaviour of sand are normally conducted with a shearing apparatus where the lateral surface of the sand specimen is covered by a rubber membrane, which transmits the cell fluid stresses to the specimen. When a sand specimen surrounded by a rubber membrane undergoes a change in the confining pressure under a drained condition, a part of the volumetric strain that occurs is caused by the sand itself as a response to the new stress state. However, another part is caused by the deflection of the membrane between the points of contact of the membrane and the grains. This phenomenon is illustrated in Fig.3.4 and is usually called membrane penetration. When a positive increment of effective confining pressure takes place, the membrane is pushed into peripheral voids and a positive volume change occurs due to the membrane effect. Conversely, when a negative increment of effective confining pressure takes place, the membrane is pushed out from the peripheral voids and a negative volume change takes place due to the membrane deflection.

Moreover, the effect of membrane penetration in an undrained test is to induce a partially drained state as a result of the membrane penetrating into (or withdrawing out of) the peripheral voids of the sand specimen. An increase in pore pressure would cause the membrane to move outwards from the interstices, and as a consequence the excess pore pressure generated will be smaller than that in a truly undrained test. Unlike in a drained test, where membrane penetration affects only volumetric strain and not the effective stress state in the sand, in an undrained test the effective stress state is directly influenced by the membrane penetra-

tion. This may have a profound influence on the measured steady state or phase transformation undrained strength of the sand, depending on the magnitude of the membrane penetration (Sivathayalan and Vaid 1998). The effective stress-path of undrained triaxial tests from Lade and Hernandez (1977) on Antelope Valley sand are shown in Fig.3.5 demonstrating the effect of membrane penetration. In this diagram the developed pore pressure, Δu , is measured by the horizontal distance from a line at 45^0 to the stress point as indicated on the figure. As can be seen, the pore pressures developed at stress obliquities below failure in the tests with reduced membrane flexibility are approximately double those developed in the tests with full effects of membrane penetration. Even higher pore pressure would be expected in tests with complete elimination of the membrane flexibility (Lade and Harnandez 1977).

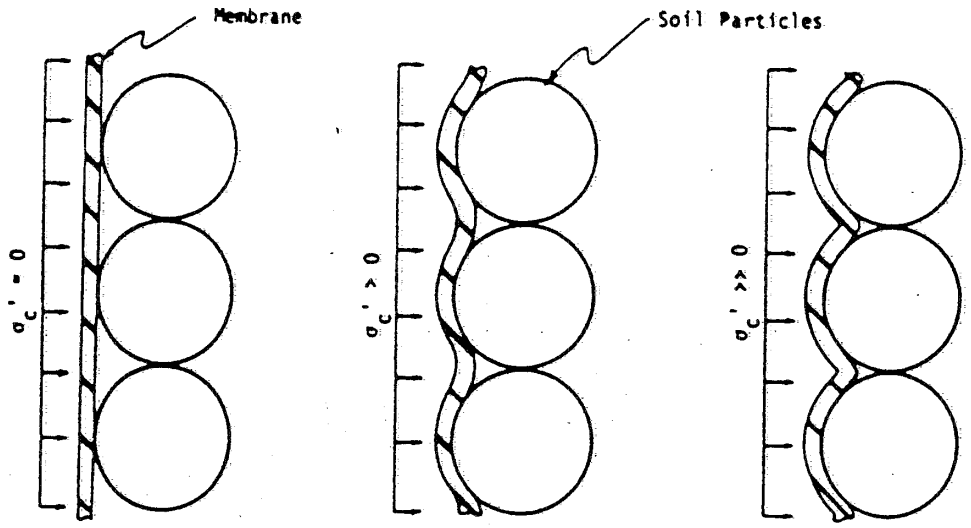

Figure 3.3 Illustration of membrane penetration (Evans and Seed 1987).

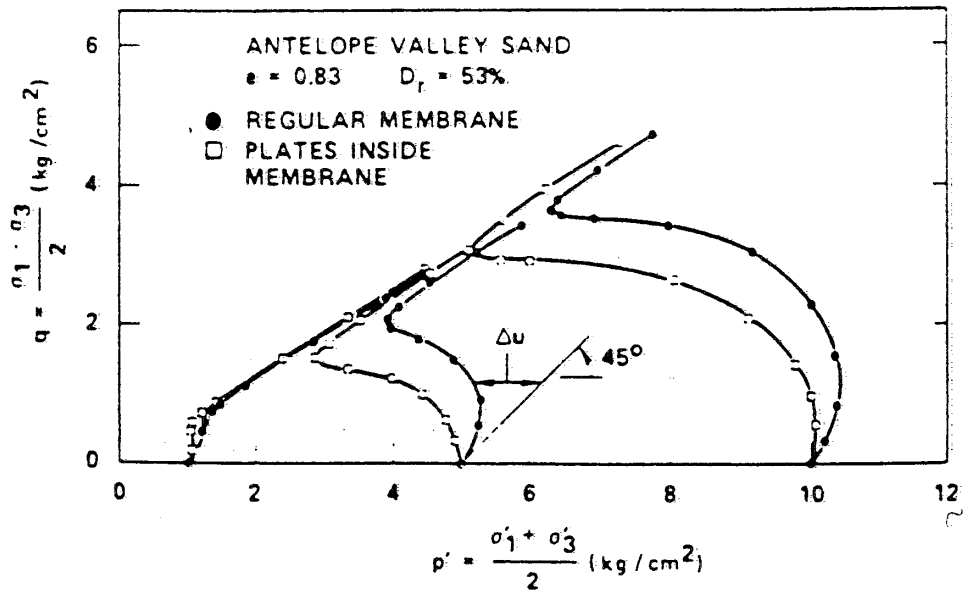

Figure 3.4 Effect of membrane penetration on undrained tests (Lade and Hernandez 1977).

Over the past 40 years there has been considerable progress made in developing methods to accurately evaluate the magnitude of membrane penetration effects. Newland and Alley (1957,1959) were the first investigators to propose a method for evaluating volumetric membrane penetration due to changes in applied effective confining pressures in triaxial testing. Assuming isotropic compression and rebound of triaxial specimens under varying hydrostatic loadings, they calculated volumetric membrane penetration as the difference between total volumetric strain and three times the measured axial strain induced by application of an isotropic stress increase in drained tests on saturated specimens. However, there is strong evidence reported by El Shohby (1964) and others

indicating that the soil behaves anisotropically even under hydrostatic loading, which makes this procedure unreliable.

Another procedure was proposed by Roscoe et al. (1963) and modified later by Raju and Sadasivan (1974). In this method, hydrostatic loading tests are conducted in several soil specimens where different size dummy brass rods of the same height as the specimen have been placed coaxially inside each specimen as illustrated schematically in Fig.3.6. As the diameter of the rods increases, the actual volume of soil volume decreases while membrane penetration is kept constant, because the surface area of the membrane remains the same. For different values of cell pressure, the total volume change versus the volume of the sand sample are plotted as shown in Fig.3.7 from Raju and Sadasivan (1974). Assuming a straight line between these two variables, the membrane penetration can be estimated by extrapolation of this curve for a diameter of the rod equal to the specimen diameter which means zero soil sample volume and, therefore, occurrence of volume change due only to membrane penetration. The linear extrapolation for a rod diameter equal to the specimen diameter can be questioned and also the inclusion of a metal rod within the specimen may cause different soil responses than a soil specimen with out a rod (Vaid et al.1984), hence this method does not provide clear reliability.

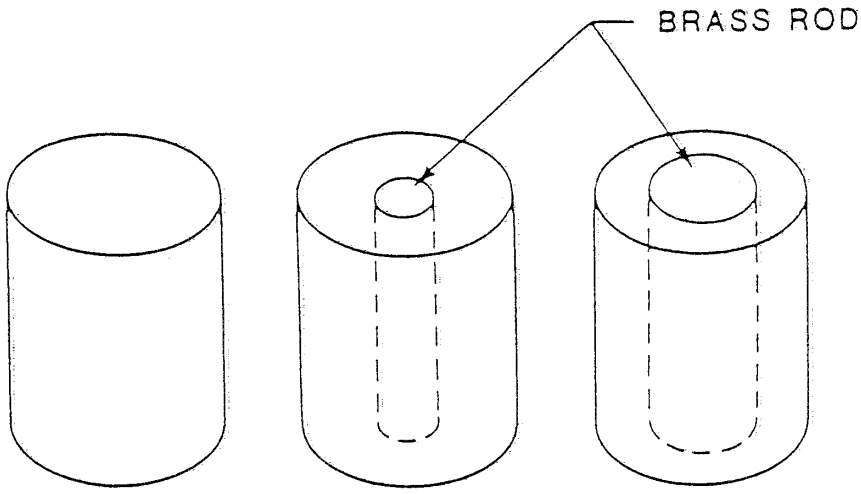

Figure 3.5 Schematic illustration of samples with central rods of various diameter (Nicholson, Seed and Anwar 1993a).

An alternative procedure to evaluate the membrane penetration has been proposed by Vaid and Negussey (1984), mainly based on the assumption that the behaviour of the soil is isotropic during the unloading steps of an isotropic consolidation test. Consequently, the membrane penetration can be assessed as the difference between the measured volumetric strain and three times the axial strain. Moreover, a second consideration that the membrane penetration is the same under loading and unloading is required and it has been proved experimentally by Vaid and Negussey (1984). This procedure to evaluate the membrane penetration seems to be the most popular in these days, mainly because of its simplicity (Verdugo 1992).

On the other hand, Baldi and Nova (1984) have developed a simplified analysis of membrane penetration that has been validated using experimental data reported with different experimental devices and with various types of membranes. Baldi and Nova proposed the following semi empirical expression to account for the volume change due to the membrane penetration phenomenon,

$$V_m = \frac{1}{2}\frac{d_g}{D} V_o \left(\frac{\sigma'_3 d_g}{E_m t_m} \right)^{1/3} \tag{3.1}$$

Where,

V_m = Volume change caused by membrane penetration

D = Diameter of the sample

V_o = Initial volume of the sample

d_g = Grain size

σ'_3 = Effective confining pressure

E_m = Young modulus of membrane

t_m = Thickness of the membrane

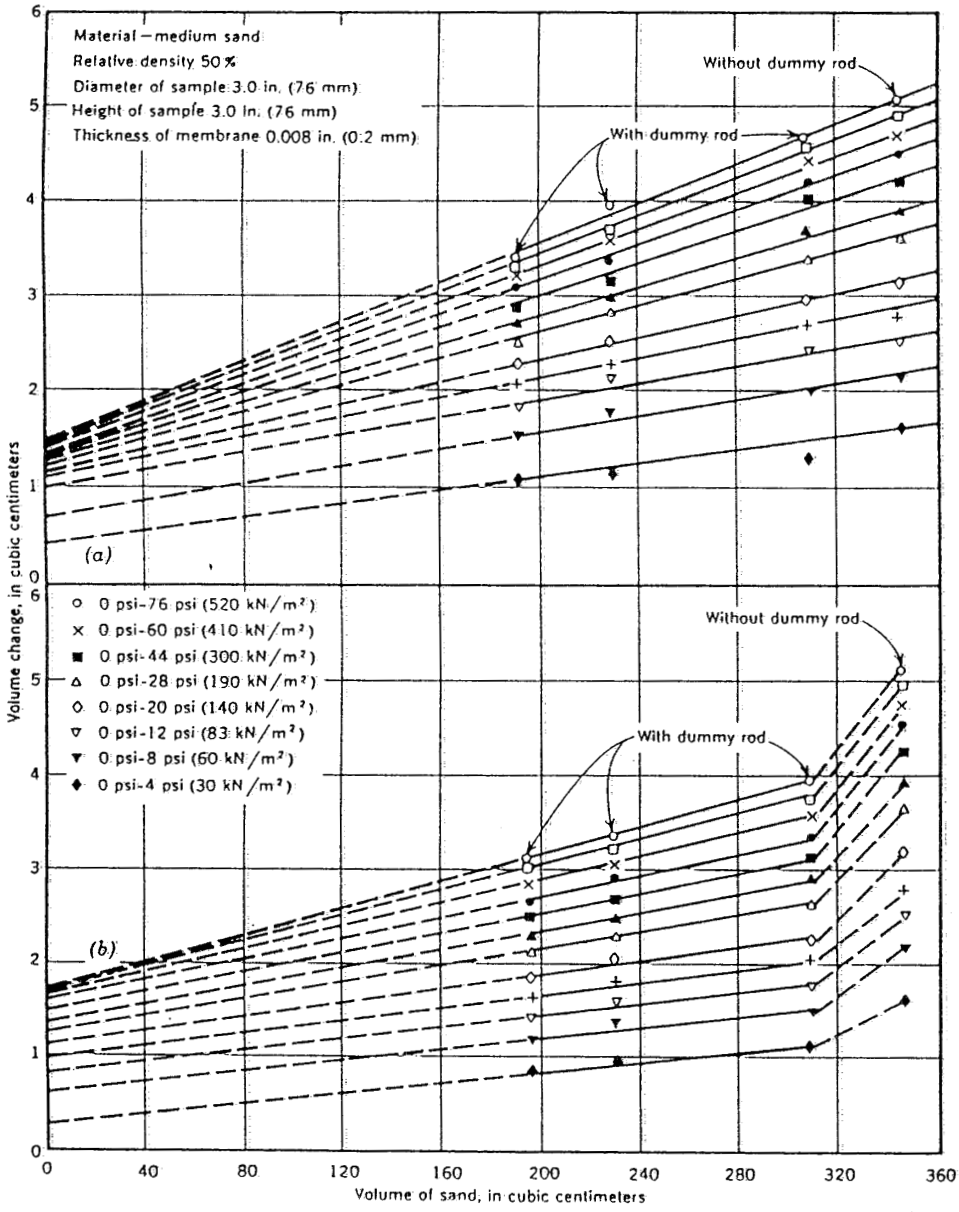

Figure 3.6 Evaluation of membrane penetration: a) annular flexible top platen, b) rigid top platen (Raju and Sadasivan 1974).

In order to compare the above equation with experimental data, Baldi and Nova used a kind of normalization and defined the unit membrane penetration, ν_m , as the ratio between V_m and the circumferential area of the specimen (the area covered by the membrane). Thus

$$\nu_m = \frac{1}{8} d_g \left(\frac{\sigma'_3 d_g}{E_m t_m} \right)^{1/3} \tag{3.2}$$

Given that different researchers have shown that membrane penetration is approximately directly proportional to the logarithmic change in the effective confining pressure, Baldi and Nova defined the normalized membrane penetration, S, as follows,

$$S = \frac{\Delta \nu_m}{\Delta \log \sigma'_3} \tag{3.3}$$

Taking the value of d_g as the mean grain size, D_{50}, the normalized membrane penetration can be easily evaluated. Sladen et al. (1985a) replotted the data presented by Baldi and Nova (1984) with additions. Fig. 3.8 shows the plot reported by Sladen et al. (1985a) indicating the normalized membrane penetration versus the mean grain size, D_{50}. In this figure the above equation proposed by Baldi and Nova for the normalized membrane penetration, S, has been plotted (see Baldi and Nova 1984). As can be seen there is a good agreement between the semi empirical expression developed by Baldi and Nova and the published experimental data. Therefore, the volume change caused by membrane penetration can be evaluated using Eq. 3.1.

Since the mathematical expression developed by Baldi and Nova shows a good fitting with the experimental data, its usage to check the membrane penetration for the present research seems reasonable.

According to the above expression, a change in the effective confining pressure of 700 kPa would produce a volume change caused by membrane penetration of 0.410 cm^3. Considering a dry soil weight of 203.37 g, the associated change in void ratio of the sample is $\Delta e = 0.005$. This variation is very small, and therefore, the void ratio of the sample was not corrected for membrane penetration effects.

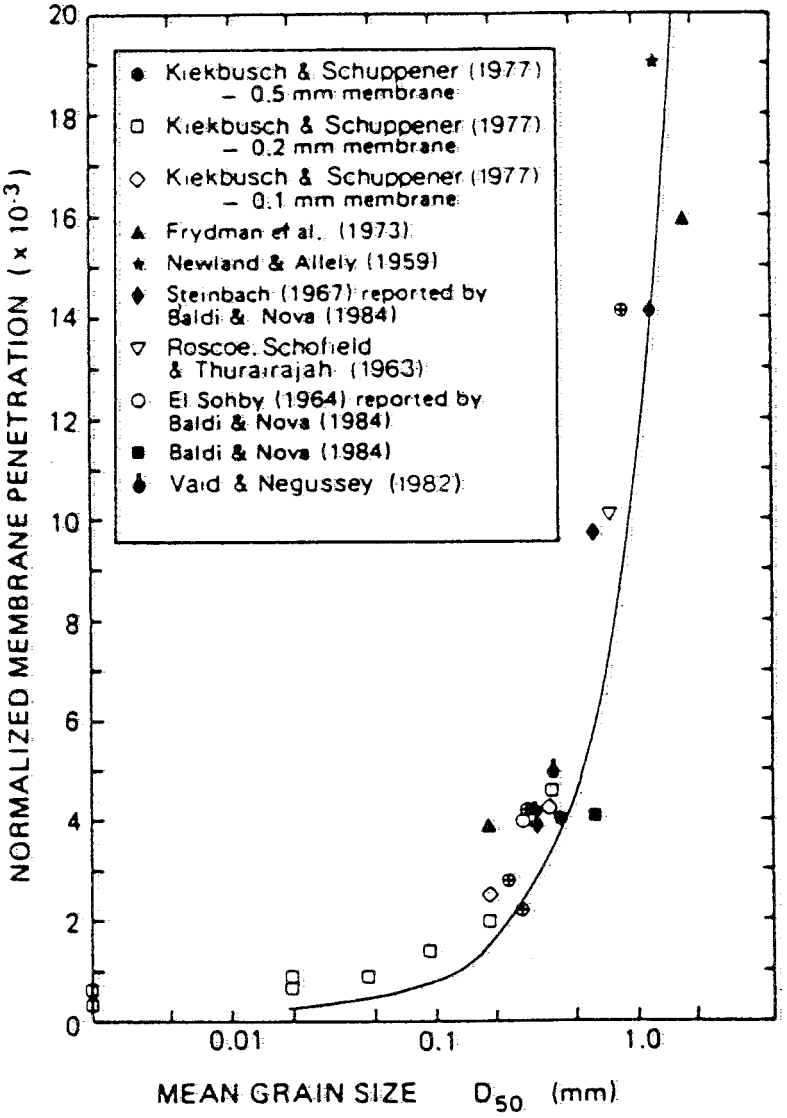

Figure 3.7 Evaluation of membrane penetration (Sladen et al,.1985a).

3.4 Material tested.

The sand used in this investigation was a uniform medium Hokksund sand. This material is commercially available and it is often used in Norway for geotechnical studies. Data presented by the Norwegian Geotechnical Institute indicates that this sand is composed of 35% quartz, 25% Sodium feldspar, 20% Potassium feldspar, 10% Mica, 5% Amphibole and 5% others. The grain size distribution curve of Hokksund sand is shown in Fig. 3.3. The physical properties of this sand are shown in Table 3.1. The maximum porosity, n_{max}, has been found by filling dry sand through a funnel into a cylinder from a negligible height The minimum porosity, n_{min}, has been found by filling moist sand into a steel cylinder in approximately 2 cm thick layers and vibrating each layer for about 30 seconds.

Table 3.1 The physical properties of Hokksund sand (Moen 1978).

Specific gravity, G_s	2.71
Coefficient of uniformity, C_u	2.04
Maximum porosity, n_{max}	48.7%
Minimum porosity, n_{min}	36.4%
d_{60}	0.5
Shape of grains	Sharp edges, cubical

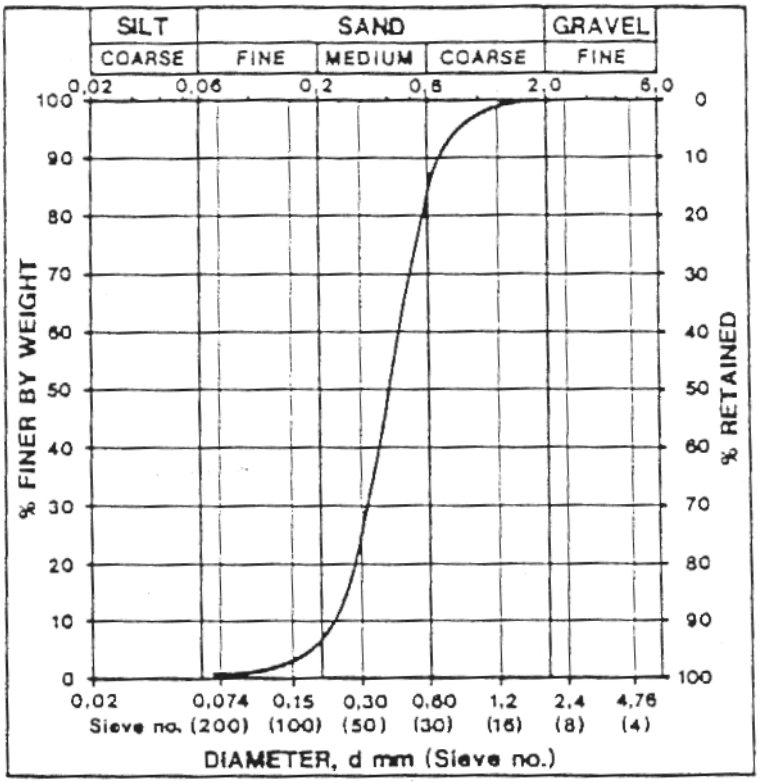

Figure 3.8 Grain size distribution of Hokksund sand.

3.5 Sample preparation.

The method of under compaction by wet tamping was used to prepare the sample. Void ratio was chosen as the control parameter because different samples were prepared with void ratios varying between the maximum and minimum void ratios.

Oven-dried, pre weighed soil was well mixed with distilled water in a proportion of 6% in weight 16 hours before use and sealed. The reason for this waiting period was to allow moisture to be evenly distributed throughout the soil. Each test sample had a 54 mm diameter and height, and was compacted in six layers in a rubber membrane confined by an air- tight split mould attached to the bottom cap of the triaxial cell.

The soil for each layer was weighed, placed in 6 separate containers and kept sealed until they were placed in the mould. Each layer was gently compacted by means of a metal mass held by a rod until the preestablished height was reached. The dimensions of the metal mass were 95 mm in height and 32 mm in diameter with a total mass of 600 g.

After the last layer was compacted, a vacuum of -96 kPa was applied to the top and bottom drainage lines and the membrane was pulled up and down around the top and bottom caps.To tighten both ends of the membrane on the two caps, double o-rings were used around each cap and then the split mold was removed from the sample. The diameter and height of the compacted sample were measured. The sample diameter was measured at three locations (top, bottom, and middle) and the average value was used for density calculation.

3.6 Test procedure.

Prior to being consolidated each sample was saturated by one of the two following procedures:

1. In the first procedure samples were saturated initially by flushing de aired water through the sample under a vacuum of -96kPa (it required to applied full vacuum to all samples in order to remove air trapped), and then applying a back pressure in increments up to a typical value of 300kPa.The value used was determined by increasing the back pressure until the B value (ratio of the change in pore-water pressure Δu to change in cell pressure $\Delta\sigma_3$) became larger than 0.96.

2. In the second procedure full saturation was achieved by first applying on the sample a vacuum of -96kPa for 12 hours. Next, carbon dioxide gas was introduced at a pressure of 30kPa at a cell pressure of 100kPa and then removed by vacuum, the purpose being to flush any remaining air from the sample. Then de-aired water was introduced under vacuum and flushed through the sample. In this technique also, the degree of saturation of the sample was sufficiently high to produce a B value of 0.96 or better.

After the saturation process was completed, the samples were isotropically consolidated by gradually increasing the cell pressure until the desired pressure was achieved with opening the drainage valve. All the samples tested were isotropically consolidated. In addition, a small axial load, sufficient to maintain the samples in an isotropic state of stress, was applied to the piston screwed into the top cap. During this phase of

the test, change in volume was recorded and the result was used to calculate the volume of the samples after consolidation and prior to shearing. The time of consolidation was 30 minutes for all samples. The consolidation was considered to be finished, if when the drainage valve closed, the pore water pressure did not change for 3 minutes.

After consolidation, in all static tests, the samples were axially loaded in the compression or extension mode under constant cell pressure. All static tests were performed under a strain controlled condition. Axial strain rate of about 4% per hour (0.036mm/min.) was used in all tests. Following the completion of the test, the samples were collected to determine their water content as a check for previous density and final void ratio calculations. In all samples, the final water contents confirmed with a good accuracy that the calculated initial densities and final void ratios were correct.

In all cyclic tests, the samples were mounted and consolidated as previously described for the static tests. After consolidation was completed, initial static shear stresses were applied to the desired values in undrained conditions. Then a sinusoidal waves form of cyclic axial loads were applied at a frequency of 0.1Hz under undrained conditions.These tests were performed under stress controlled conditions.

In the current study a cyclic stress ratios $q_{cyc}/(2\sigma'_{3c})$ ranging from 0.2 to 0.6 were used, to develop a pore water pressure equal to the applied confining stress and different shear strain amplitudes.

3.7 Testing program

The tests performed in connection with this research were:-

1. CU:- Isotropically consolidated undrained monotonic loading tests.

2. CD:- Isotropically consolidated drained monotonic loading tests.

3. CUC:- Isotropically consolidated undrained cyclic loading tests.

Most of the monotonic loading tests were performed in the compression mode. However, a limited number of undrained monotonic loading tests were carried out in the extension mode in order to see possible behaviour differences due to the modes of loading and to locate the phase transformation lines in the extension stress path plane. In addition to the conventional undrained tests, some consolidated constant volume (CCV) tests were also performed. These tests were carried out by controlling the cell pressure in such a way that $\Delta\varepsilon_p = 0$ throughout the test. In this way the undrained condition is ensured and the effective stress path is followed throughout the test.

The main purpose of this testing program was to study the behaviour of saturated sands under different loadings and to establish a link between undrained monotonic and undrained cyclic loading conditions.

The monotonic triaxial loadings were performed on isotropically consolidated samples having the following initial relative densities:-

- Relatively loose, relative density of 30%. This corresponds to a

porosity of 45.5%.

- Medium dense, relative density of 57%. This corresponds to a porosity of 42.33%.

- Dense, relative density of 87%. This corresponds to a porosity of 38.3%.

In all monotonic triaxial tests the consolidation pressure were varied from 125kPa to 700kPa.

The cyclic triaxial tests were performed on isotropically consolidated samples with an initial relative density of 30% and an effective confining pressure of 125kPa.

3.8 Test data interpretation.

The parameters, which are used to describe the response of the samples, are calculated from the measurements taken during the tests. These parameters are:-

- Strains.

Axial strain, $\varepsilon_a = \frac{\Delta L}{L_o}$ (3.4)

Volumetric strain, $\varepsilon_p = \frac{\Delta V}{V_o}$ (3.5)

Radial strain, ε_r

For drained tests, $\varepsilon_r = (\varepsilon_p - \varepsilon_a)/2$ (3.6)

For undrained tests, $\varepsilon_r = (-\varepsilon_a)/2$ (3.7)

Shear strain, $\varepsilon_q = \frac{2}{3}(\varepsilon_a - \varepsilon_r)$ (3.8)

Where ΔL = change of length

L_o = initial length

ΔV = change of volume

V_o = initial volume

- Stresses

Axial stress, $\sigma = \frac{N}{A}$ (3.9)

Deviatoric stress, q = $(\sigma_1 - \sigma_3)$ (3.10)

Mean stress, p = $(\sigma_1 + 2\sigma_3)/3$ (3.11)

Where N = normal force

A = the true cross sectional area

In triaxial test the cross sectional area of the sample changes continuously during loading. Therefore one should make area corrections in order to get the correct responses of the sample. In this investigation, it was assumed that the sample deforms as a right cylinder keeping its original shape. The corrected areas for the drained and undrained tests were calculated using the following equations respectively (see appendix A).

A = $A_o\left(1 + \varepsilon_r + \varepsilon_r^2\right)$ (3.12)

A= $A_o\left(1 + \varepsilon_a + \frac{1}{4}\varepsilon_a^2\right)$ (3.13)

- Shear and bulk modulus

$$G = \frac{\Delta q}{3\Delta \varepsilon_q} \tag{3.14}$$

$$K = \frac{\Delta p'}{\Delta \varepsilon_p} \tag{3.15}$$

Chapter 4
Monotonic triaxial test results

4.1 Introduction.

In this chapter, the monotonic triaxial test results are presented and discussed. The tests were conducted on isotropically consolidated samples sheared at a constant rate of axial strain 0.036 mm/min. in triaxial compression and extension. The test series were organized so that the effects of initial relative density and consolidation pressure were examined successively in all types of tests.

Samples were formed at a fixed initial void ratio e_i using the wet tamping method as described in section 3.5 and series of tests performed after consolidated to various levels of initial confining pressures. A similar

series of tests were then repeated on samples formed at another fixed initial void ratio. In this manner, three initial void ratio states were covered. This enable investigation of undrained and drained behaviour that covered a wide range of initial states (e_c and σ'_{3c}) of the sand. In this testing programme a total of 34 samples were tested. All tests were performed with an initial back pressure of 300kPa.

4.2 Drained monotonic compression test results.

A series of conventional triaxial tests with constant confining pressure were carried out under a drained condition of loading. The samples were consolidated at confining pressures of, 125, 225,425, 700kPa. The relative densities of the samples in a set were, 30%, 57% and 87%.

For each relative density, Fig.4.1 to 4.3 shows the stress path, deviatoric stress versus axial strain and volumetric strain versus axial strain. From these figures, one can see clearly the effect of confining pressure and relative density on the behaviour of drained sand.

For all levels of confining pressure, the results on dense specimens (Fig. 4.1) show that the deviatoric stress increases to a peak then drops with increasing the axial strain. The increase in deviatoric stresses are associated with a slight initial volumetric contraction, followed by a gradually increasing rate of volume expansion (dilation). The post-peak reduc-

tion in deviatoric stress is associated with a decreased rate of dilation until shear at a constant volume occurs at a steady state. Dilation is gradually decreased as the confining pressure increases. The value of deviatoric stress increases until a maximum deviatoric stress is reached then the mean and deviatoric stresses decrease until a steady state is observed. Since these tests are drained tests, the stress path (q-p‘) diagram displays a straight line with a slope of 1:3

Fig.4.2 shows the results of tests on samples with an initial relative density of 57%. Although these samples also display a dilative behaviour for the range of the pressure used, the maximum deviatoric stresses are significantly less in comparison to those observed at a relative density of 87%.

As the relative density further decreases to 30%, the maximum deviatoric stresses continue to decrease significantly (Fig.4.3). The volumetric strains become contractive at the two levels of confining pressures (σ'_3 = 425kPa and 700kPa). While for the other two confining pressures (σ'_3 =125kPa and 225kPa), the sand shows dilative behaviour at large axial strain levels. Here also the value of q and p‘ increase gradually to a maximum.

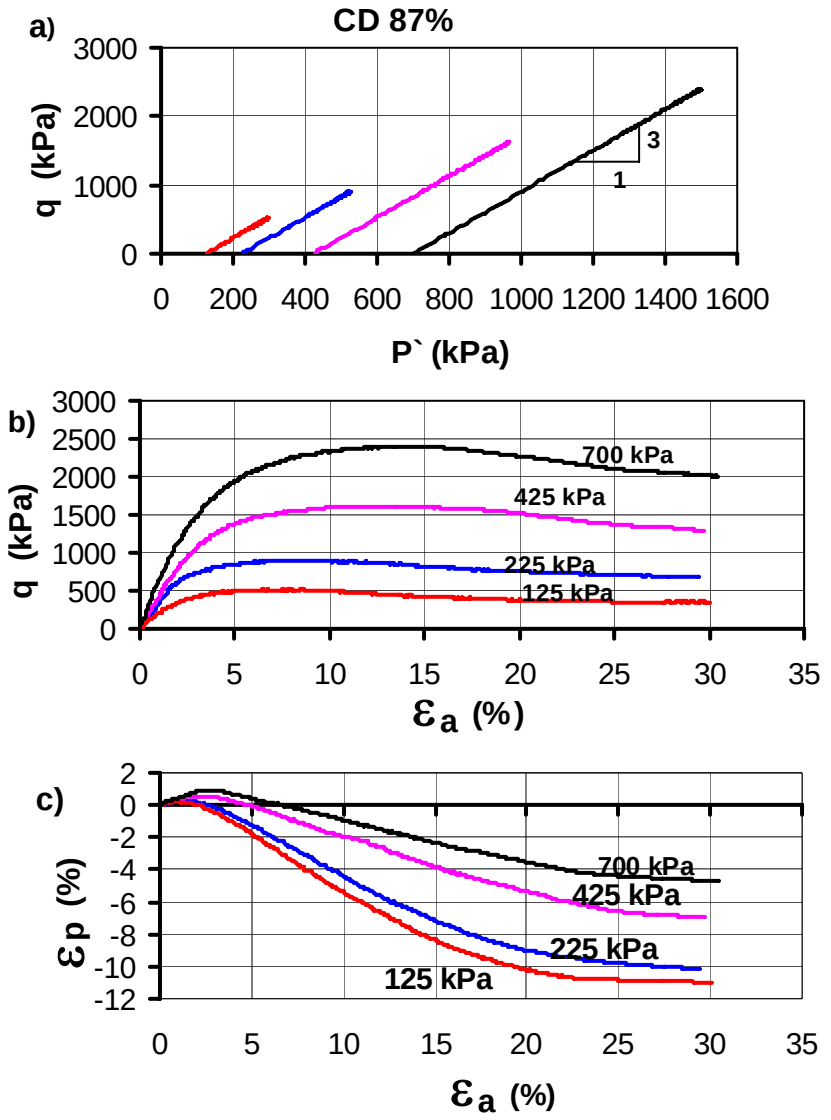

Figure 4.1 Drained monotonic compression loading behaviour of initially dense sand under different confining pressures. a) Effective stress paths, b) stress-strain curves and c) volumetric strain versus axial strain curves.

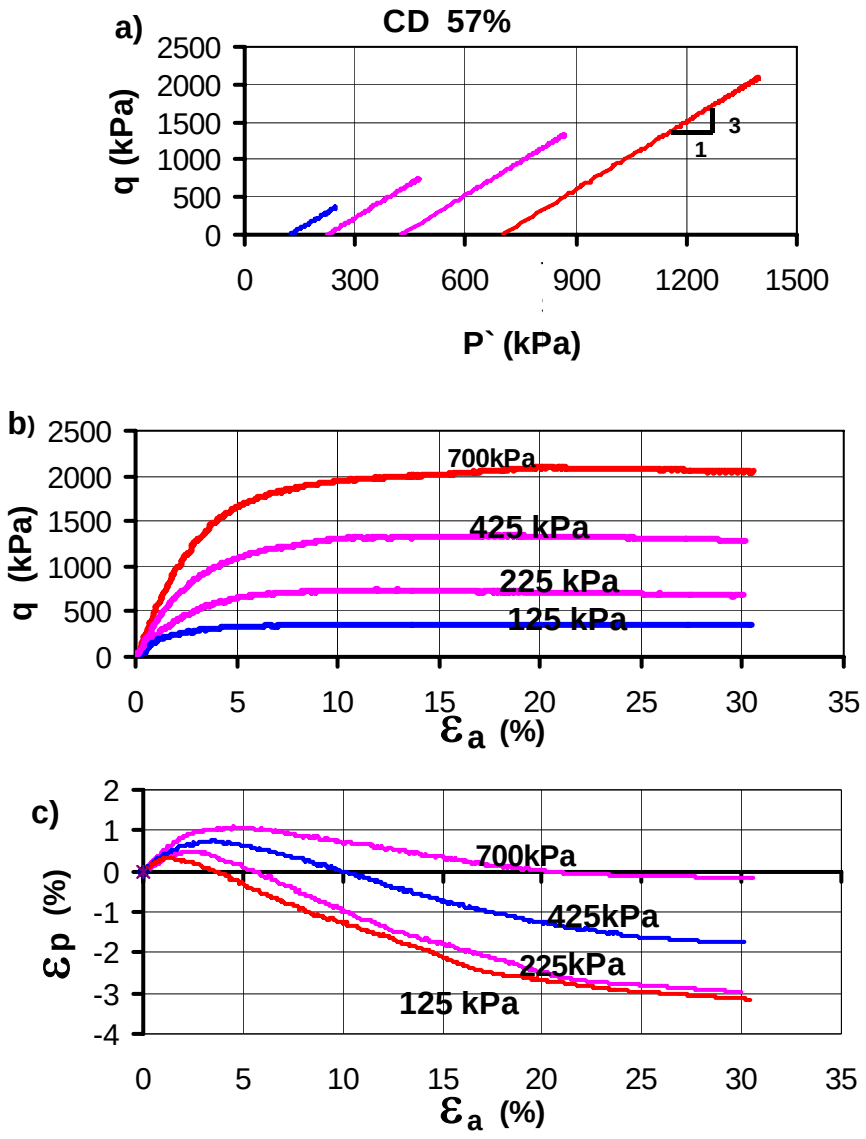

Figure 4.2 Drained monotonic compression loading behaviour of initially medium dense sand under different confining pressures. a) Effective stress paths, b) stress-strain curves and c) volumetric strain versus axial strain curves.

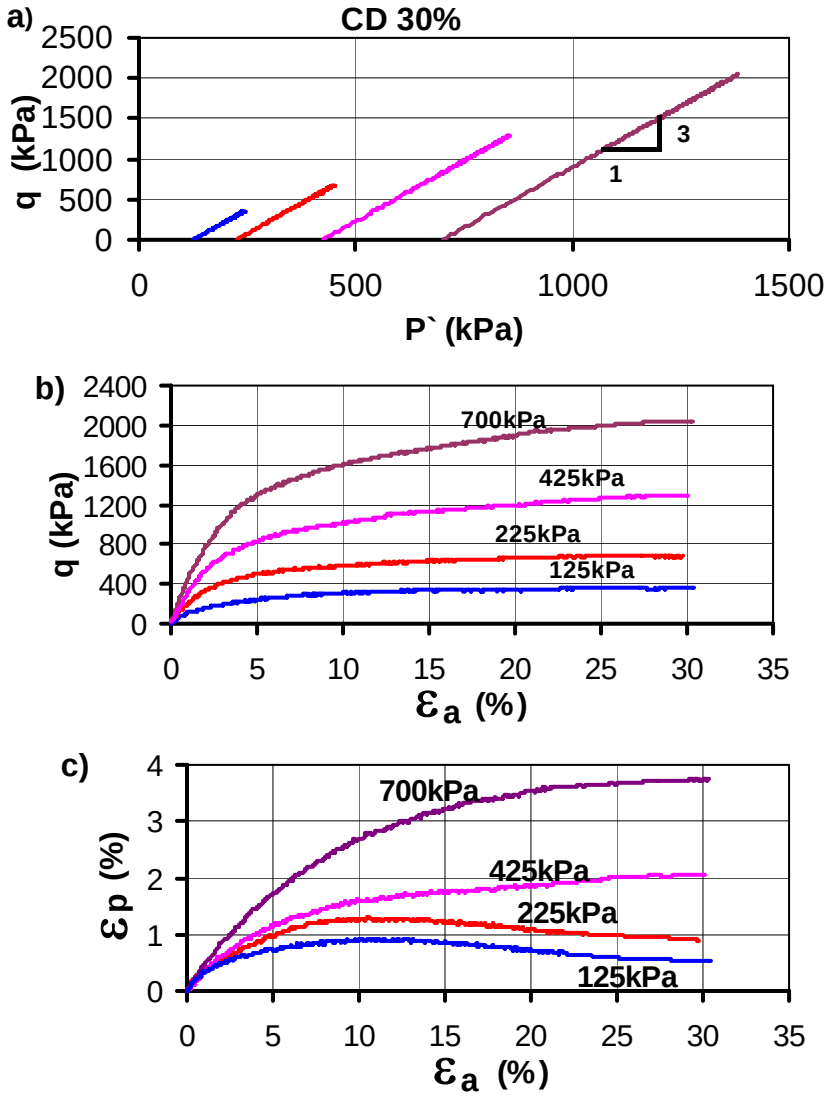

Figure 4.3 Drained monotonic compression loading behaviour of initially loose saturated sand under different confining pressures. a) Effective stress paths, b) stress-strain curves and c) volumetric strain versus axial strain curves.

4.3 Undrained monotonic compression test results.

Undrained monotonic triaxial compression tests were conducted on loose, medium dense and dense sand samples subjected to an initial effective isotropic confining pressures ranging from 125 to 700kPa. Stress paths, stress-strain curves and developed pore water pressures for the three relative densities are shown in Figs. 4.4 to 4.6. It may be noted that the range of observed undrained response covers the range of behaviour from partially liquefied to dilative.

For the effective confining pressures of 225 and 425kPa, the samples having an initial relative density of 30% developed a deviator stresses plateau over a certain range of strain before the shear resistances started to increase once again due to dilation with further straining (Fig. 4.4(b) and (c)). It may also be seen that the stress-strain curves after the plateau were flatter than that in the initial stage of loadings. While for the 125kPa confining pressure, the deviatoric stress was increased very rapidly for the first few strains and then after it was monotonically increased at a decreasing rate. On the other hand, the effective stress paths of these samples move at the beginning to the left and then bend sharply upwards and to the right. It may be observed that for all levels of confining pressures the samples required high strains before phase transformation states occurred. Furthermore, once the samples passed the phase transformation state, their effective stress paths approached the common failure envelope rather quickly with further loading.

The results of tests on samples with an initial relative density of 57% are presented in Fig. 4.5. It can be seen that for the range of pressure used, the response is always with a dilative portion where the pore pressure increments are negative and therefore, the effective stress paths move up to the right after initially moving to the left.

Fig.4.6 shows the results of tests on samples with an initial relative density of 87%. For all levels of confining pressures, the response of the samples is always after initially being contractive, dilative and forming cavitation at the end. As the pore water pressure-strain curves make clear, the pore water pressure in each test begins at the imposed back pressure value, but after a small initial positive pore water pressure it decreases until cavitation occurs at a pore water pressure of roughly -96kPa. From the effective stress paths, it also possible to see the developed cavitation. In each test the initial paths are nearly the same. When cavitation occurs, the slope changes abruptly to become equal to the drained value of 1:3. If one projected the drained stress path back down to the level of zero deviatoric stress, it intersects the mean stress axis at exactly the value of the initial confining stress. The soil starts to develop cavitation when the pore water pressure fails to prevent the interlocking disrupter, i.e. $\Delta\varepsilon_p$ is no longer equal to zero. This means that the failure condition is controlled by the same mechanism as failure under drained condition. In contrast to the loose soil, these samples reached the phase transformation states at a very early stage (Fig. 4.6a) and they required relatively high stress increments to reach the common failure envelope.

4.4 Undrained monotonic extension test results.

An additional series of triaxial tests were performed in undrained extension. In a manner similar to that used in undrained compression, a series of undrained extension samples were prepared and isotropically consolidated to the same stress levels as the compression tests. Undrained shearing was performed by reducing the axial stress by applying tension to the loading rod, which was threaded into the sample top cap. In this method of loading, the axial stress becomes the minor principal stress, while the intermediate and major principal stresses are equal and represented by the lateral stress.

At large strains, specimens tested in extension are prone to nonuniform straining, resulting in formation of a “neck” or portion of the specimen with reduced diameter. In this testing program, the onset of necking was observed to occur at axial strains of approximately 10%. All samples, however, reached the phase transformation states prior to the appearance of such nonuniformities.

The results of the undrained extension tests are plotted in Figs. 4.7 and 4.8, which compare the stresses-strains and the effective stress paths of these tests with those of the compression tests illustrated in Figs. 4.4, 4.5 and 4.6. By comparing pairs of samples in Figs. 4.7 and 4.8 and that have been consolidated to the same stress level and have the

same void ratios but loaded by the two different methods, it consistently appears that the samples tested in extension are considerably weaker and more contractive than those tested in compression. The phase transformation lines in extension appear to have slightly less slope to that in compression.

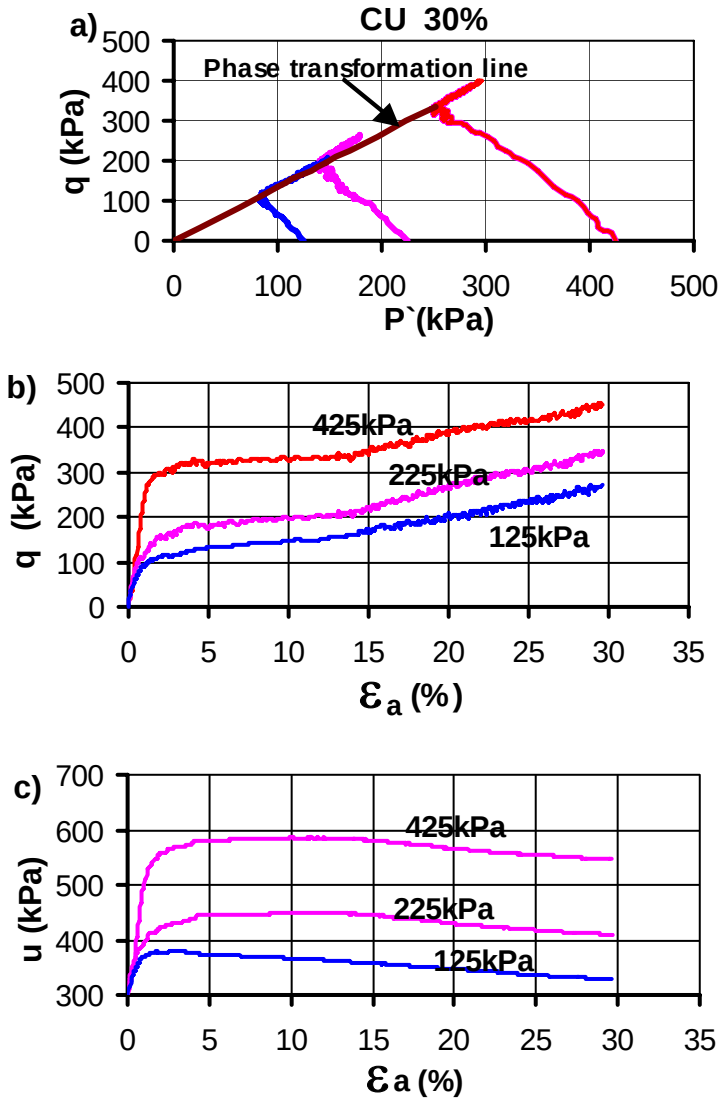

Figure 4.4 Undrained monotonic compression loading behaviour of initially loose sand under different confining pressures. a) Effective stress paths, b) stress-strain curves and c) pore water pressure versus strain curves.

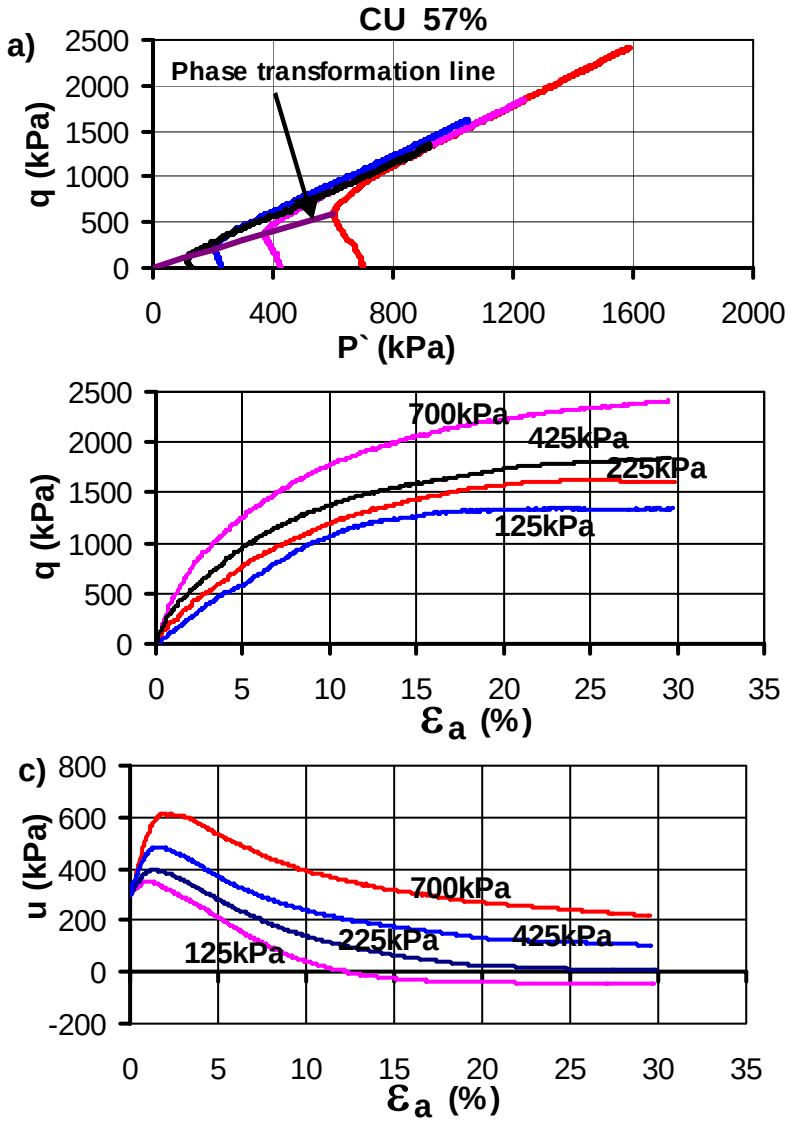

Figure 4.5 Undrained monotonic compression loading behaviour of initially medium dense sand under different confining pressures. a) Effective stress paths, b) stress-strain curves and c) pore water pressure versus strain curves.

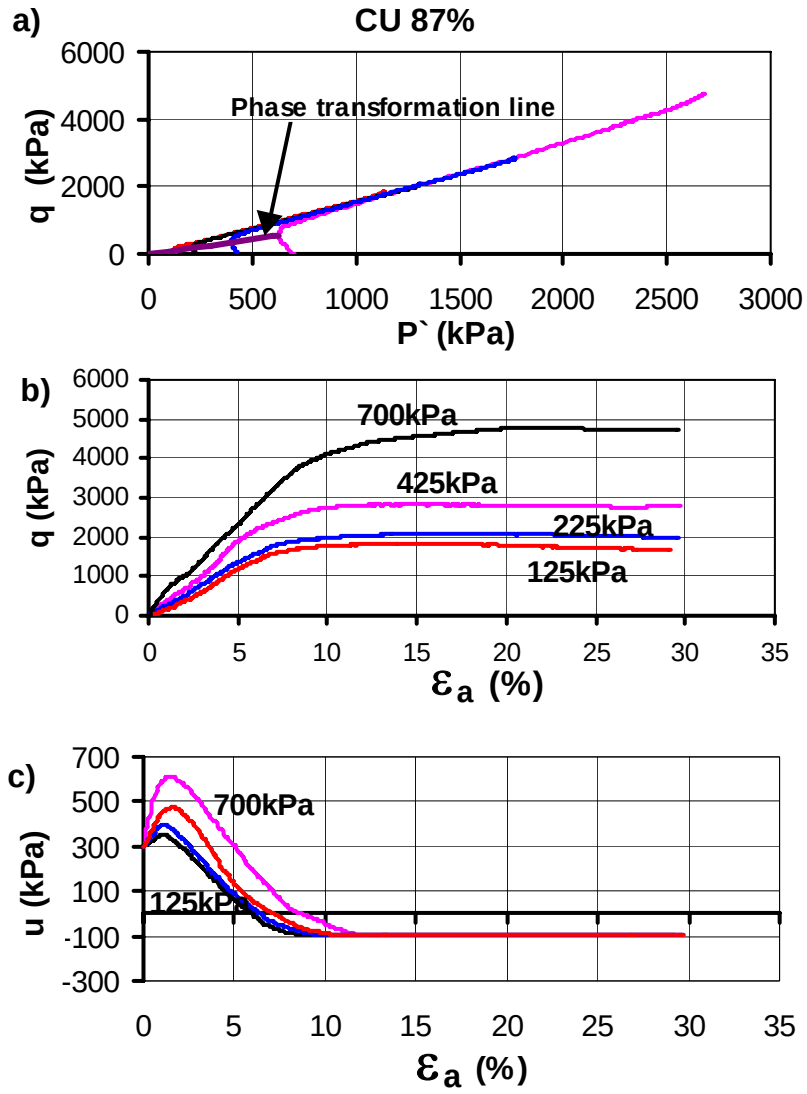

Figure 4.6 Undrained monotonic compression loading behaviour of initially dense sand under different confining pressures. a) Effective stress paths, b) stress-strain curves and c) pore water pressure versus strain curves.

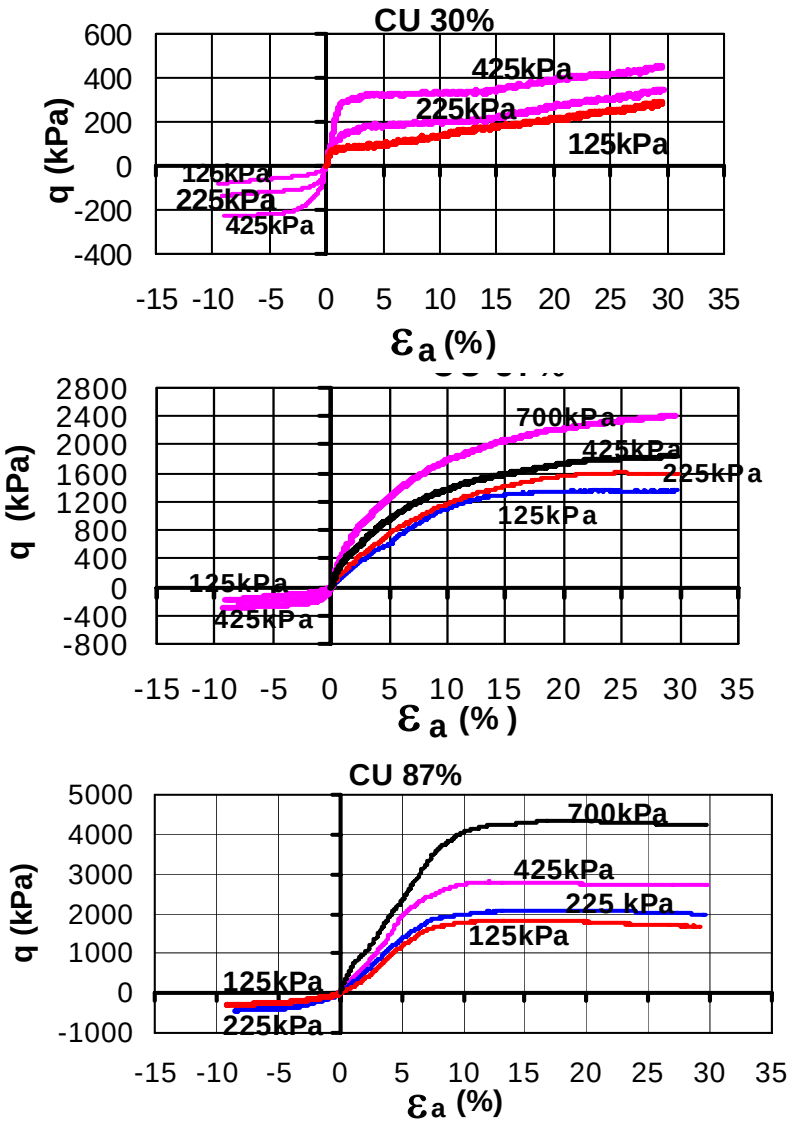

Figure 4.7 Stress-strain plots of both triaxial compression and extension tests performed on loose, medium dense and dense samples.

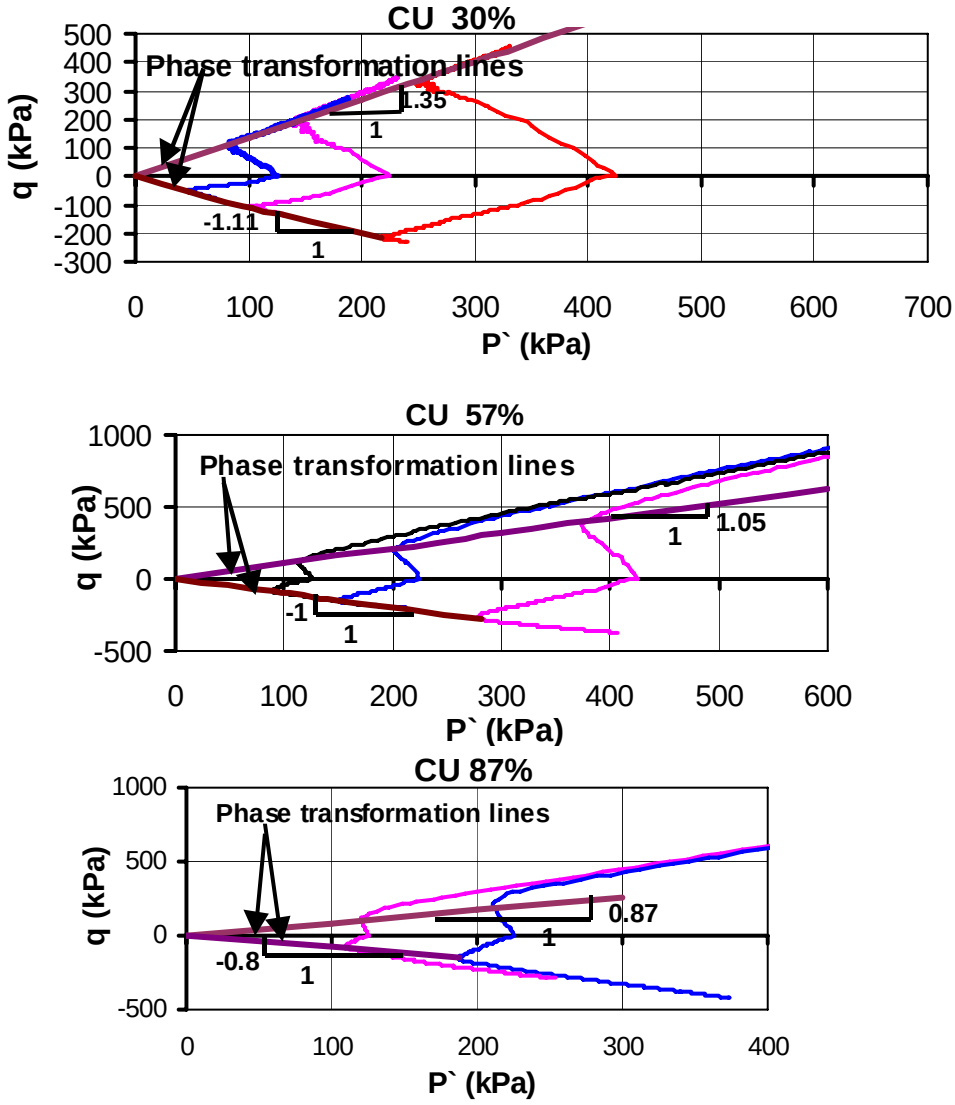

Figure 4.8 Effective stress path plots of both triaxial compression and extension tests performed on loose, medium dense and dense samples.

4.5 Steady state from drained and undrained compression tests.

Irrespective of the initial state of the samples, when the strain level is large enough, the soil mass tends to approach a condition of continuous deformation under constant shear stress and volume. This stage of the soil response is certainly apparent in most of the drained and undrained test results shown in Figs. 4.1 to 4.6 when the axial strains are larger than 20-25%. However, as can be observed from the same figures, there are also some test results where the deviatoric stress and the mean stress are still increasing after an axial strain of 27%. Nevertheless, the increments are small, hence in these cases, the stresses at an axial strain around 27% have been taken as ultimate or steady state of the samples.

Fig. 4.9 shows the paths in terms of void ratio-mean effective stress for drained and undrained compression tests. The marked points shown in Figs. 4.9 and 4.10 indicate the ultimate conditions achieved by the two types of tests and which suppose to be the steady state of the soil under investigation. As can be observed, there is a good correlation between the sample void ratios and the effective mean stress developed at large deformation, irrespective of the type of the test and the initial state of the sample. However, it is important to note that the scatter in the experimental results obtained from drained tests is more significant than the undrained tests. Accordingly, it seems that drained tests are not the most suitable tests to evaluate the steady state line. In undrained test on dense sand, when the pore water pressure reaches to a maximum suction value (approx. -96kPa), the nature of the loading changes from und-

rained to drained. That means after cavitation occurs in the pore water, the volume of the sample changes continuously. In this study this volume change was not recorded and because of this the results of the dense samples are not included in Figs. 4.9 and 4.10.

Stresses at steady state obtained from both the undrained and drained triaxial tests are shown on a plot of q versus p‘ in Fig. 4.11. The data fall in a relatively narrow band and close to a reasonably straight line. The average ratio of $q/(p' + a)$ at the steady state (M) is 1.5; this corresponds to an effective angle of internal friction of 36.9^0 and an attraction of 10kPa. This result indicated that at the steady state the angle of internal friction of Hokksund is not affected by packing density, type of tests and stress levels.

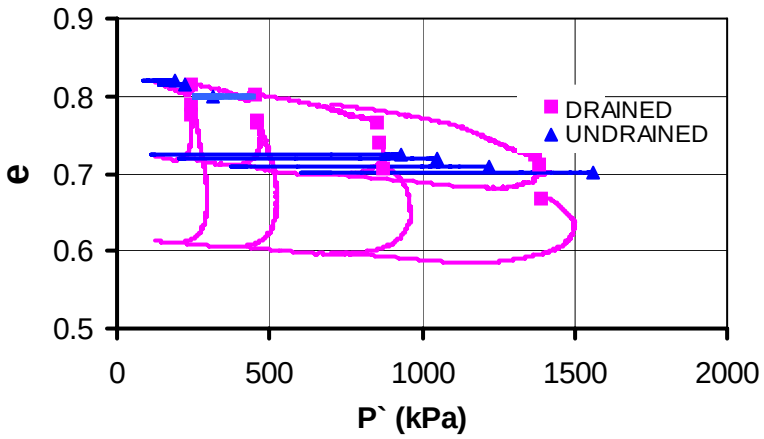

Figure 4.9 Variations of void ratio with effective mean stress in drained and undrained compression tests.

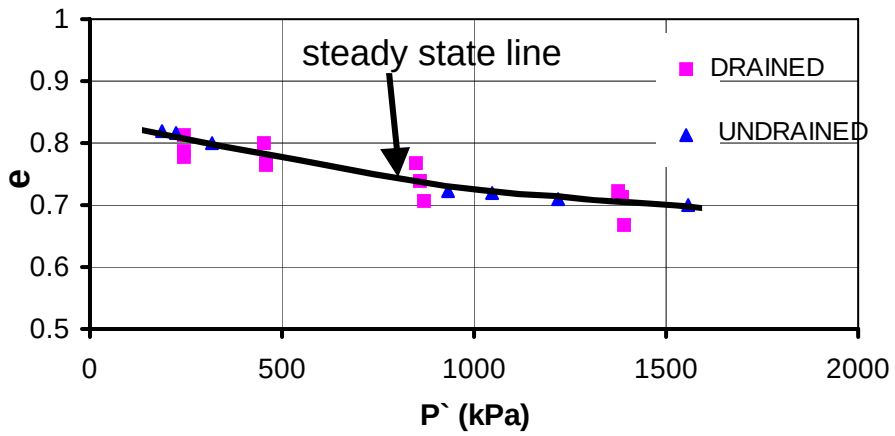

Figure 4.10 Steady state data from drained and undrained triaxial compression tests and steady state line.

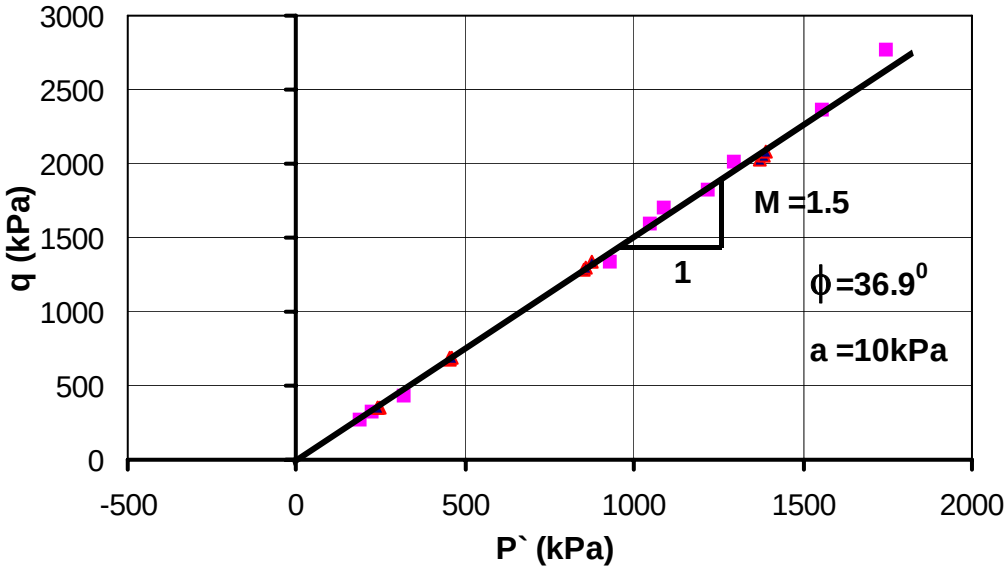

Figure 4.11 Strength envelope at the steady state

Shear and bulk modulus

The shear and bulk modulus of the material under investigation were calculated from the initial slopes of the deviatoric stress versus shear strain and mean stress versus volumetric strain curves using Eqs. 3.14 and 3.15. Both theoretical considerations and practical experiments show that the initial tangent modulus are generally dependent on the mean stress p‘ according to Nordal (1996).

$$G = g_o P_a \left(\frac{p' + a}{P_a}\right)^{1-n} \tag{4.1}$$

$$K = k_o P_a \left(\frac{p' + a}{P_a}\right)^{1-n} \tag{4.2}$$

In which P_a is atmospheric pressure expressed in the same units as G, K and p‘. g_o and k_o are non-dimensional moduli numbers, and n is an exponent determining the rate of variations of G and K with p‘.

The bulk and shear modulus calculated from results of the undrained and drained compression tests are plotted in double logarithmic coordinate systems as shown in Figs. 4.12 and 4.13. The parameters g_o, k_o and n in Eqs. (4.1) and (4.2) are determined from these figures.The intercepts of the best- fitting straight line for the data shown in Figs. 4.12 and 4.13 with $\left(\frac{p' + a}{P_a}\right) = 1$ are the values of g_o and k_o, and n is the slopes of the lines. As can be seen from these figures for a given void ratio, the two elastic parameters vary linearly with the mean stress.

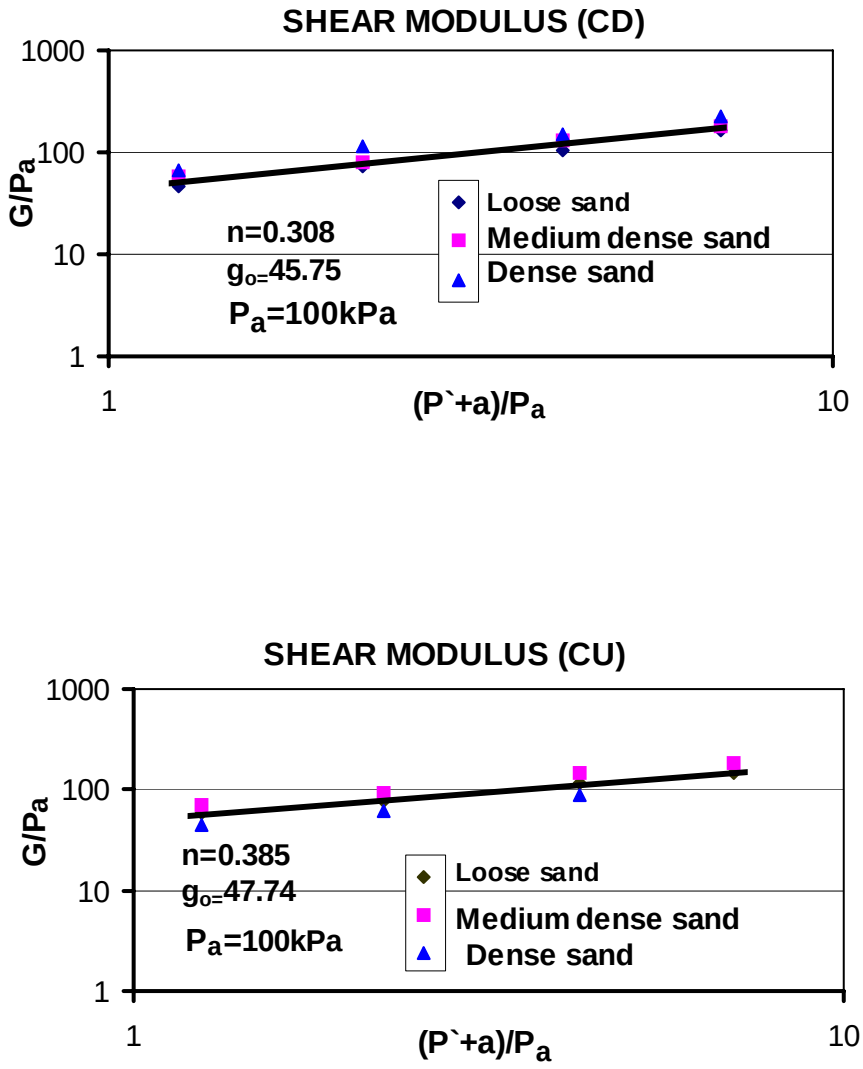

Figure 4.12 Variations of shear modulus in drained and undrained tri-axial compression tests.

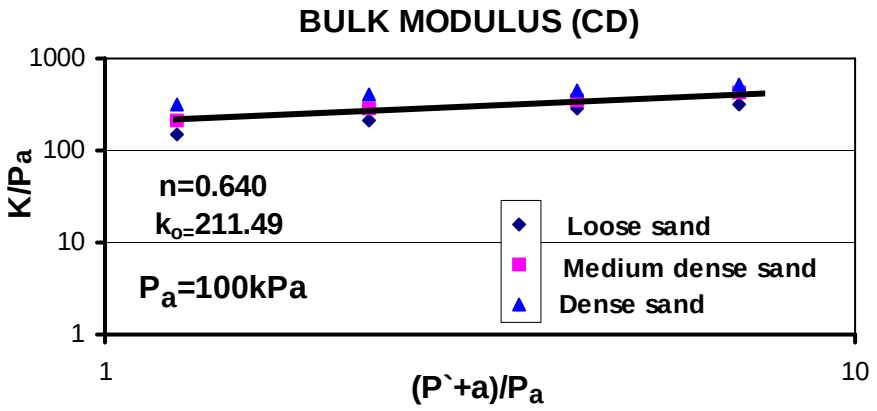

Figure 4.13 Variation of bulk modulus in drained compression test.

From the results of the tests described in the present chapter, the following conclusions can be drawn.

- The undrained and drained behaviour of saturated sand depends on both the void ratio after consolidation and the effective confining stress.

- For a given initial void ratio, the stress level to which samples are consolidated prior to shearing has significant effect on the developed shear strength in both drained and undrained tests. Samples consolidated to higher stresses consistently exhibited higher strength over a wide range of strain.

- In loose sands, the phase transformation line is inclined very close to the common (ultimate) stress paths. Hence, very small stress increments are required to reach the common stress path after crossing the phase transformation states. On the other hand, it is found that for dense sands high stress increments are required to reach the common stress path after the phase transformation states.

- When a dense sample is sheared with low back pressure in undrained compression tests, cavitation will takes place before it reaches to failure. Due to this the response of the sand starts to deviate from the common stress path. Failure occurs when the stress path reaches the drained failure envelope.

- For a given initial void ratio and confining pressure, samples tested in extension show considerably weaker and significantly more contractive behaviour than those tested in compression.

- At a given relative density, the effective stress ratio at the phase transformation state is slightly less in extension than in compression.

- When a loose sample is sheared in undrained tests, the deviator stress tends to increase continuously after it reaches a plateau over a certain range of strains. The rate of such an increase with strain, however, is very small. Therefore, the stress values at 27% strain are used to estimate the steady state.

- The same steady state line is obtained from undrained and drained tests. However, some scatter is evident on the test results computed

from drained tests. Therefore, drained tests are not recommended to establish the steady state line.

- From compression tests it appears that the friction angle mobilized at steady state is unique for the sand. It is independent of both the initial state (void ratio and confining pressure) and the type of the test (undrained or drained).

Chapter 5
Cyclic triaxial test results

5.1 Introduction.

Undrained cyclic loading causes a progressive increase in pore-water pressure and cyclic deformation in saturated sand with increasing number of cycles. However, two distinct types of responses may be obtained with regard to the development of strain. As it was discussed in Chapter 2, these two responses are called flow liquefaction and cyclic mobility respectively. In the first type of response, the sand may loose large portion of its resistance and deform continuously. In the second type of response, large deformations may results from progressive stiffness degradation.

Although both flow liquefaction and cyclic mobility result in large deformations which are generally unacceptable for engineering purposes, the

mechanisms of strain development as a consequence of flow liquefaction and cyclic mobility are quite different. It is generally believed that relative density is the most important initial state parameter of sand controlling the development of strain under cyclic loading. Sand with low relative density is considered to be susceptible to flow liquefaction, while sand with high relative density is susceptible to cyclic mobility.

This Chapter describes the results of saturated samples prepared at three different initial relative densities, to illustrate the mechanisms of flow liquefaction and cyclic mobility for strain development under cyclic loading. In this testing programme 14 cyclic triaxial tests were conducted under the same confining pressure. Back pressure of 300kPa was applied in all tests. The Skempton‘s pore water pressure coefficient (B-value) was greater than 0.96 for all samples.

5.2 Test results.

Typical cyclic triaxial test results on samples of loose, medium and dense sands are shown in Figs. 5.1, 5.2 and 5.3. The failure envelope shown in Fig. 4.11 and phase transformation lines obtained from monotonic compression and extension loading test results are also plotted together with the cyclic stress paths of the three samples. In all tests, the effective stress paths moved toward the failure envelopes during cyclic loading and finally they traced the steady loops which were tangent to failure envelopes.

The results of a typical triaxial cyclic loading test on a sample of loose sand are shown in Fig. 5.1. The test data in this figure shows the effec-

tive stress path, strain versus number of cycles and pore-water pressure with number of cycles for an initial effective confining pressure of 125kPa. It may be seen that, the pore water pressure accumulated progressively and the developed strain is small until the effective stress path touches for the first time the phase transformation line in the extension side. Further cyclic loading beyond this phase transformation line caused the sample to loose its shear resistance, which was accompanied by the development of large deformation (characteristics of flow liquefaction) and a sharp increase in pore water pressure.

As it can be seen from Fig. 5.1(b), the developed strain amplitude was increased from 0.3% to 0.66% for the first 5 cycles. However, the application of the 6^{th} cycle of loading produced a disproportionate effect. The axial strain during this stress cycle increased to about 1.64%. The strain amplitude increased further from 1.64% to 20% in the next two stress cycles. From pore water pressure versus number of cycles curves, it may be noted that during the 6^{th} cycle the sample showed a decrease in pore water pressure when the maximum shear stress was reached. The effective stress state at which the sample starts to developed significant amount of strain was found to be essentially the same as the phase transformation line obtained from undrained monotonic loading. Similar to undrained monotonic loading, the phase transformation state in the cyclic loading also signifies the onset of significant deformation of dilative samples. After crossing the phase transformation line, very few stress cycles were applied to reduced the effective stress to zero and at the same time, to produce complete liquefaction of the sample.

Typical effective stress paths, strain versus number of cycles and pore

water pressure responses for medium and dense samples are shown in Fig. 5.2 and 5.3 respectively. As in the case of loose sand, the sample withstood a number of stress cycles with no significant deformations, but after the effective stress paths reach the phase transformation line the strain amplitude begins to increase markedly. However, in contrast to loose sands, the strain amplitude increased relatively slowly with increasing number of cyclic stresses. Each cyclic stress after crossing the phase transformation line causes a large increase in pore water pressure, which also brings the sample close to the transient state of zero effective stress, but with very little change in deformation. Repetition of this phenomenon of stress state moving alternatively into the region beyond the phase transformation line with cycles of loading ultimately results in a transient state of zero effective stress, which is responsible for further accumulation of deformation. In contrast to the behaviour on the compression side, the effective cyclic stress path on the extension side forms a closed loop on the phase transformation line as the cyclic extension strains steadily increase. Here also it was found that, the effective stress states at which the samples start to dilate were the same as the phase transformation lines obtained from undrained monotonic loading tests on the two samples.

The above discussion can be made more clear by looking further into details of the development of strains and pore-water pressure in dense sand. As may be seen from Fig. 5.3(b) that, the sample accumulated very small deformations until the effective stress state reached the phase transformation line. From the first cycle until 11 cycles of loading, the strain amplitude increased from 0.13% to 0.15%. However, during the

12^{ve} stress cycle the deformation increased to a value 0.22%. In the next 40 cycles the strain amplitude increased further from 0.22% to about 1%. From Fig. 5.3 (a) and (c) it is apparent that starting from the 12^{ve} cycles the sample showed a decrease in pore water pressure when the maximum shear stress was reached. After the stress state crossed the phase transformation line, unloading of shear stress during the stress cycle resulted in an increase in pore water pressure with very little change in deformation. On the other hand, reloading caused the sample to develop relatively large deformation with an accompanying drop in pore water pressure.

The influence of the density of the sand on the strain amplitudes that develop after crossing the phase transformation line and initial liquefaction (In this investigation, initial liquefaction or 100% pore pressure was defined when the pore-water pressure of the samples became equal to the applied confining pressure during the course of cyclic stress application) is clearly shown in Fig. 5.4. It can be seen from this figure that:

- The loose sand developed large strains immediately after crossing the phase transformation line, whereas the dense sand developed much smaller strains and exhibited a much slower rate of strain increase.

- In loose sand, the number of stress cycles required to reach the phase transformation line and initial liquefaction are almost the same, whereas in dense sand there is a great difference in the required number of stress cycles to reach the phase transformation line and initial liquefaction.

- In contrast to loose sand, the dense sand continued to effectively resist large deformations for a number of cycles following initial liquefaction.

The unsymmetrical deformation shown by the dense sand sample (Fig. 5.3(b)) is characteristic of the behaviour of all sand samples tested during this investigation. This behaviour for all samples was markedly anisotropic and relatively larger strains occurred in extension.

The result of cyclic shear stress ratio $q_{cyc}/(2\sigma'_3)$ versus number of cycles to develop 5% D.A. (double amplitude) axial strain due to flow liquefaction or cyclic mobility are shown in Fig. 5.5. It may be seen from the diagram that for a sand at a given void ratio under a given initial effective confining pressure, the number of cycles required to cause 5% D.A. axial strain increases as the cyclic shear stress ratio decreases. Furthermore, for a given confining pressure, the cyclic shear stress ratio required to cause 5% D.A. axial strain increases as the relative density of the sand increases.

It has become a routine practice to take the cyclic shear stress ratio required to cause 5% D.A. axial strain under 20 stress cycles as a factor quantifying the liquefaction resistance of sands under a given state of packing as represented by void ratio or relative density. This cyclic shear stress ratio is represented by $(q_{cyc}/(2\sigma'_3))_{20}$, and is sometimes referred to as the cyclic strength (Ishihara, K. 1994). The cyclic strengths required to cause 5% D.A. axial strain for the three relative densities of Hokksund sand are tabulated in Table 5.1.

Table 5.1 Cyclic strengths required to cause 5% D.A. axial strain.

D_r	30%	57%	87%
$\left(\frac{q_{cyc}}{2\sigma'_3}\right)_{20}$	0.332	0.423	0.595

The following conclusions may be made on the basis of the cyclic triaxial test results presented above.

- In all samples, the effective stresses at which the samples start to develop significant amount of strains were found the same as the phase transformation lines obtained from undrained monotonic loadings.

- Repetition of stress state moving into the region beyond the phase transformation line is responsible for further accumulation of deformations.

- For a given cyclic shear stress, the rate of development of strain after the phase transformation line depends on the initial relative density of the sample. In loose sand, the strain increases rapidly and failure due to flow liquefaction occurs within a very few stress cycles. On the contrary, in dense sand as a result of progressive stiffness degradation strain increases more slowly with increasing number of cycles.

- After the stress state crosses the phase transformation line, unloading of shear stress during the stress cycles results in an increase in pore water pressure with very little change in deformation. On the other hand, reloading caused the sample to develop relatively large deformation with accompanying drop in pore water pressure.

- In all samples, the effective cyclic stress paths on the extension sides formed a closed loop on the phase transformation lines.

- Dense sand has a capacity to resist large deformations for a number of cycles following initial liquefaction.

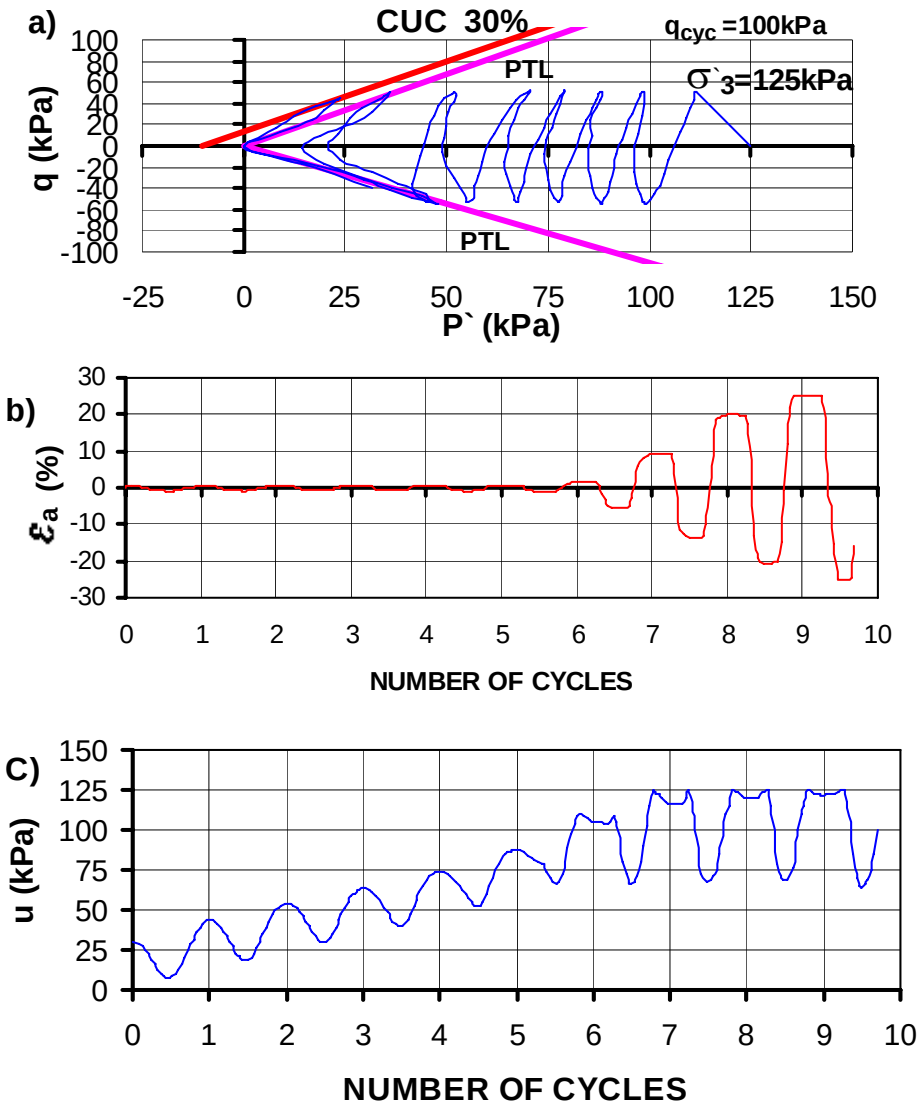

Figure 5.1 Typical cyclic triaxial test results on loose sand. a) Effective stress path, b) strain versus number of cycles and c) pore water pressure versus number of cycles.

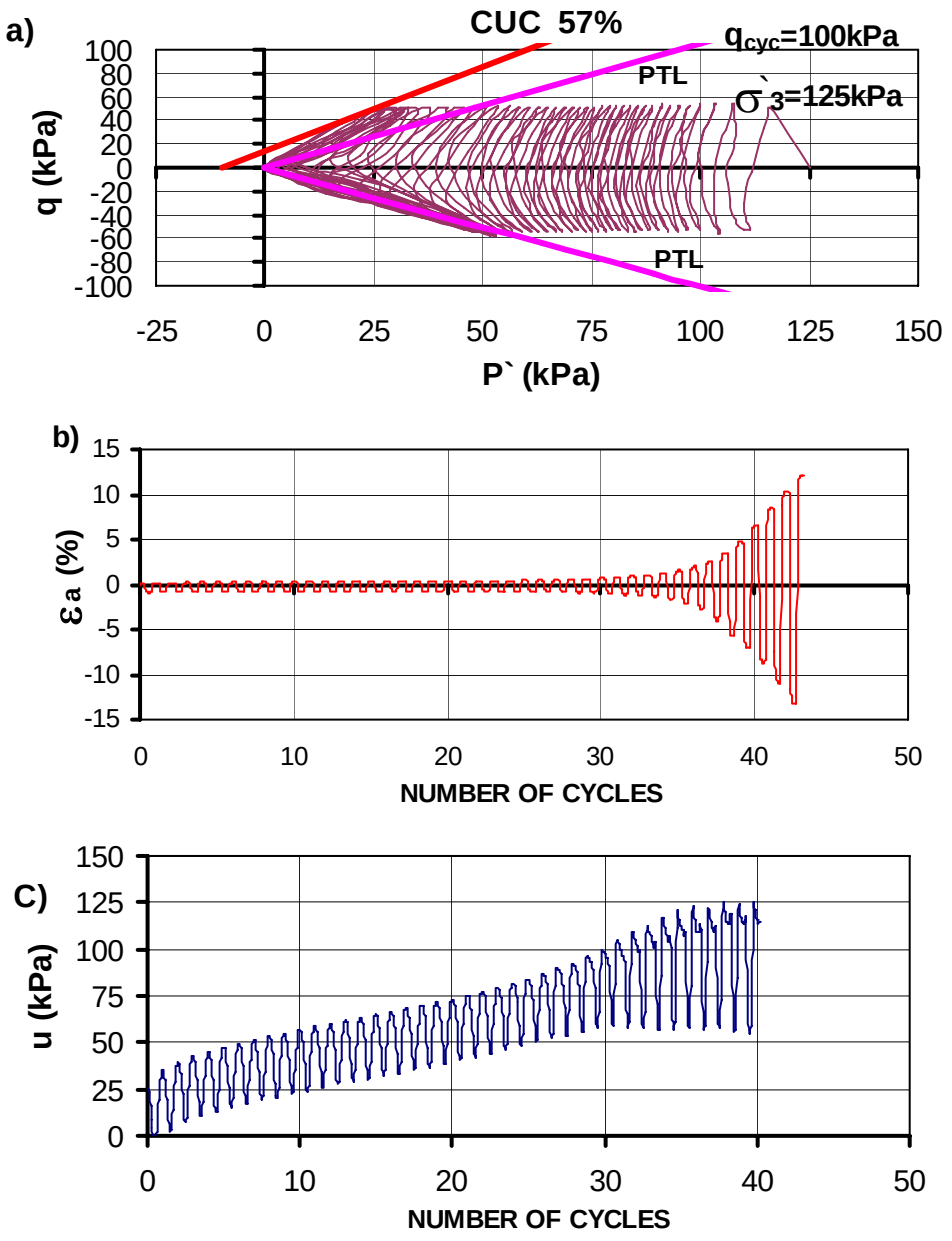

Figure 5.2 Typical cyclic triaxial test results on medium dense sand. a) Effective stress path; b) strain versus number of cycles and c) pore water pressure versus number of cycles.

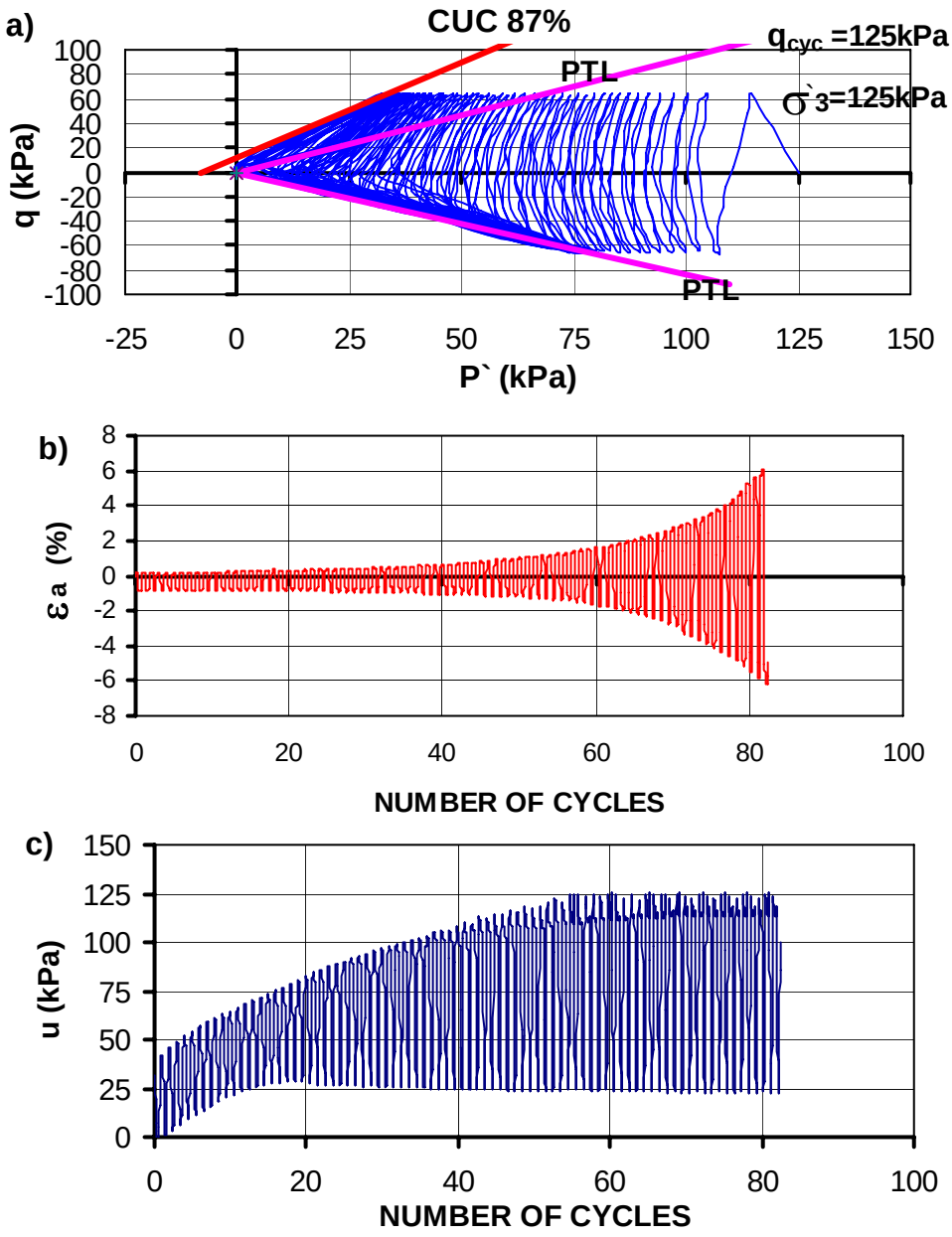

Figure 5.3 Typical cyclic triaxial test results on dense sand. a) Effective stress path, b) strain versus number of cycles and c) pore water pressure versus number of cycles.

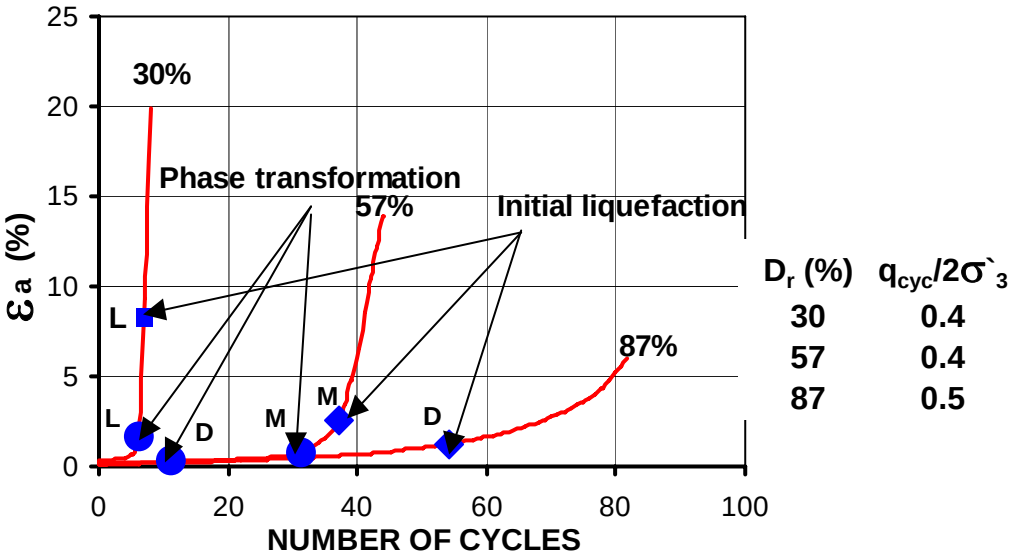

Figure 5.4 Strain developments versus number of cycles for loose, medium and dense sands.

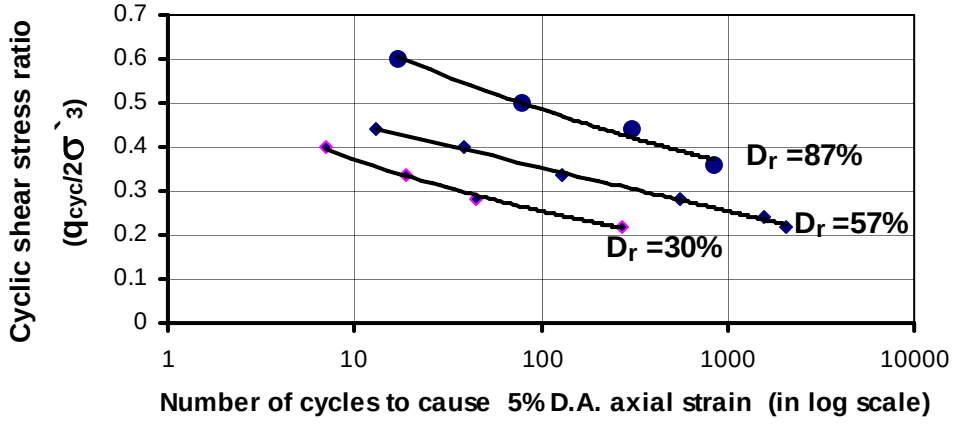

Figure 5.5 Cyclic shear stresses required to cause 5% D.A. axial strain for initially loose, medium and dense sands.

5.3 Link between undrained monotonic and cyclic loadings.

As was shown in the previous section, there is an apparent link between the effective stresses at which samples start to dilate under monotonic and cyclic loadings and the phase transformation lines in monotonic tests and cyclic strengths. The tendency to dilate during monotonic and cyclic loadings causes a change in particle arrangement, which may include the formation of metastable holes (Nemat-Nasser and Takahashi 1984; Youd 1977). Unloading after hitting the phase transformation line reduced drastically the number of contact points between neighboring grains. Accordingly the sand structure tends to collapse, producing a correspondingly large increase in pore water pressure. In short, phase transformation lines define the onset of large deformations during monotonic undrained and cyclic loadings.

The relationship between undrained monotonic and cyclic loading tests can be illustrated by examining the cyclic stress paths shown in Fig. 5.6, in relation to the monotonic stress paths and the phase transformation lines, for loose, medium dense and dense sands. In all samples, when the cyclic stress paths reached the phase transformation line deformations increased rapidly. The cyclic stress paths on the extension sides formed a closed loop on the phase transformation lines and flow liquefaction or cyclic mobility occurred depending on the relative density of the samples.

As it was indicated in Chapter 4, for all samples tested, that the response of the samples in extension was weaker than in compression.

The cyclic strengths are therefore assumed to be governed by the phase transformation lines on the extension sides. Based on the foregoing observation a relationship between the phase transformation line on the extension side and flow liquefaction or cyclic mobility, the cyclic shear stress ratios required to cause 5% D.A. axial strain after 20 cycles $(q_{cyc}/(2\sigma'_3))_{20}$ has been plotted against the effective stress ratios at the phase transformation states (Fig. 5.7). It can be seen from this figure that the cyclic strength of the soil under investigation can be uniquely determined from the monotonic effective stress ratio at the phase transformation state.

For a given sand, the effective stress ratio at the phase transformation line mainly depends on the relative density of the sand. For loose sand, the effective stress ratio at the phase transformation line is slightly smaller than the larger effective stress ratio at failure line. In this case as shown in Fig. 5.7, the cyclic shear stress required to develop 5% D.A. axial strain is very small.

As the relative density of the sand increases, the phase transformation lines move away from the failure lines, since dilation would prevail at much lower effective stress ratio. Accordingly, in dense sands, as shown in Fig. 5.7 the cyclic shear stress required to develop 5% D.A. axial strain is large.

It may be important to point out one of the features of Fig. 5.7. A limited number of undrained monotonic triaxial tests are required in order to find the effective stress ratios at the phase transformation states. Then

using these ratios, a figure like Fig. 5.7 can be used to predict the cyclic shear stress which will cause 5% D.A. axial strain in 20 cycles. This approach may be enabling a first hand identification of the cyclic strength of the given soil.

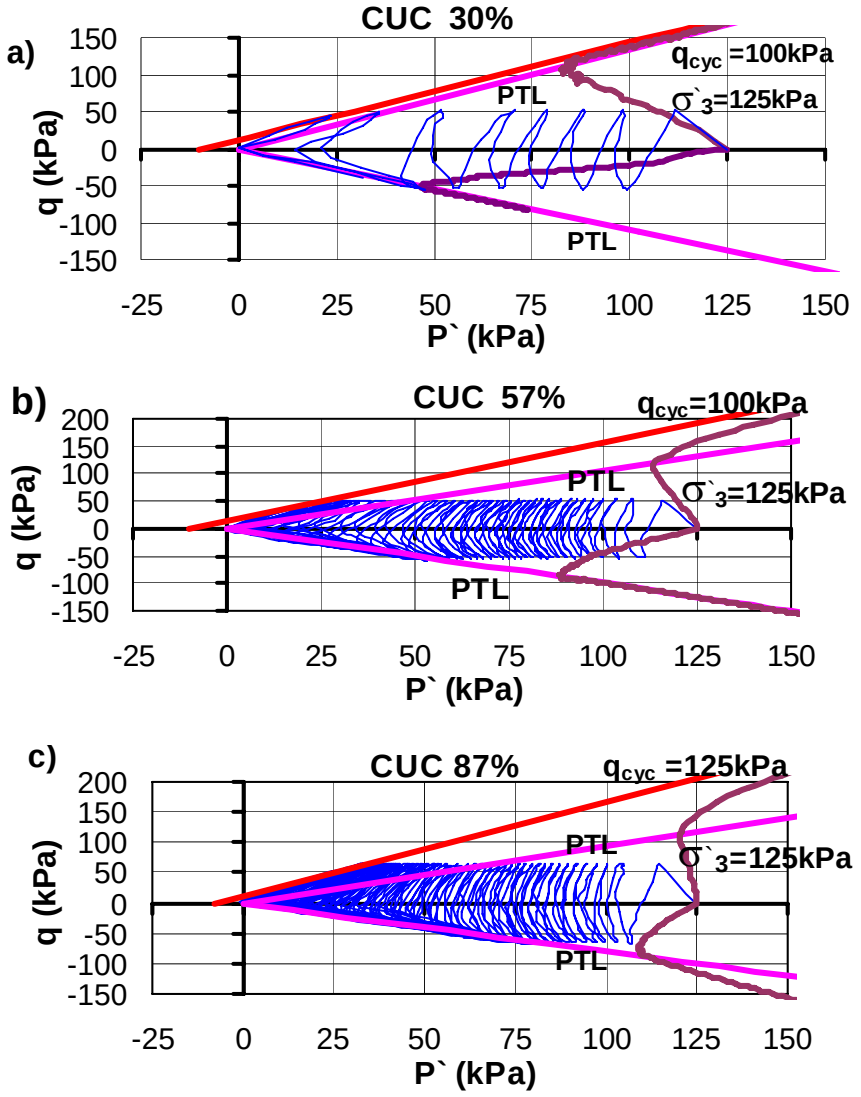

Figure 5.6 Comparison of undrained monotonic and cyclic stress paths: a) loose sample; b) medium dense sample and c) dense sample

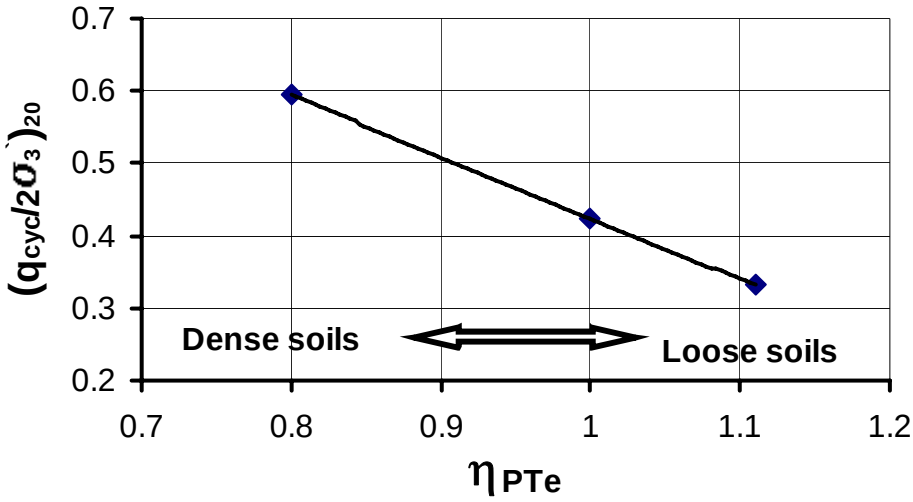

Figure 5.7 Relationship between cyclic strengths and effective stress ratios at phase transformation states.

Chapter 6
Conclusions and recommendations

6.1 Conclusions.

Monotonic and cyclic loading behaviour of a saturated sand has been studied under triaxial tests. The range of behaviour covered from contractive to dilative under monotonic loading and flow liquefaction and cyclic mobility under cyclic loading. Flow liquefaction refers to the loss in shear strength accompanied by the development of large deformation of a saturated sand under monotonic or cyclic loading, while cyclic mobility refers to the gradual development of deformation due to reduction in stiffness of a saturated sand under cyclic loading. These definitions of flow liquefaction and cyclic mobility currently get a general acceptance among researchers.

In view of the expense of running cyclic triaxial tests, it is most convenient to estimate the cyclic strength of saturated sands from the results of monotonic undrained triaxial tests. Comparison of the phase transformation lines obtained from undrained monotonic and the effective stress paths of cyclic loading shows that a connection exists between the two types of loading conditions. On the basis of this connection a relationship can be established so that the cyclic strengths can be estimated from the results of monotonic undrained tests.

The following conclusions may be stated based on the result of the experiments presented in this study.

1.The drained and undrained behaviour of saturated sands depend on both the void ratio after consolidation and the effective confining pressure.

2. In undrained monotonic triaxial testing all of the stress paths for the sand tested passed through the phase transformation states.These states defined by points in a q-p‘ plane at which the mean effective stress increments , $\Delta p'$, are zero.

3. For a given initial void ratio and confining pressure, sample tested in extension is considerably weaker and highly contractive than that tested in compression. It was also observed that under extension loading, the effective stress ratios at the phase transformation state is slightly less than that in compression.

4. At large strain level, the same steady state line is obtained from monotonic undrained and drained compression tests. This indicates that the large strain level needed to develop the steady state is able to transform the initial soil structure to a new soil structure which is the same for all samples tested under these two conditions of loading.The result also confirms that the steady state is an ultimate condition absolutely common to both undrained and drained loading conditions.

5.The friction angle mobilized at steady state is unique for the sand. It is independent of both the initial state (void ratio and confining pressure) and the type of the test (undrained or drained).

6. The effective stress ratio at which the samples start to develop significant amount of deformations appear to be the same for undrained monotonic and cyclic tests. Therefore, the stress conditions which initiate the development of large deformations are not influenced by the type of load (monotonic or cyclic) applied.

7. Under cyclic loading, the strain development could be due to flow liquefaction or cyclic mobility. If flow liquefaction develops after the effective stress path crossing the phase transformation line, the axial strains rapidly accelerated and take the soil to a complete liquefaction stage. If cyclic mobility develops after the effective stress path crossing the phase transformation line and then cycled through or close to zero mean effective stress conditions, the cyclic axial strains increased at steady rate to large values.

8.A relationship is developed between the effective stress ratios at the

phase transformation lines on the extension sides from undrained monotonic loading and the cyclic strengths from the cyclic triaxial loading conditions. This relationship can be used to estimate the cyclic strength of the soil under investigation from the undrained monotonic loading tests.

6.2 Recommendations for future work.

The present work has attempted to investigate experimentally the behaviour of saturated uniform medium sand subjected to monotonic and cyclic loading conditions. However, the present investigation has not covered all the areas of sand behaviour. In view of this, it would be desirable to extend the present work in the following areas.

1.Some more tests are needed to verify the hypothesis proposed for other sands with different gradations and shapes. A study of more well graded soils would in this respect be very interesting.

2. To conduct a series of undrained monotonic stress controlled triaxial tests aim at softening mechanism leading to liquefaction. Testing samples under stress controlled conditions is a useful demonstration of the potentially catastrophic effects of liquefaction in the field, where many conditions approximate load control. The dramatic postpeak axial deformation shown by the samples loaded under these conditions may also show clearly the concepts of steady state deformation.

3. To study the effect of intermediate principal stress on the behaviour of the soil. In a conventional triaxial test, it is not possible to have a truly stress state, but at least, two principal stresses must be equal. Consequently, the state of the stresses is always axially symmetric. Field conditions on the other hand, almost always involve three-dimensional stress conditions, and only rarely are axisymmetric stress conditions encountered in-situ. It is therefore recommendable to conduct a true triaxial test, to investigate the influence of the intermediate principal stress on the behaviour of the soil.

4.To study the behaviour of the soil under anisotropically consolidated conditions. Due to orientation or segregation of particles during deposition and due to orientation arising from its subsequent history, soil structure (fabric) may in fact be significantly anisotropic. Anisotropic consolidation is therefore of importance both in studying the stress-strain behaviour of consolidated samples and in examining the deformation and volume change characteristics during consolidation.

5.Peizocone penetration test (CPTU) is commonly used in Norway to measure the in-situ strength and pore- water pressure of a naturally deposited soils. Therefore this equipment may be used to measure the strength of the soil and to develop a relationships with the laboratory data.

References.

1.Alarcon-Guzman, A.,Leonards,G.A.and Chameau,J.I.(1988a). Discussion to liquefaction evaluation procedure. Journal of Geotechnical Engineering, ASCE, Vol.114, No.2, pp.232-236.

2.Alarcon-Guzman, A.,Leonards,G.A.and Chameau,J.I.(1988b). Undrained monotonic and cyclic strength of sands. Journal of Geotechnical Engineering, ASCE, Vol.114, No.10, pp.1089-1109.

3.Arulanandan,K.and Muraleetharan,K.(1988). Discussion to liquefaction evaluation procedure.Journal of Geotechnical Engineering, ASCE, Vol.114, No.10, pp.236-239.

4. Baldi,G.and Nova, R.(1984). Membrane penetration effects in triaxial testing.Journal of Geotechnical Engineering, ASCE, Vol.110, No.3, pp.403-420.

5.Baldi, G., Hight, D.W. and Thomas, G.E. (1986). A reevaluation of conventional triaxial test method. State of the Art Paper, Advanced Triaxial Testing of Soil and Rock, ASTM STP 977, pp.219-263.

6.Been, K.and Jefferies, M.G.(1985).A state parameter for sands. Geotechnique, Vol.35,No.2, pp.99-112.

7.Been,K.,Jefferies,M.G. and Hachey,J.(1991). A critical state of sands. Geotechnique, Vol.41,No.3, pp.365-381.

8.Bishop, A.W.(1966). Strength of soils as engineering materials. 6th Rankine Lecture, Geotechnique, Vol.16, pp.81-130.

9.Bishop, A.W. and Henkel, D.J. (1962). The measurement of soil properties in the triaxial test. Edward Arnold(Publisher) LTD.

10.Britto, A.M. and Gunn, M.J.(1987). Critical state soil mechanics via finite elements. John Wiley and Sons.

11.Casagrande, A. (1936). Characteristics of cohesionless soils affecting the stability of slopes and earth fills. Journal of the Boston Society of Civil Engineering, January, pp.13-32.

12.Casagrande, A. (1936a). Notes on the shearing resistance and stability of cohesionless soils and their relation to the design of earth dams. Proceedings, First International Conference on Soil Mechanics

and Foundation Engineering, Vol.III, pp.58-60.

13.Casagrande, A. (1938).The shearing resistance of soils and its relation to the stability of earth dams. Proceedings, Soils and Foundation Conference of the U.S. Engineer Department, Boston.

14.Casagrande, A. (1970). On liquefaction phenomena. Lecture, Reported by Green and Ferguson, Geotchnique, Vol. 21, No. 3, (1971), pp.197-202.

15.Casagrande, A. (1975). Liquefaction and cyclic deformation of sands-a critical review. Fifth Panamerican Conference on Soil Mechanics and Foundation Engineering, Buenos Aires, Argentina.

16.Castro, G. (1969). Liquefaction of sands. Ph.D. Thesis, Harvard University, Cambridge, Mass.

17.Castro, G. (1975). Liquefaction and cyclic mobility of saturated sands. Journal of Geotechnical Engineering, ASCE, Vol.101, No.GT6, June, pp.551-569.

18.Castro, G. and Christian, J.T. (1976). Shear strength of soils and cyclic loading. Journal of Geotechnical Engineering, ASCE, Vol.102, No.GT9, Sept., pp.887-894.

19.Castro, G. and Poulos, S.J. (1977). Factors affecting liquefaction and cyclic mobility. Journal of Geotechnical Engineering, ASCE, Vol. 103, No. GT6, pp. 501-516.

20.Castro, G. and Poulos, S.J.,France, J.W. and Enos, J.L. (1982). Liquefaction induced by cyclic loading. Inc., Report Submitted to National Science Foundation, March.

21.Castro, G., Poulos, S.J. and Leathers, F. D. (1985). Re-examination of slides lower San Fernando dam. Journal of Geotechnical Engineering, ASCE, Vol. 111, No. 9,Sept., pp.1093-1107.

22.Castro, G., Seed, R.S., Keller, T. O. and Seed, H. B. (1992). Steady-state strength analysis of lower San Fernando dam slide. Journal of Geotechnical Engineering, ASCE, Vol. 118, No.3, pp. 406-427.

23.Chu, J. (1992). Discussion to minimum undrained strength versus steady-state strength of sands. Journal of Geotechnical Engineering, Vol. 118, No. 2.

24.Chu, J. (1992). Discussion to minimum undrained strength of two sands. Journal of Geotechnical Engineering, Vol.118, No. 3.

25.Chu, J. (1995). An experimental examination of the critical state and other similar concepts for granular soils. Canadian Geotechnical Journal , Vol. 32, pp. 1065-1075.

26.De Alva, P. (1988). Discussion to liquefaction evaluation procedure. Journal of Geotechnical Engineering, ASCE, Vol. 114, No. 2, Feb., pp. 239-241.

27.DeGregorio, V.B. (1990). Loading systems, sample preparation, and liquefaction. Journal of Geotechnical Engineering, ASCE, Vol.

116, No. 5, pp.805-821.

28.Dennis, N. P. (1988). Discussion to liquefaction procedure. Journal of Geotechnical Engineering, ASCE, Vol. 114, Feb., pp. 241-243.

29.Dobry, R. and Ladd, R.S (1980). Discussion to soil liquefaction and cyclic mobility evaluation for level ground during earthquakes, and liquefaction potential-science versus practice. Journal of Geotechnical Engineering, ASCE, Vol. 106, No. GT6, June, pp. 720-724.

30.Dobry, R., Ladd, R.S., Yokel, F.Y., Chung, R.M. and Powell, D. (1982). Prediction of pore water pressure buildup and liquefaction of sands during earthquake by the cyclic strain method. Building Science Series 138, National Bureau of Standards, U.S. Department of Commerce, U.S. Governmental Printing Office, Washington, D.C.

31.El-Shohby, M.a. (1964). The behaviour of particulate material under stress. Ph.D. Thesis, Manchester University.

32. Fukushima, S. and Tatsuoka, F. (1984). Strength and deformation characteristic of saturated sand at extremely low pressures. Soils and Foundations, Vol. 24, No. 4, pp. 30-48.

33.Georgiannou, V.N., Burland, J.B. and Hight, D.W, (1990). The undrained behaviour of clayey sands in triaxial compression and extension. Geotechnique, Vol.40, No. 3, pp. 431-449.

34.Hanzawa, H. (1980). Undrained strength and stability analysis for quick sand. Soils and Foundations, Vol. 20, No. 4, pp. 30-48.

35.Henkel, D.J. and Gilbert, G.D. (1952). The effect of the rubber membrane on the measured triaxial compression strength of clay samples. Geotechnique, Vol. 3, pp. 20-29.

36.Hird, C.C. and Hassona, F.A. (1990). Some factors affecting the liquefaction and flow of saturated sands in laboratory tests. Engineering Geology Vol. 28, pp.149-170.

37.Holtz, R.D. and Kovacs, W.D. (1981). An introduction to geotechnical engineering. Prentice Hall, Englewood Cliffs USA.

38.Hrcyciw, R,D., Vitton, S. and Thomann, T.G. (1990). Liquefaction and flow failure during seismic exploration. Journal of Geotechnical Engineering, ASCE, Vol. 116, No. 12, pp. 1881-1889.

39.Hyodo, M., Murata, H., Yasufuku, N. and Fujii, T. (1989). Undrained cyclic shear strength and deformation of sands subjected to initial static shear stress. Proceedings of the Fourth International Conference on Soil Dynamics and Earthquake Engineering, Mexico City, Oct., pp. 81-103.

40.Ibsen, L.B. (1994). The stable state in cyclic triaxial testing on sand. Soil Dynamics and Earthquake Engineering, Vol.13, pp. 63-72.

41.Ibsen, L.B. (1995). The static and dynamic strength of sand. Proceedings of the Eleventh European Conference on Soil Mechanics and Foundation Engineering, Copenhagen, May, pp. 69-75.

42.Ibsen, L.B. and Lade, P.V. (1997). The role of the characteristic line in the behaviour of sand under static and cyclic loading. Proceedings

of the Fourth International Workshop on Localization and Bifurcation Theory for Soils and Rock, Adachi, Oka and Yashima, eds. Gifu, Japan.

43.Ishihara, K. (1985). Stability of natural deposits during earthquakes. Proceedings 11th International Conference on Soil Mechanics, San Francisco, Vol. 1, pp. 321-376.

44.Ishihara, K. (1993). Liquefaction and flow failure during earthquakes. Thirty-third Rankine Lecture, Geotechnique, Vol. 43, No. 3, pp. 351-451.

45.Ishihara, K., Tatsuoka, F. and Yasuda, S. (1975). Undrained deformation and liquefaction of sand under cyclic stresses. Soils and Foundations, Vol. 15, No. 1, pp.29-44.

46.Ishihara, K., Yasuda, S. and Yoshida, Y. (1990). Liquefaction induced flow failure of embankments and residual strength of silty sands. Soils and Foundations, Vol. 30, No. 3, pp.69-80.

47.Ishihara, K. and Watanabe, T. (1976). Sand liquefaction through volume decrease potential. Soils and Foundations, Vol. 16, No. 4 pp. 61-70.

48.Kiekbusch, M. and Schuppener, B. (1977). Membrane penetration and its effect on pore pressure. Journal of Geotechnical Engineering, ASCE, Vol. 103, No. GT11, pp.1267-1279.

49.Kirkpatrick, W.M. and Belshaw, D.J. (1968). On the interpretation of the triaxial test. Geotechnique, Vol. 18, No. 3, pp. 336-350.

50.Kirkpatrick, W.M and Younger, J.S. (1970). Strain conditions in compression cylinder.Journal of the Soil Mechanics and Foundations Division, ASCE, Vol. 96, No. SM5, Proc. Paper 7504, Sept., pp. 1683-1695.

51.Kirkpatrick, W.M and Younger, J.S. (1971). Patterns of strain in strength test samples.Proceedings of the First Australia and New Zealand Conference on Geomechanics, Vol.1, Melbourne, Australia.

52.Konrad, J.M. (1990a). Minimum undrained strength of two sands. Journal of Geotechnical Engineering, ASCE, Vol. 116, No. 6, June, pp. 932-947.

53.Konrad, J.M. (1990b). Minimum undrained strength versus steady-state strength of sand. Journal of Geotechnical Engineering, ASCE, Vol. 116, No. 6, June, pp. 948-963.

54.Konrad, J.M. (1993). Undrained response of loosely compacted sands during monotonic and cyclic compression tests. Geotechnique, Vol. 43, No. 1, pp. 69-89.

55.Kramer, S.L. (1989). Uncertainty in steady-state liquefaction evaluation procedures. Journal of Geotechnical Engineering, ASCE, Vol. 115, No. 10, pp. 1402-1419.

56.Kramer, S.L. and Seed, H.W. (1988). Initiation of soil liquefaction under static loading conditions. Journal of Geotechnical Engineering,

ASCE, Vol. 114, No. 4, pp.412-430.

57.Kutter, B.L. (1988). Discussion to liquefaction evaluation procedure. Journal of Geotechnical Engineering, SACE, Vol. 114, No. 2, Feb. pp.243-246.

58.Ladd, R.S. (1974). Specimen preparation and liquefaction of sands. Journal of the Geotechnical Engineering Division, ASCE, Vol. 100, No. GT10, pp.1180-1184.

59.Lade, P.V. (1988). Effects of voids and volume changes on the behaviour of frictional materials. International Journal for Numerical and Analytical Methods in Geomechanics, Vol. 12, pp. 351-371.

60.Lade, P.V. (1992). Static instability and liquefaction of loose fine sandy slopes. Journal of Geotechnical Engineering, ASCE, Vol. 118, No. 1, pp.51-71.

61.Lade, P.V. and Hernandez, S. (1977). Membrane penetration effects in undrained tests. Journal of Geotechnical Engineering, ASCE, Vol. 103, No. GT2, pp. 109-125.

62.Lee, I.K. and Seed, H.B. (1964). Discussion of importance of free ends in triaxial testing by Rowe, P.W. and Barden, L. Journal of the Soil Mechanics and Foundations Division, ASCE, Vol. 90, No. SM6, pp.173-175.

63.Lee, K.L., (1965). Triaxial compressive strength of saturated sands under seismic loading conditions. Ph.D. dissertation, University of California, Berkeley.

64.Lee, K.L. (1978). End restraint effects on undrained static triaxial strength of sand. Journal of Geotechnical Engineering, ASCE, Vol. 104, No. 6, pp. 687-704.

65.Lee, K.L. and Fitton, J.A. (1969). Factors affecting the cyclic loading strength of soils. Vibration Effects of Earthquakes on Soils and Foundations, ASTM STP 450, pp. 71-95.

66.Lee, K.L. and Seed, H.B. (1967a). Cyclic stress conditions causing liquefaction of sand. Journal of Soil Mechanics and Foundations Division, ASCE, Vol. 93, No. SM1, Jan., pp.47-70.

67.Lee, K.L. and Seed, H.B. (1967c). Drained strength characteristic of sands. Journal of Soil Mechanics and Foundations Division, ACSE, Vol. 93, No. SM6, Nov., pp.117-141.

68.Lindenberg, J. and Koning, H.L. (1981). Critical density of sand. Geotechnique, Vol.31, No. 2, pp. 231-245.

69.Lo, K.Y. and Roy, M. (1973). Response of particulate materials at high pressures. Soils and Foundations, Vol. 24, No. 1, pp.77-89.

70.Luong, M.P. (1980). Stress-strain aspects of cohesionless soils under cyclic and transient loading. International Symposium on Soils under Cyclic and Transient loading, Swansea, U.K., pp. 315-324.

71.McRoberts, E.C. and Sladen, J.A. (1992). Observations on static and cyclic sand-liquefaction methodologies. Canadian Geotechnical Journal, Vol. 29, pp. 650-665.

72.Miura, N., Murata, H.and Yaswfuku,N. (1984). Stress-strain characteristics of sand in a particle-crushing region. Soils and Foundations, Vol.24, No. 1, pp.77-89.

73.Moen, T.I. (1978). Hokksund sand. Undersøkelse av sandens rutinedata, setnings-og skjærfasthetsegenskaper. F. 78.04, Geot. Div., NTH.

74.Mohamad, R. and Dobry, R. (1986). Undrained monotonic and cyclic triaxial strength of sand. Journal of Geotechnical Engineering, Vol. 112, No. 10, Oct., pp.941-958.

75.Negussey, D. and Islam, M.S. (1994). Uniqueness of steady state and liquefaction potential. Canadian Geotechnical Journal, Vol. 31, pp. 132-139.

76.Negussey, D., Wijewickreme, W.K. and Vaid, Y.P. (1988). Constant-volume friction angle of granular materials. Canadian Geotechnical Journal, Vol. 25, pp. 50-55.

77.Nemat-Nasser, S. and Takahashi, K. (1984). Liquefaction and fabric of sand. Journal of Geotechnical Engineering, ASCE, Vol.110, No. 9, pp.1291-1306.

78. Newland, P.L. and Allely, B.H. (1959). Volume changes during undrained triaxial tests on saturated dilatant granular materials. Geotechnique, Vol. 9, No. 4, pp. 174-182.

79.Nordal, S. Kavli, A. and Askevold, A. (1996). Description of the mobilized friction model (MFM). SINTEF Geotechnical Engineering,

The Norwegian Institute of Technology.

80.Norris, G., Siddharthan, R., Zafir, Z. and Madhu, R. (1997). Liquefaction and residual strength of sands from drained triaxial tests. Journal of Geotechnical and Geoenvironmental Engineering, ASCE, Vol. 123, No. 3, pp. 220-228.

81.Olson, R.R. and Campbell, L.M. (1964). Discussion on importance of free ends in triaxial testing. Journal of the Soil Mechanics and Foundations Division, ASCE, Vol. 90, No. SM6, pp. 167-173.

82.Peacock, W.H. and Seed, H.B. (1968). Sand liquefaction under cyclic loading simple shear conditions. Journal of the Soil Mechanics and Foundations Division, ASCE, Vol. 94, No.SM3, May, pp. 689-708.

83.Poulos, S.J. (1981). The steady state of deformation. Journal of Geotechnical Engineering, ASCE, Vol. 107, No. 5, May, pp. 553-562.

84.Poulos, S.J. (1971). The stress-strain curves of soils. Geotechnical Engineers, Inc., Winchester, Mass.

85. Poulos, S.J., Castro, G. and France, J.W. (1985a). Liquefaction evaluation procedure.Journal of Geotechnical Engineering, ASCE, Vol. 111, No. 6, pp. 772-792.

86.Poulos, S.J., Castro, G. and France, J.W. (1988). Liquefaction evaluation procedure.Replay.Journal of Geotechnical Engineering, ASCE, Vol. 114, No. 2,Feb., pp. 232-256.

87.Pyke, R. (1988). Discussion to liquefaction procedure. Journal of Geotechnical Engineering, ASCE, Vol. 114, No. 2, Feb., pp. 246-247.

88.Raju, V.S. and Sadasivan, S.K. (1974). Membrane penetration in triaxial tests on sands. Journal of Geotechnical Engineering, ACSE, Vol. 100, No. GT4, pp.281-288.

89.Reynolds, O. (1885). The dilating of media composed of rigid particles in contact. Philosophical Magazine, S.5., Vol. 20, No. 127, pp. 469-481, London.

90.Riemer, M.F. and Seed, R.B. (1997). Factors affecting apparent position of steady state line. Journal of Geotechnical and Geoenvironmental Engineering, ASCE, Vol. 123, No. 3, pp.281-288.

91.Roscoe, K.H., Schofield, A.N. and Wroth, C.P. (1958). On yielding of soils. Geotechnique, Vol. 8, No. 1, pp. 22-53.

92.Roscoe, K.h., Schofield, A.N. and Thurairajah, A. (1963). An evaluation of test data for selecting a yield criterion for soils. Proc. Laboratory Shear Testing of Soils , ASTM, Special Publication, No. 361,pp. 111-128.

93.Rowe, P.W. and Barden, L. (1964). Importance of free ends in triaxial testing. Journal of Soil Mechanics and Foundations Division, ASCE, Vol. 90, No. 1, pp. 1-27.

94.Schofield, A.N. and Worth, C.P. (1968). Critical state soil mechanics, McGraw-Hill, London.

95.Seed, H.B. (1979). Soil liquefaction and cyclic mobility evaluation for level ground during earthquakes. Journal of Geotechnical Engineering, ASCE, Vol. 105, No. GT2, pp. 201-255.

96.Seed, H.B. (1987). Design problems in soil liquefaction. Journal of Geotechnical Engineering, ASCE, Vol. 113, No. 8, August, pp. 827-845.

97.Seed, H.B. A and Idriss, I.M. (1971). Simplified procedures for evaluating soil liquefaction potential. Journal of Soil Mechanics and Foundations Division, ASCE, Vol.97, No. SM9, pp. 1249-1273.

98.Seed, H.B. and Lee, K.L. (1966). Liquefaction of saturated sands during cyclic loading. Journal of Soil Mechanics and Foundations Division, ASCE, Vol. 92, No. SM6, Nov. pp. 105-134.

99.Seed, H.B. and Lee, K.L. (1967). Undrained strength characteristics of cohesionless soils. Journal of Soil Mechanics and Foundations Division, ASCE, Vol. 93, No. SM6, pp. 333-360.

100.Seed, H.B., Tokimatsu, K., Harder, L.F. and Chung, R.M (1985). Influence of SPT procedures in soil liquefaction resistance evaluations. Journal of Geotechnical Engineering, ASCE, Vol. 12, pp. 1425-1445.

101.Selig, E.T. and Chang, C.S. (1981). Soil failure modes in undrained cyclic loading. Journal of Geotechnical Engineering, ASCE, Vol. 107, No. GT5, pp.539-551.

102.Sivathayalan, S. and Vaid, Y.P. (1998). Truly undrained response of granular soils with no membrane-penetration effects. Canadian Geotechnical Journal, Vol.35, pp. 1683-1695.

103.Sladen, J.A., D'Hollander, R.D. AND Krahn, J. (1985a). The liquefaction of sands, a collapse surface approach. Canadian Geotechnical Journal, Vol. 22, pp. 564-578.

104.Sladen, J.A. and Oswell, J.M. (1989). The behaviour of very loose sand in the triaxial compression test. Canadian Geotechnical Journal, Vol. 26, pp. 103-113.

105.Talaganov, K. (1986). Determination of liquefaction potential by cyclic strain approach. Proceedings of the Eight European Conference on Earthquake Engineering.

106.Tatsuoka, F. and Haibara, O. (1985). Shear resistance between sand and smooth or lubricated surfaces. Soils and Foundations, Vol. 25, No. 1, pp.89-98.

107.Tatsoka, F., Sakamoto,M., Kawamura,T. and Fukushima, S. (1986). Strength and deformation characteristics of sand in plane strain compression at extremely low pressure. Soils and Foundations, Vol.26, No. 1, pp. 65-84.

108.Taylor, D.W. (1948). Shearing strength determinations by undrained cylindrical compression tests with pore pressure measurments. Proceedings of the Second International Conference on Soil Mechanics, Vol. 5, pp. 45-49.

109.Terzaghi, K. and Peck, R.B. (1948). Soil mechanics in engineering practice, John Wiley and Sons.

110.Vaid, Y.P. and Chern, J.C. (1984). Effect of static shear on resistance to liquefaction. Soils and Foundations, Vol. 23, No. 1, pp. 47-60.

111.Vaid, Y.P. and Chern, J.C. (1985). Cyclic and monotonic undrained response of saturated sands. Advances in the Art of Testing Soils Under Cyclic Conditions, ASCE, Edited by V.Khosi.

112.Vaid, Y.P., Chern, J.C. and Tumi, H. (1985). Confining pressure, grain angularity and liquefaction. Journal of the Geotechnical Engineering Division, ASCE, Vol. 111, No.10, pp. 1229-1235.

113.Vaid, Y.P., Chung, E.K. and Kuerbis, R.H. (1989). Preshearing and undrained response of sand. Soils and Foundations , Vol. 29, No. 4, pp. 49-61.

114.Vaid, Y.P., Chung, E.K. and Kuerbis, R.H. (1990). Stress path and steady state. Canadian Geotechnical Journal, Vol. 27, pp. 1-7.

115.Vaid, Y.P. and Finn, W.D.L. (1979). Static shear and liquefaction potential. Journal of Geotechnical Engineering Division, ASCE, Vol. 105, No. GT10, pp. 1233-1246.

116.Vaid, Y.P., and Negussey, D. (1984). A critical assessment of membrane penetration in the triaxial test. Geotechnical Testing Journal, Vol. 7, No. 2, pp. 70-76.

117.Vaid, Y.P. and Sivathayalan. S. (1996). Static and cyclic liquefaction potential of Fraser Delta sand in simple shear and triaxial tests. Canadian Geotechnical Journal, Vol. 33, pp. 281-289.

118.Vaid, Y.P. and Thomas, J. (1995). Liquefaction and post liquefaction behaviour of sand. Journal of Geotechnical Engineering, ASCE, Vol. 121, No. 2, pp. 163-173.

119.Vasquez-Herrera, A. and Dobry, R. (1988). The behaviour of undrained contractive sand and its effect on seismic liquefaction flow failures of earth structures. Department of Civil Engineering Polytechnic Institute, USA.

120.Verugo, R. (1992). Characterization of sandy soil behaviour under large deformation. Ph.D. Thesis, Department of Civil Engineering, University of Tokyo.

121.Vesic, A.S. and Clough, G.W. (1968). Behaviour of granular materials under high stresses. Journal of the Soil Mechanics and Foundations Division, ASCE, Vol. 94, No. SM3, pp. 661-688.

122.Wood, D.M. (1990). Soil behaviour and critical state soil mechanics , Cambridge University, press.

123.Yamamuro. J.A. and Lade. P.V. (1997). Static liquefaction of very loose sands. Canadian Geotechnical Journals, Vol.34, pp. 905-917.

124.Youd, T.L. (1977). Packing changes and liquefaction susceptibility. Journal of Geotechnical Engineering, ASCE, Vol. 103, No. GT8. pp. 918-923.

125.Youd, T.L. (1984b). Geological effects- liquefaction and associated ground failure. Proceedings, Geologic and Hydrologic Hazards Training Program, Open File Report 84-760, U.S. Geological Survey, Menlo Park, California, pp. 210-238.

Appendix A

A.1 Area corrections.

The axial stress was computed by dividing the piston force by the effective area, assuming that the sample deformed as a right cylinder keeping its original shape as shown in Fig. A1. Visual inspection of the samples showed that this assumption was reasonable both during and shearing stages of the tests.

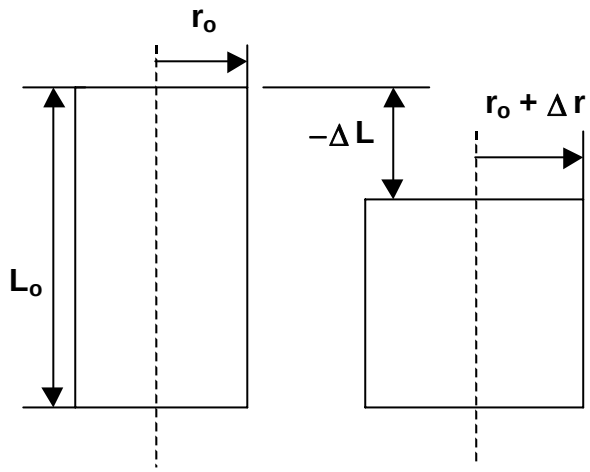

Figure A.1 Area corrections during drained and undrained triaxial tests.

The corrected areas for drained and undrained tests are calculated as follows:

Let r_o denote the initial radius, L_o the initial length and A_o the initial cross-sectional area. If $r_o + \Delta r$ is the radius after a change ΔL in length, then the cross-sectional area of the sample at this stage is given by:

$$A = \pi(r_o + \Delta r)^2 \tag{A.1}$$

$$= \pi r_o^2\left(1 + \frac{\Delta r}{r_o}\right)$$

but $\pi r_o^2 = A_o$

then $$A = A_o(1 + 2\varepsilon_r + \varepsilon_r^2) \tag{A.2}$$

In the compression undrained test on saturated soils volumetric strain is zero and hence the corrected area is a function of only axial strain.

$$-\varepsilon_a + 2\varepsilon_r = 0 \tag{A.3}$$

$$\varepsilon_a = 2\varepsilon_r \tag{A.4}$$

Substituting this into Eq. (A.2) gives

$$A = A_o\left(1 + \varepsilon_a + \frac{1}{4}\varepsilon_a^2\right) \tag{A.5}$$

A.2 Monotonic triaxial test results.

In this section of the appendix some of the monotonic triaxial test results which are not covered in the main body of this thesis are presented.

In Figs. A.2 and A.3 conventional consolidated undrained (CU) and consolidated constant volume (CCV) test results are plotted together. As seen in these figures, the CCV tests give a stress paths quite similar to the stress paths of the undrained tests, except that they avoid cavitation caused by large negative pore-water pressures (approx. at -96kPa).

In order to see the responses of the sand during unloading-reloading, different tests under undrained and drained loading conditions were conducted. As can be seen from Figs. A.4, A.5, and A.6, for all tests the initial stress paths were followed during in all stages of reloading.The stress path plot shown in Fig. A.4 shows that in all stages of unloading-reloading the stress paths have a slope similar to a conventional drained test (i.e 1:3). For further reference the unloading shear stiffness were calculated from the plots of stress versus shear strain and shown in the same figures.

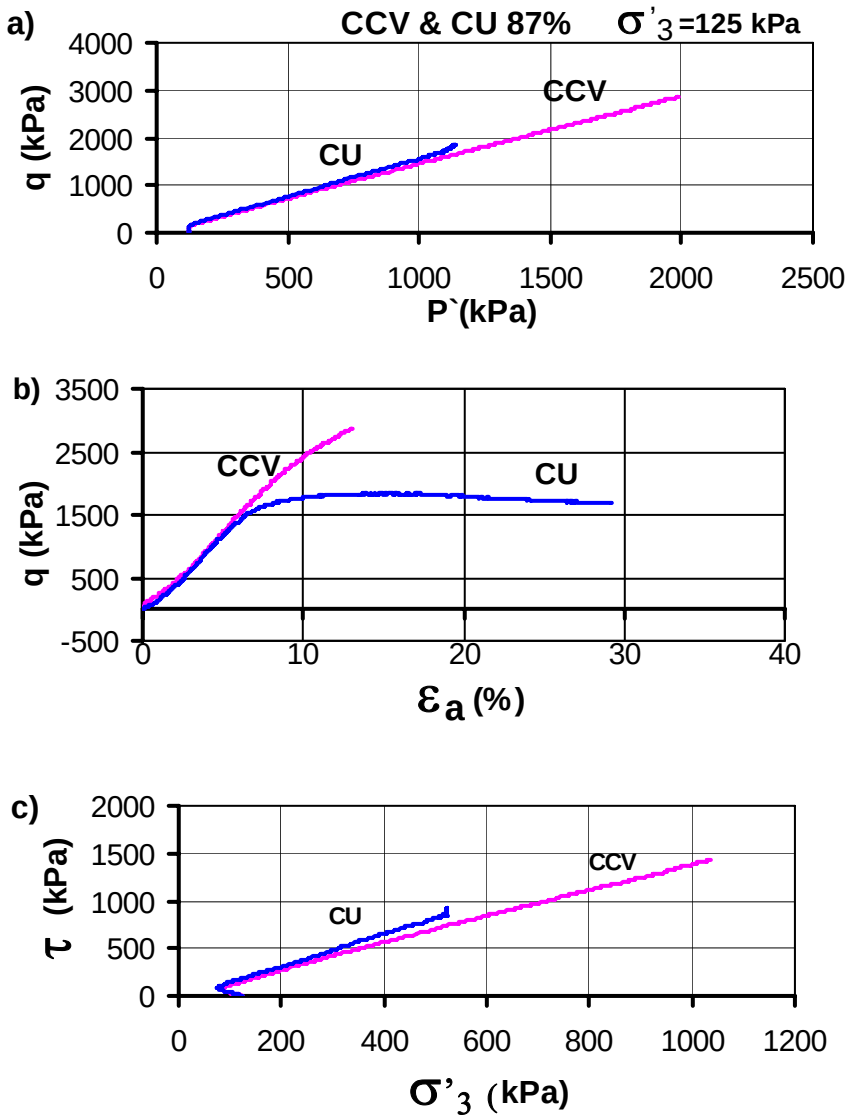

Figure A.2 Consolidated constant volume and consolidated undrained test results on dense sample. a) stress path, b) stress versus strain and c) shear stress versus effective confining pressure.

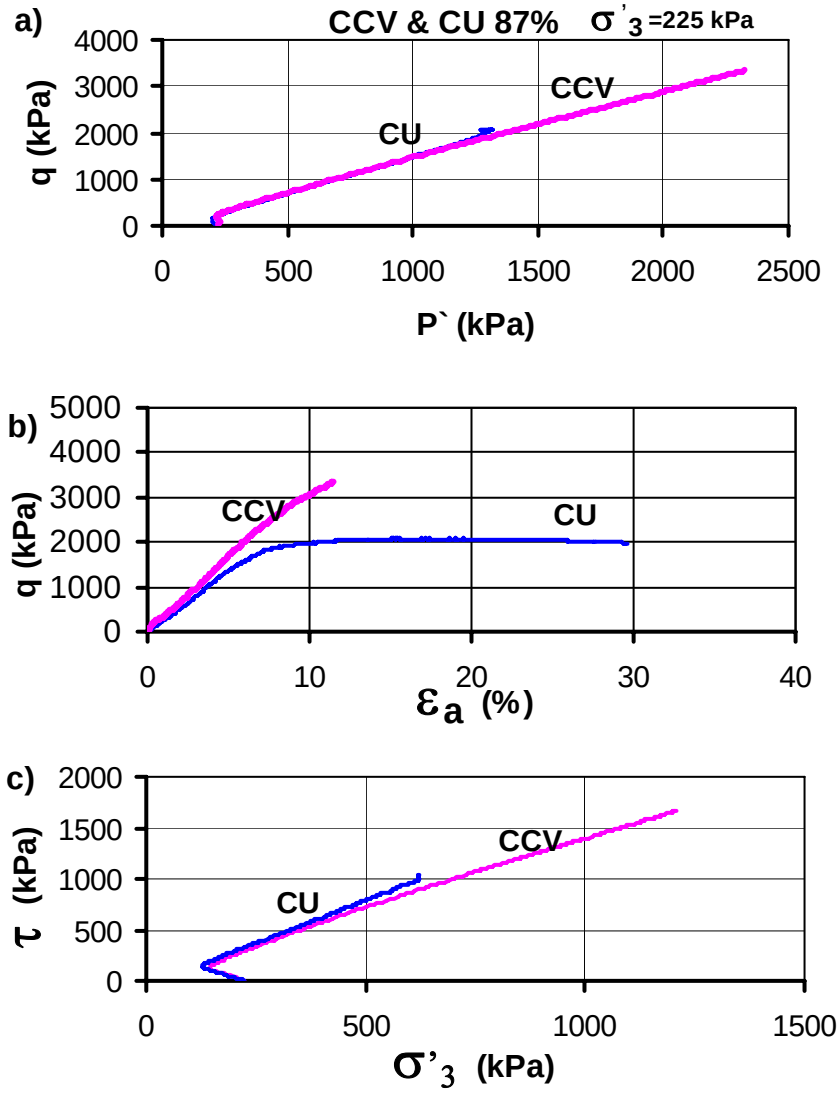

Figure A.3 Consolidated constant volume and consolidated undrained test results on dense sample. a) stress path, b) stress versus strain, and c) shear stress versus effective confining pressure.

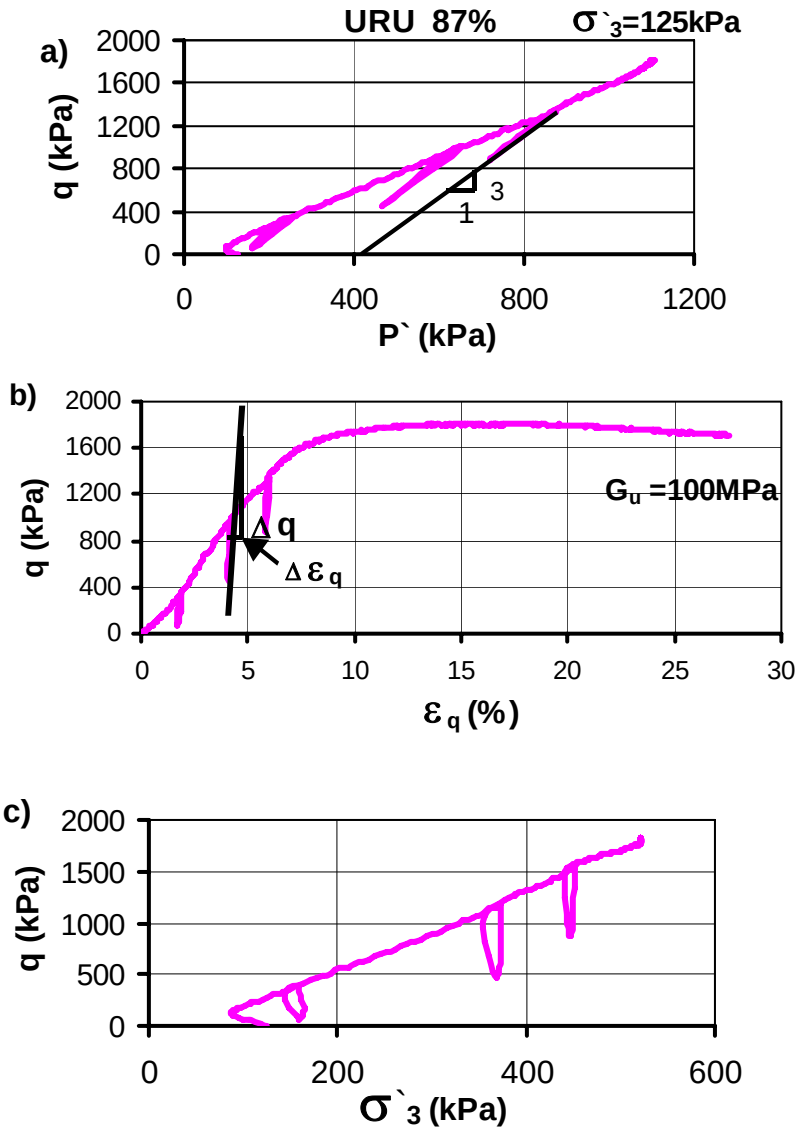

Figure A.4 Unloading-reloading consolidated undrained test results on dense sample. a) stress path, b) stress versus shear strain and c) deviatoric stress versus effective confining pressure.

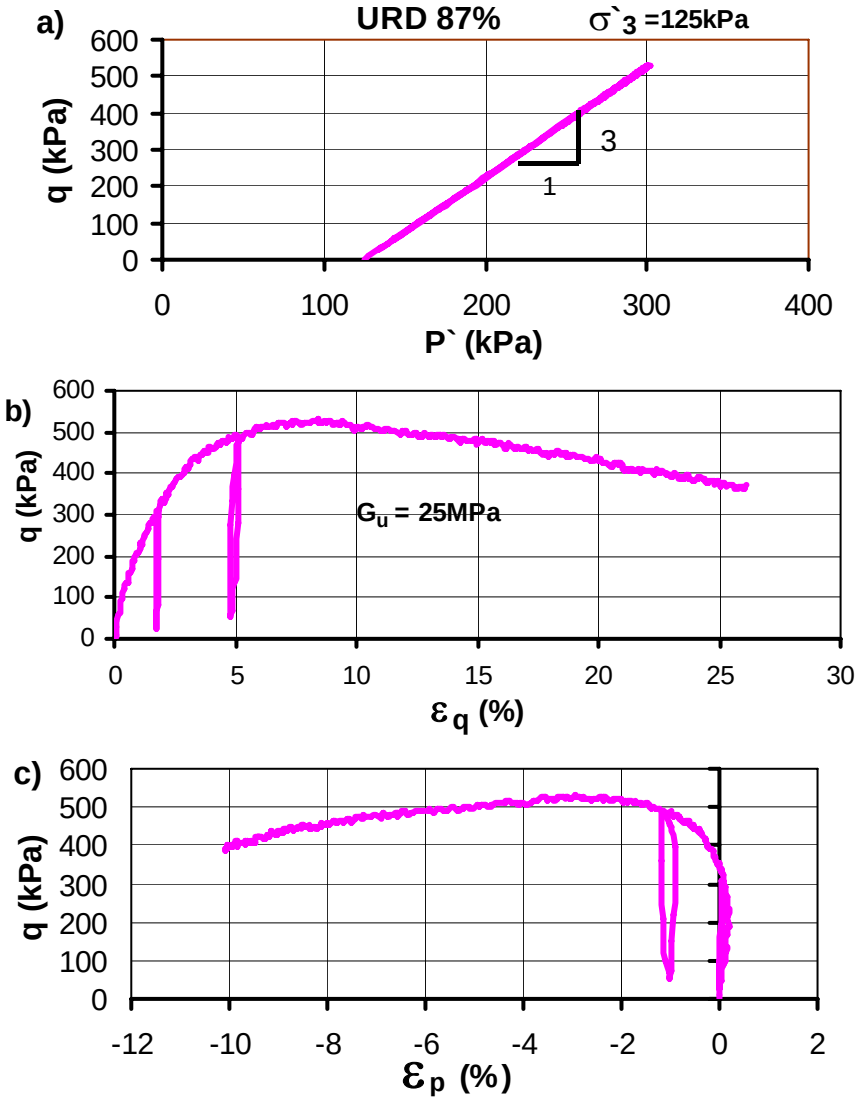

Figure A.5 Unloading-reloading consolidated drained test results on dense sample. a) stress path, b) stress versus shear strain and c) deviatoric stress versus volumetric strain.

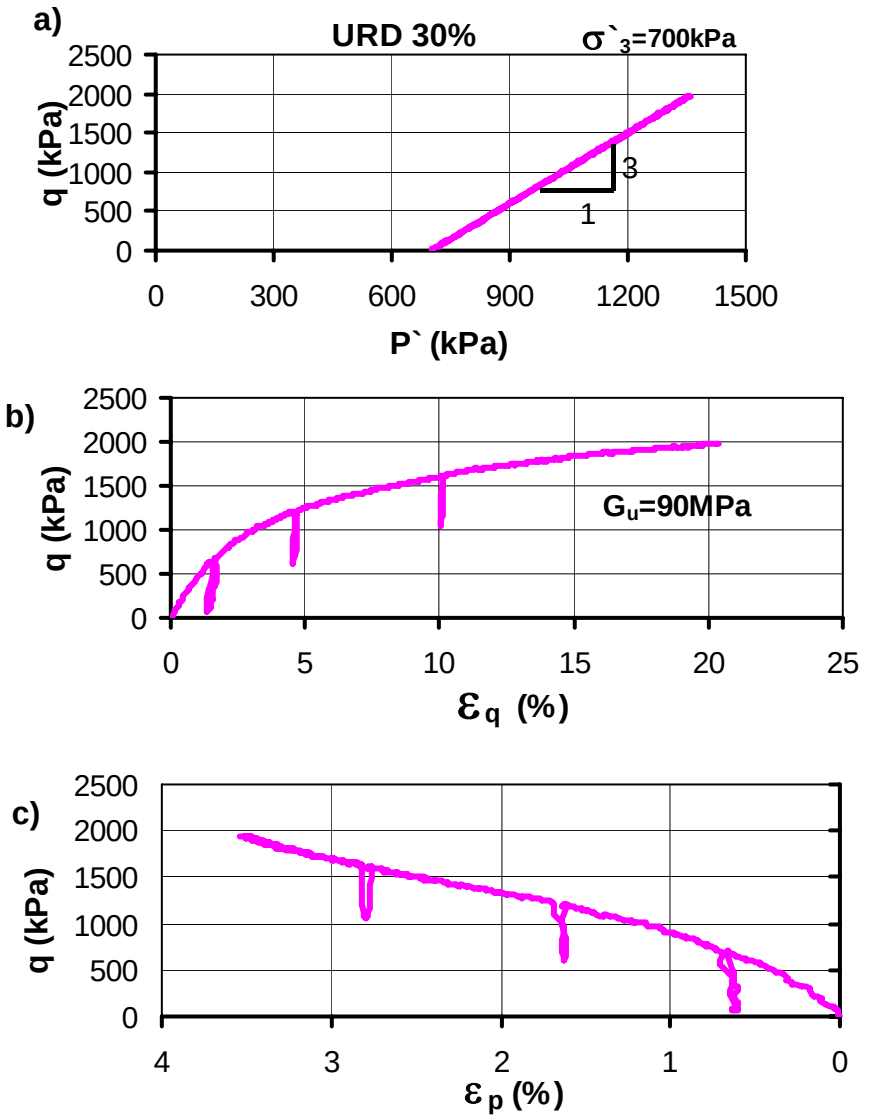

Figure A.6 Unloading-reloading consolidated drained test results on loose sample. a) stress path, b) stress versus shear strain and c) deviatoric stress versus volumetric strain.

Appendix B

B.1 Cyclic triaxial test results.

The cyclic test results in terms of a) effective stress paths (q-p'), b) the relationships between deviator stress (q) and axial strain (ε_a) and c) the relationships between the developed pore-water pressure and number of cycles are presented in Figs. B.1 to B.9. Table B.1 shows some of cyclic tri-axial tests conducted in this program.

Table B.1Cyclic triaxial tests.

Test name	Relative density (%)	Cyclic stress (q_{cyc})	Initial conditions
CUC 30%	30	84	Isotropically consolidated at σ'_3 = 125kPa
CUC 30%	30	70	
CUC 30%	30	55	
CUC 57%	57	110	
CUC 57%	57	85	
CUC 57%	57	70	
CUC 87%	87	150	
CUC 87%	87	110	
CUC 87%	87	90	

Fig. B.10 shows the effect of monotonic loading to a sample of dense sand. The sample was first brought to reach an initial liquefaction stage by the cyclic loading shown in Fig. B.10(a). When the cyclic loading was stopped the pore water pressure in the sample was equal to the applied confining pressure. At this stage the sample was subjected to monotonic loading at constant rate of strain. As can be seen from Fig. B.10, the sample dilate and developed a resistance to deformation at a much small strain level. It may be conclude from this that liquefied layers of dense sand will regain their strength at low level of deformations.

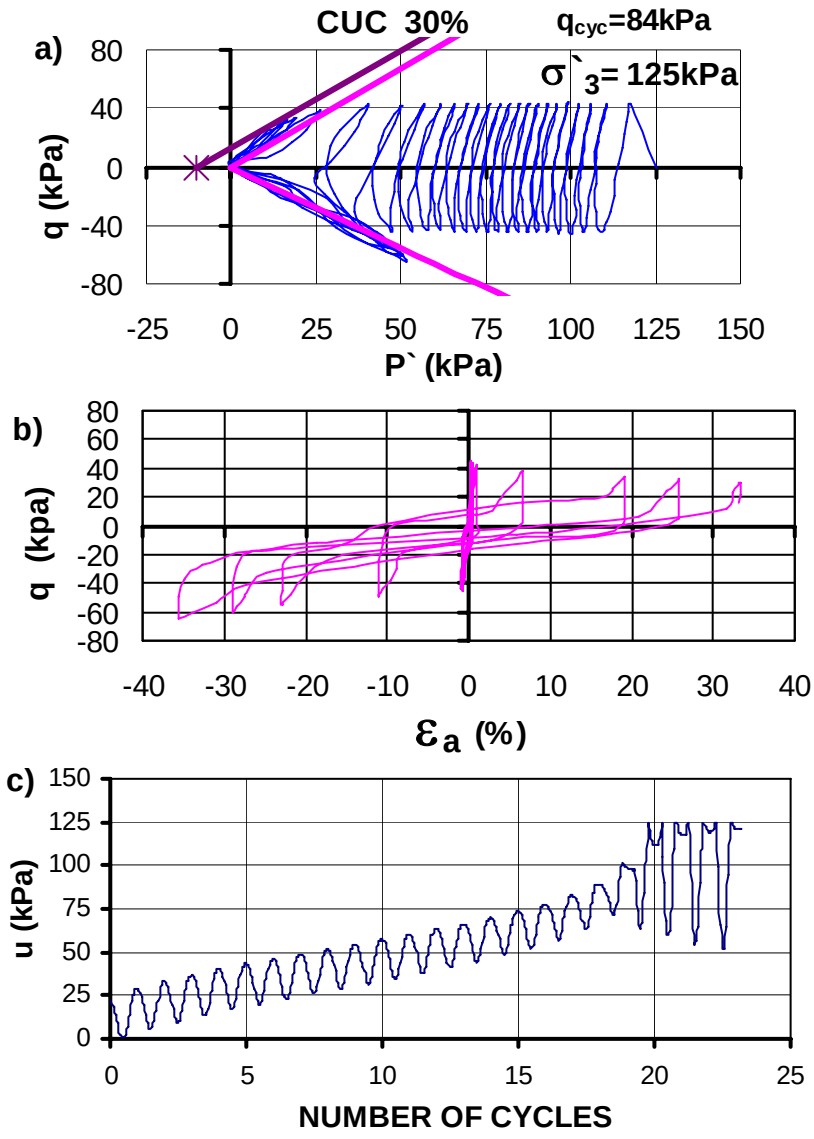

Figure B.1Cyclic triaxial test results on loose sand. a) Effective stress path, b) stress versus axial strain and c) pore water pressure versus number of cycles.

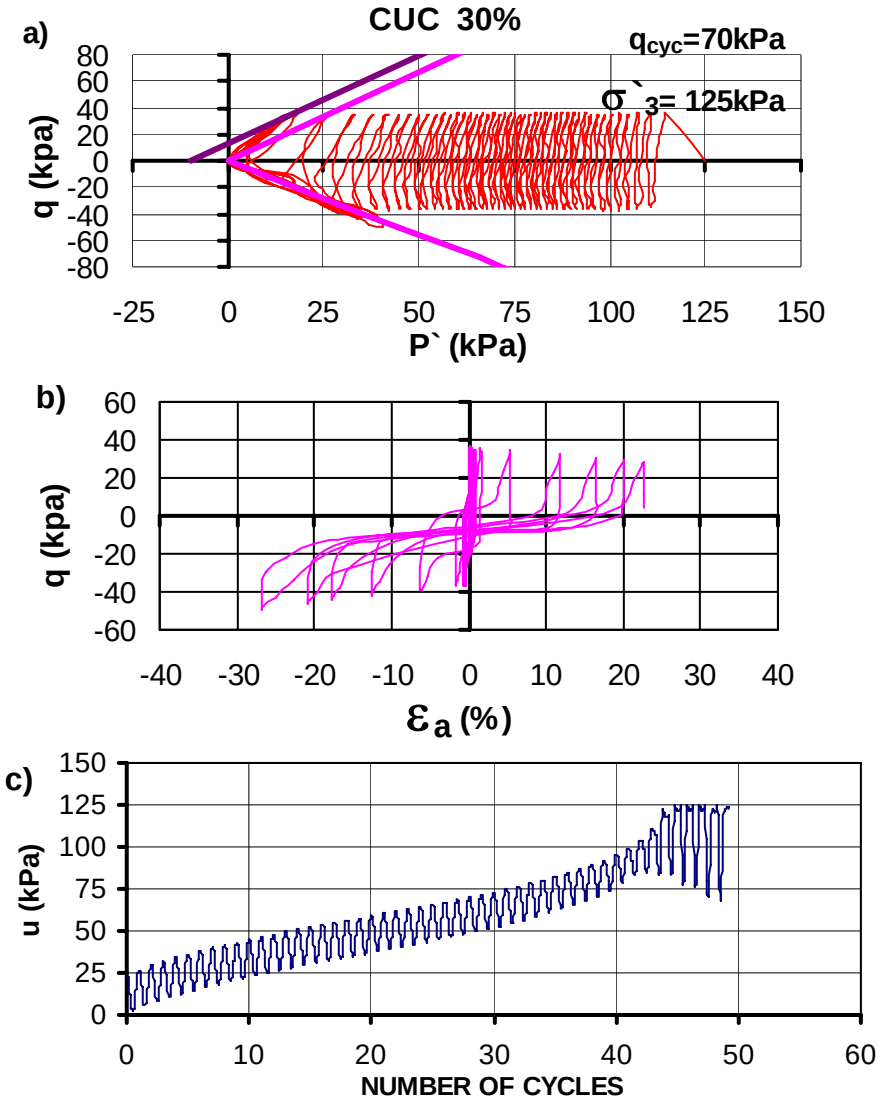

Figure B.2 Cyclic triaxial test results on loose sand. a) Effective stress path, b) stress versus axial strain and c) pore water pressure versus number of cycles.

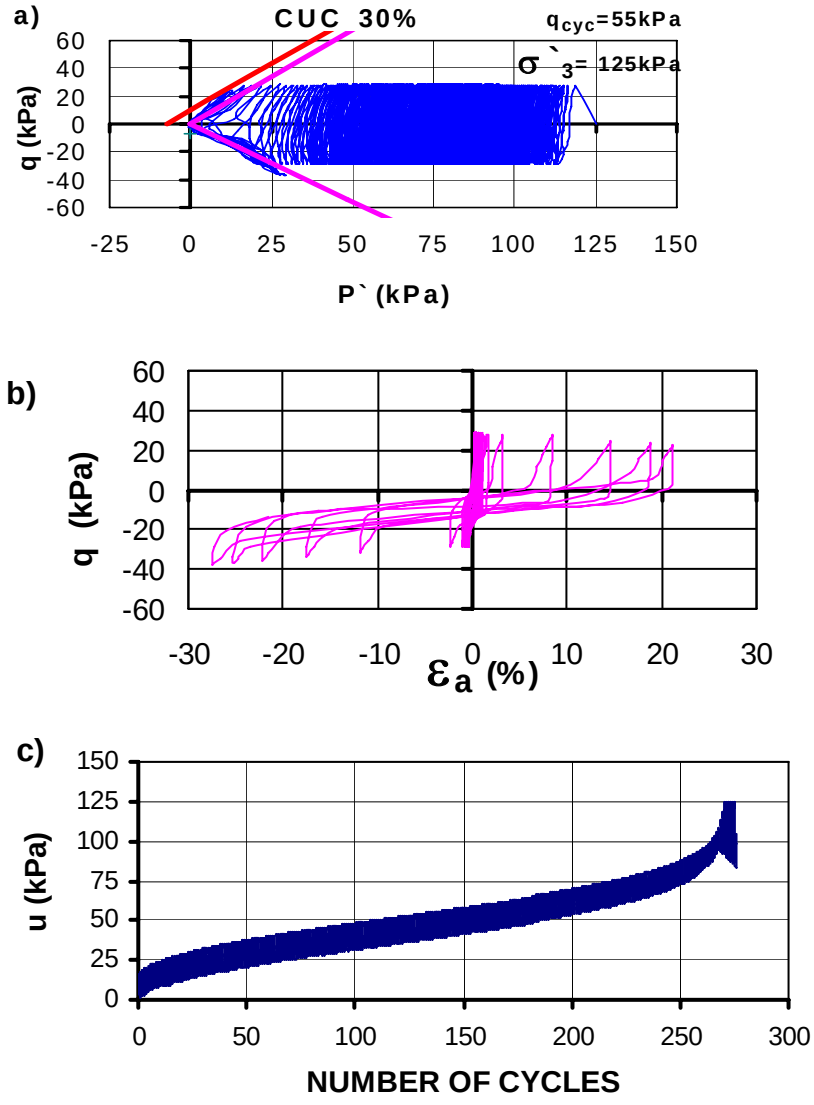

Figure B.3 Cyclic triaxial test results on loose sand. a) Effective stress path, b) stress versus axial strain and c) pore water pressure versus number of cycles.

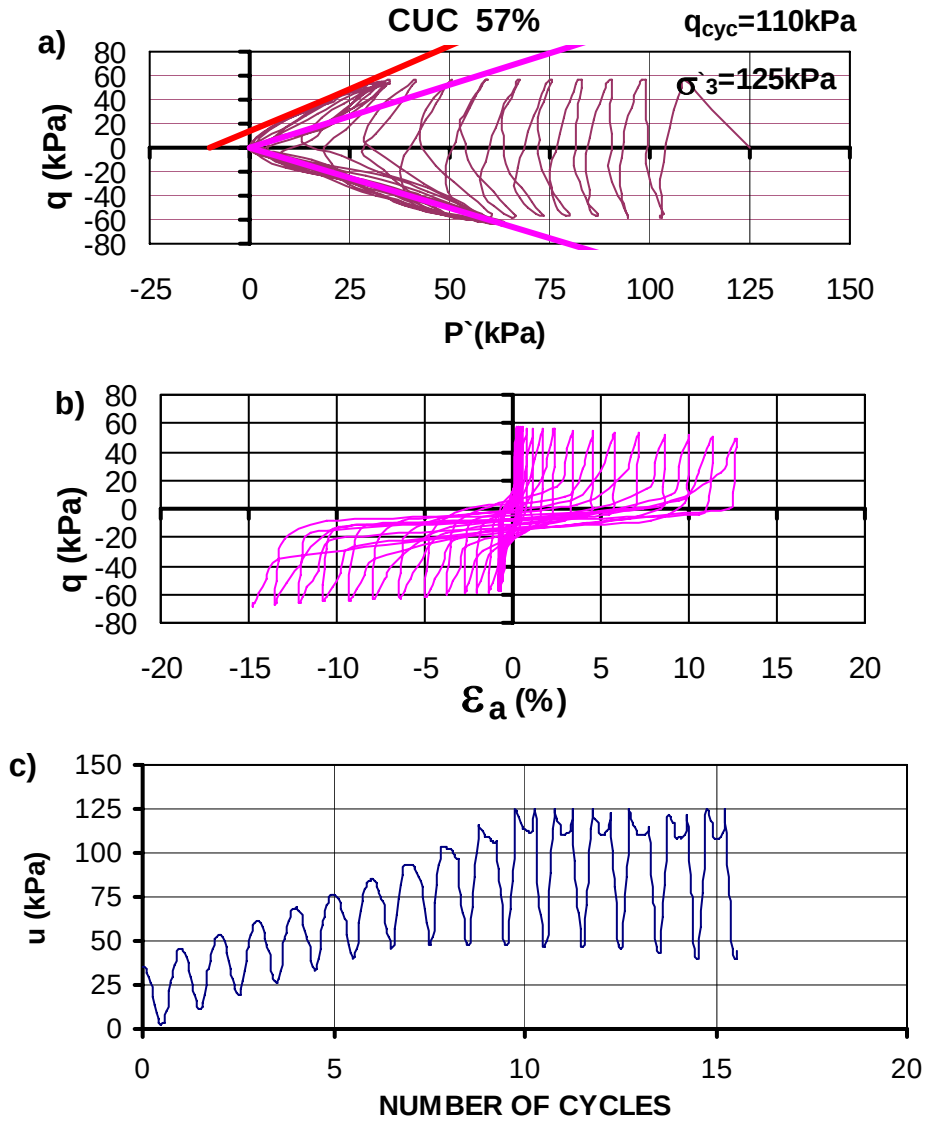

Figure B.4 Cyclic triaxial test results on medium dense sand. a) Effective stress path, b) stress versus axial strain and c) pore water pressure versus number of cycles.

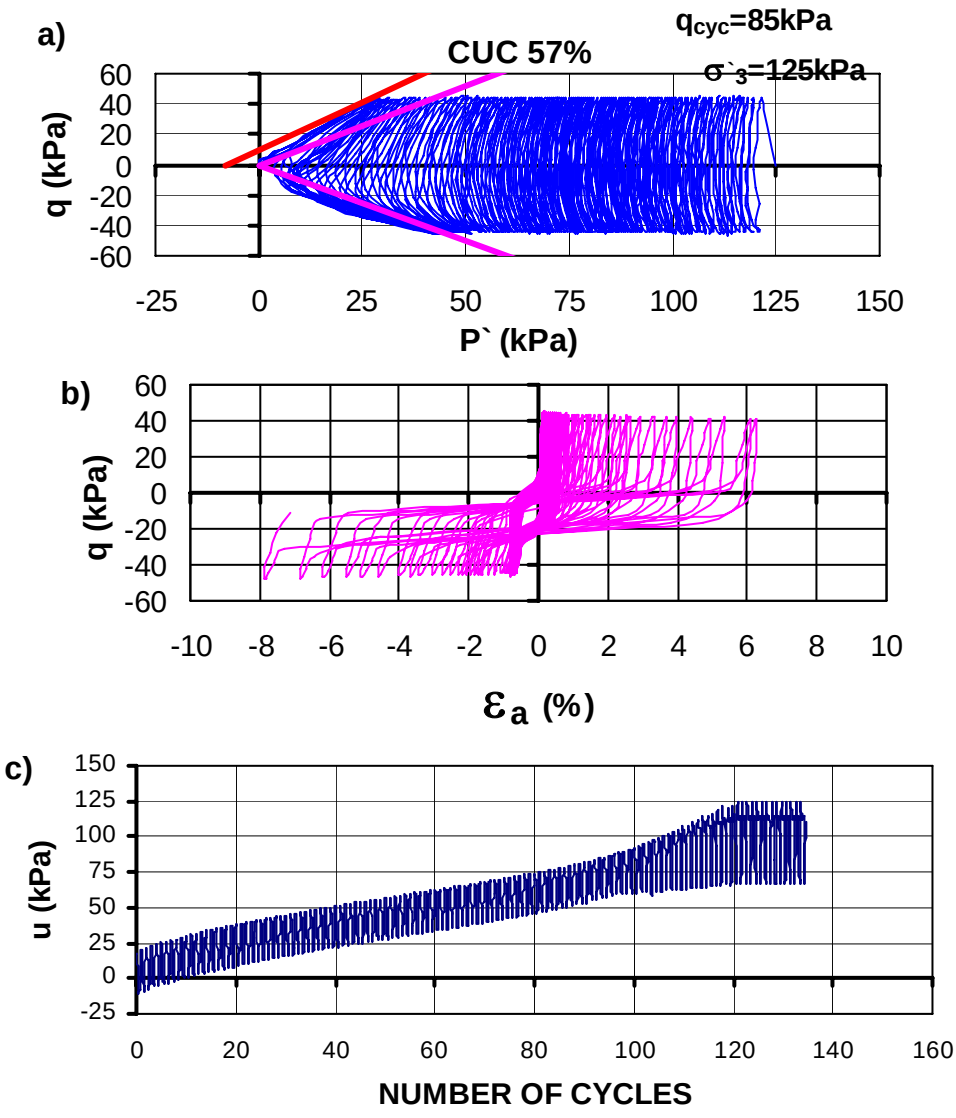

Figure B.5 Cyclic triaxial test results on medium dense sand. a) Effective stress path, b) stress versus axial strain and c) pore water pressure versus number of cycles.

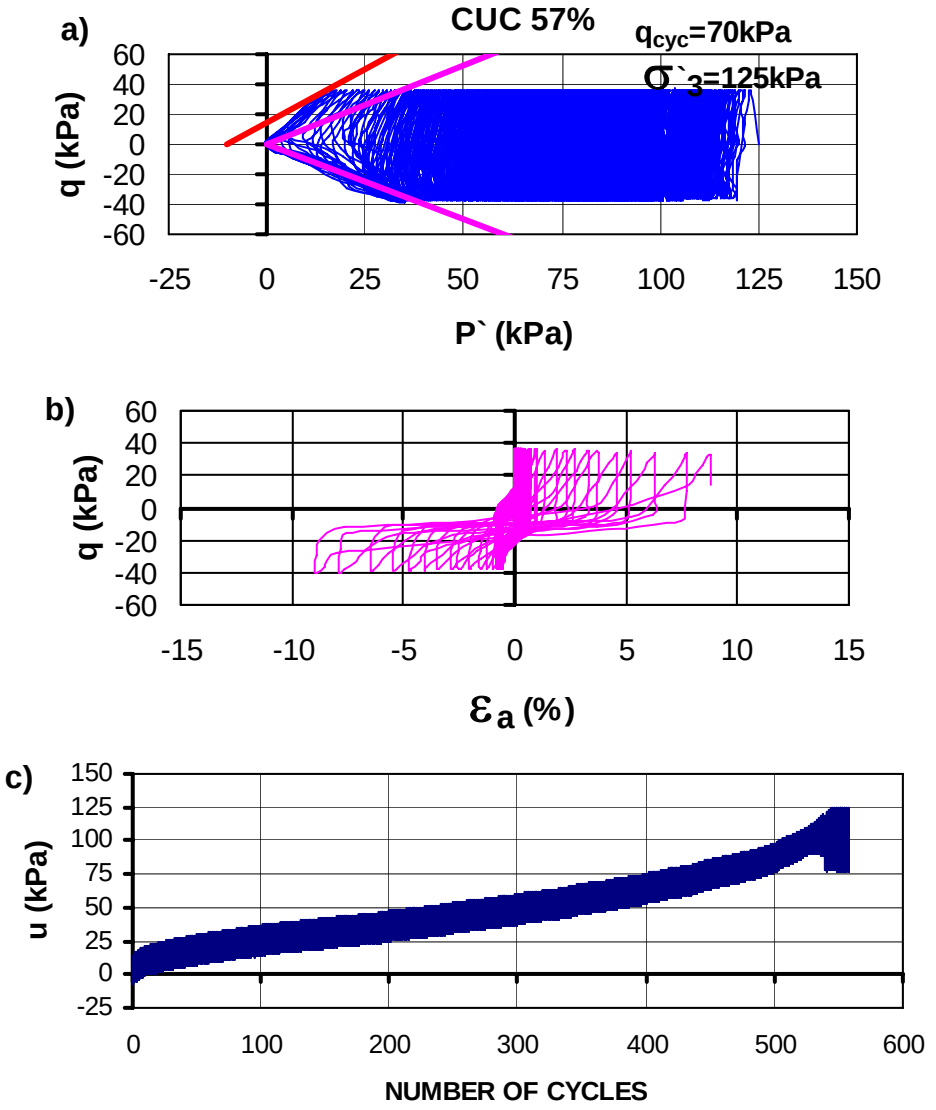

Figure B.6 Cyclic triaxial test results on medium dense sand. a) Effective stress path, b) stress versus axial strain and c) pore water pressure versus number of cycles.

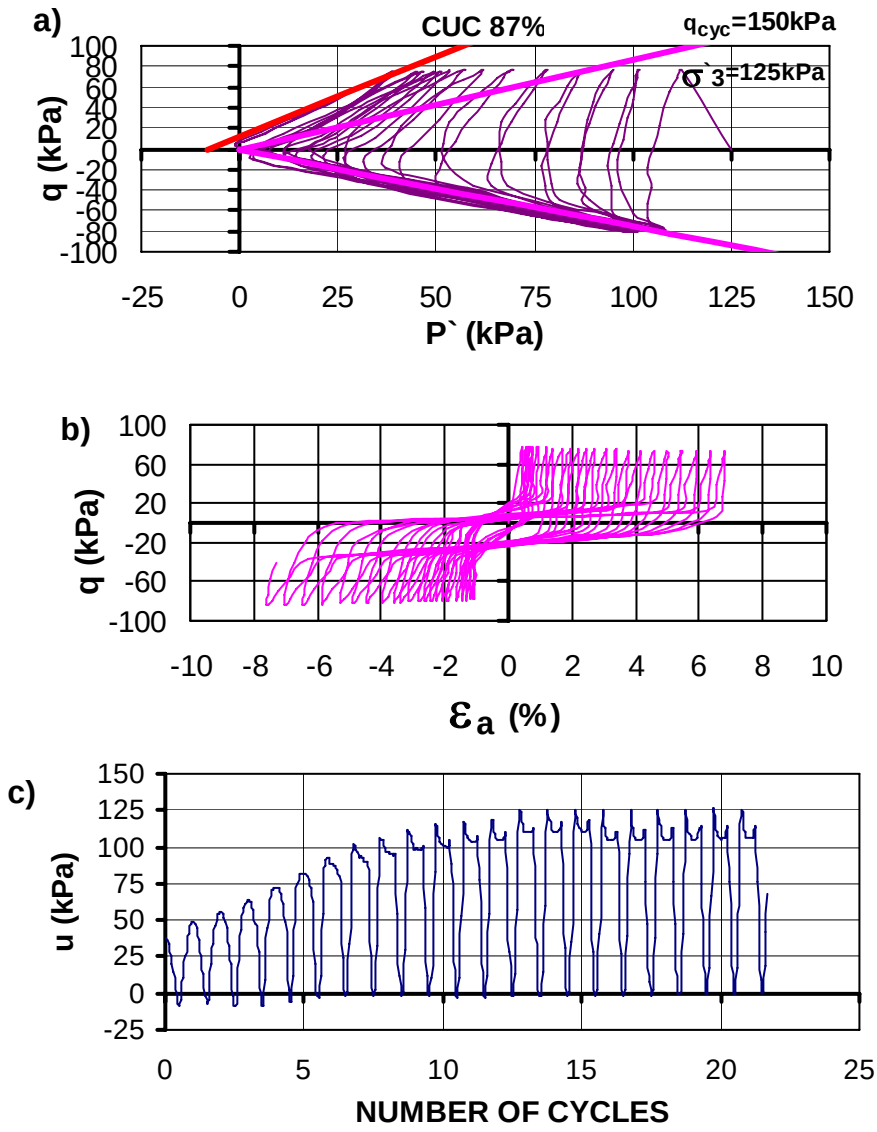

Figure B.7 Cyclic triaxial test results on dense sand. a) Effective stress path, b) stress versus axial strain and c) pore water pressure versus number of cycles

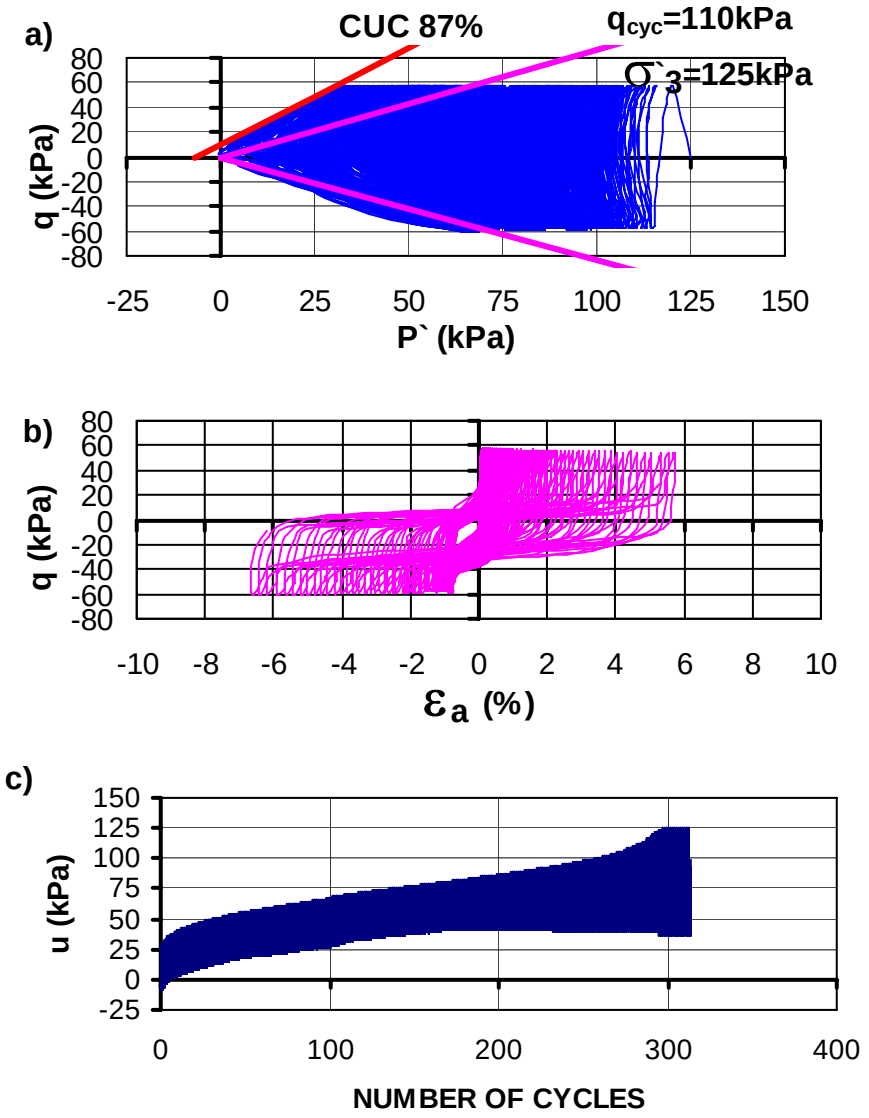

Figure B.8 Cyclic triaxial test results on dense sand. a) Effective stress path, b) stress versus axial strain and c) pore water pressure versus number of cycles.

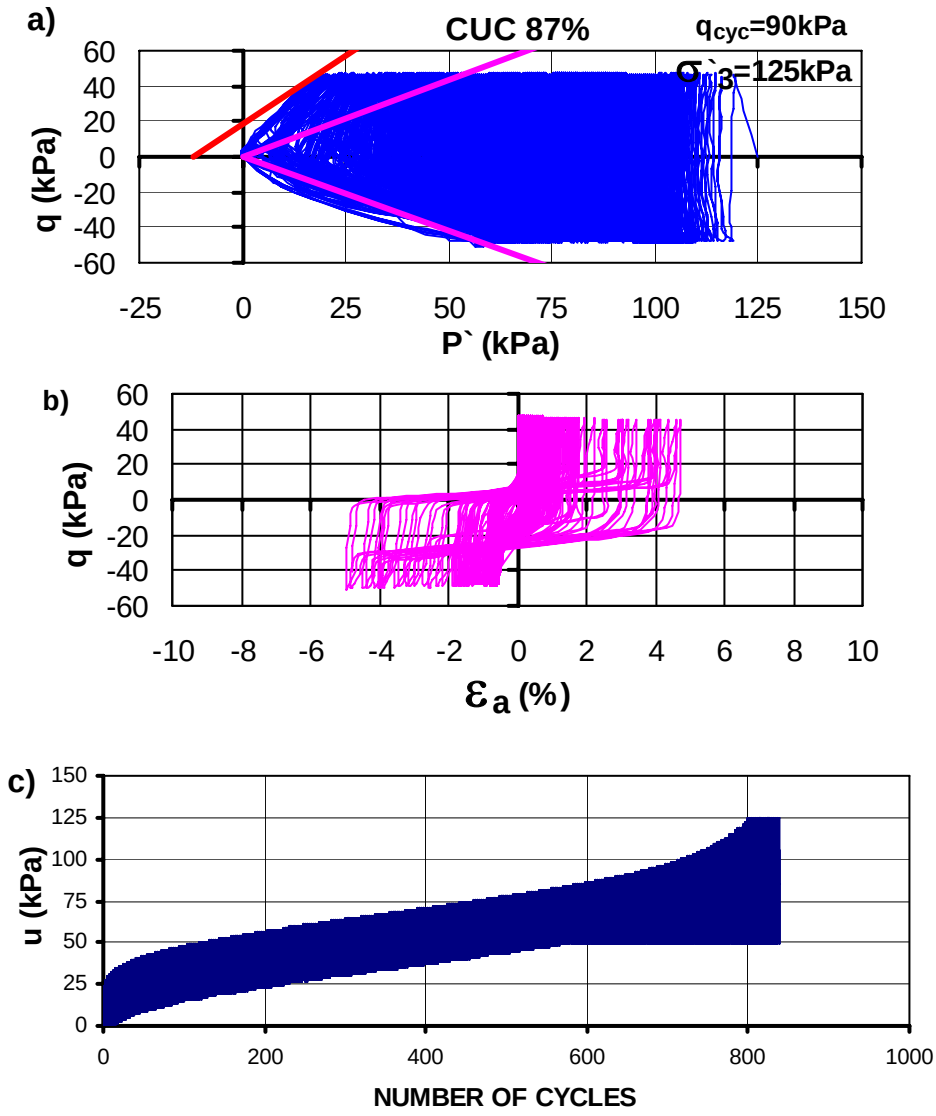

Figure B.9 Cyclic triaxial test results on dense sand. a) Effective stress path, b) stress versus axial strain and c) pore water pressure versus number of cycles.

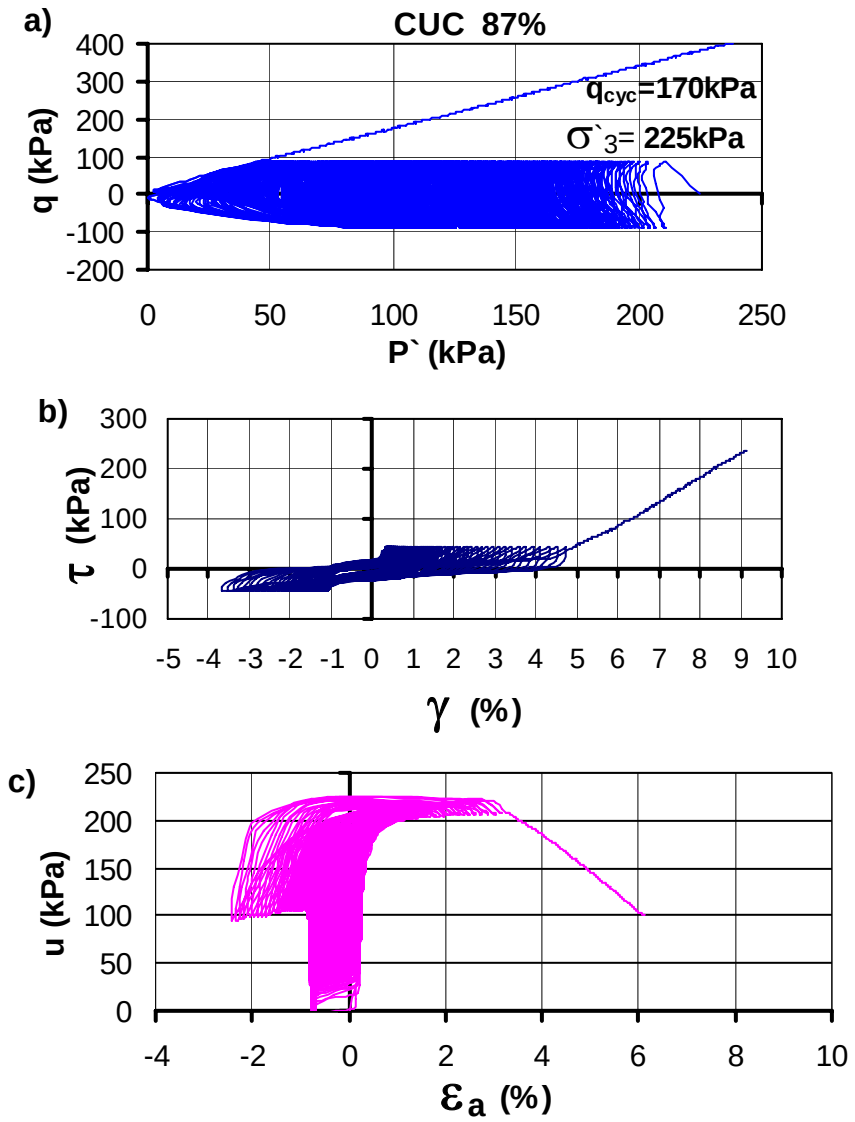

Figure B.10 Results of cyclic triaxial loading followed by monotonic loading test on dense sand. a) Effective stress path, b) shear stress versus shear strain and c) pore water pressure versus axial strain.

Corrections

1) The second figure of Fig. 4.12 should be replaced by the following figure.

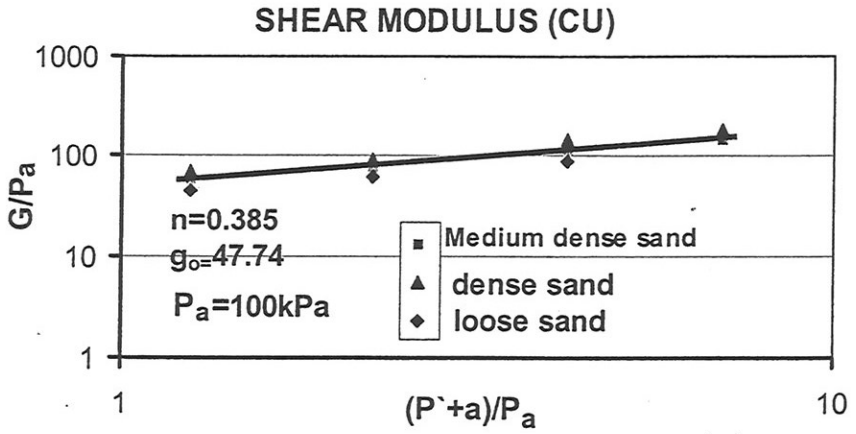

2) Appendix A, page A-2, line 5 should be replaced by

$$r_o^2\left(1+\frac{\Delta r}{r_o}\right)^2$$